BENEFICIAL USE OF PRODUCED WATER AND CARBON DIOXIDE IN DEPLETED OIL RESERVOIRS: IN-SITU MICROBIAL CONVERSION OF CRUDE OIL TO METHANE

By

BABAK SHABANI

Bachelor of Science in Petroleum Engineering-Drilling
Petroleum University of Technology
Ahwaz, Iran
2008

Master of Science in Petroleum Engineering-Drilling and Production
Amirkabir University of Technology (Polytechnic)
Tehran, Iran
2011

Submitted to the Faculty of the
Graduate College of the
Oklahoma State University
in partial fulfillment of
the requirements for
the Degree of
DOCTOR OF PHILOSOPHY
May, 2019

BENEFICIAL USE OF PRODUCED WATER

AND CARBON DIOXIDE IN DEPLETED

OIL RESERVOIRS: IN-SITU MICROBIAL

CONVERSION OF CRUDE OIL TO METHANE

Dissertation Approved:

Dr. Javier Vilcáez

Dissertation Adviser

Dr. Jack C. Pashin

Dr. Todd Halihan

Dr. Sumit Mukhopadhyay

Dr. Prem Bikkina

ACKNOWLEDGEMENTS

I would like to express my deepest appreciation to all who provided me the possibility to complete this dissertation.

I would like to express my sincere gratitude to my advisor Dr. Javier Vilcáez for the continuous support of my Ph.D. study, for his patience, motivation, and immense knowledge. His guidance helped me in all the time of research and writing of this dissertation.

Besides my advisor, I would like to thank the rest of my dissertation committee: Dr. Jack Pashin, Dr. Todd Halihan, Dr. Sumit Mukhopadhyay, and Dr. Prem Bikkina for their insightful comments and support.

I deeply appreciate the support of the Boone Pickens School of Geology, its faculty and staff during last four years. My special thanks goes to Dr. Mohamed Abdelsalam, Dr. Jim Puckette, and Dr. Mary Hileman.

I very much appreciate the Geological Society of America research grant, the Oklahoma Water Resources Center grant, Martin Family foundation fellowship, and Professor Hermann Burchard Holistic Science Prize award.

I thank my fellow officemates for the stimulating discussion, their help and support, and all the fun we have had. Also, I appreciate my friends who have treated me like a family member in last four years. I would like to give my deepest appreciation to Aghayans, Bagheris, Davanis, Estefanny, Georgina, Habibpours, Hamid Rahnema, Jenny, Liang, Mahmoodis, Pouyan, Ross, Sahar, and Zares.

Last but not the least, I would like to thank my family: my parents and my brothers for supporting me spiritually throughout writing this dissertation and my life in general.

Name: BABAK SHABANI

Date of Degree: MAY, 2019

Title of Study: BENEFICIAL USE OF PRODUCED WATER AND CARBON DIOXIDE IN DEPLETED OIL RESERVOIRS: IN-SITU MICROBIAL CONVERSION OF CRUDE OIL TO METHANE

Major Field: GEOLOGY

Abstract:

Produced water from oil and gas reservoirs contains high levels of organic chemicals and heavy metals whose concentrations, in many cases, exceeds USA drinking water standards. To prevent the contamination of underground sources of drinking water, produced water from oil and gas reservoirs is commonly disposed into deep highly porous and permeable media such as saline aquifers. However, produced water also contains indigenous microbial communities that are well adapted to deep underground conditions. This property of petroleum produced water can be used to convert remaining crude oil (mostly n-alkanes) in depleted oil reservoirs to methane (CH_4) gas. This can be done by stimulating the activity of methanogenic and crude oil-degrading microbial communities present in produced water by combining the supply of protein-rich matter and CO_2.

The goal of my research was to numerically assess the feasibility of microbial conversion of CO_2 and crude oil to CH_4 in depleted oil reservoirs. To achieve this goal, I developed a non-iterative fugacity-activity thermodynamic model to predict the mutual solubility of CO_2-CH_4-H_2S-N_2 gas mixtures and brine, and also expanded the capability of a thermodynamic model to calculate the solubility of CO_2-CH_4-H_2S-H_2 gas mixtures in brine. After that, I included these thermodynamic models into multiphase-multicomponent fluid flow simulators TOUGH2 and TOUGHREACT. The flow capabilities of the developed TOUGH2 and TOUGHREACT modules were verified by comparing their simulation results with other reliable multiphase simulation programs including the ECO2N module of TOUGHREACT, the EOS7C module of TOUGH2, and CMG-GEM©. The final step was to apply relevant changes in the reactive part of the developed TOUGHREACT module, named CO2Bio. The CO2Bio can simulate the multiphase-multicomponent reactive transport of CO_2-CH_4-H_2S-H_2 gas mixtures and brine under biotic conditions. Using CO2Bio, a simulation study was conducted in a section of Cushing oil reservoir in Oklahoma. The results of this simulation showed that it is feasible to produce CH_4 from biodegradation of the remaining crude oil in depleted oil reservoirs.

PUBLICATION DISSERTATION OPTION

This dissertation has been organized in two sections. The first section briefly outlines the dissertation structure and introduces the scientific questions that have been investigated in this research. The second section presents the three published papers and one in-preparation manuscript out of this research.

Paper 1: Shabani, B. and Vilcáez, J., 2017. "Prediction of CO_2-CH_4-H_2S-N_2 gas mixtures solubility in brine using a non-iterative fugacity-activity model relevant to CO_2-MEOR," J. of Petroleum Science and Engineering, (150), pp. 162-179.
https://doi.org/10.1016/j.petrol.2016.12.012

Paper 2: Shabani, B. and Vilcáez, J., 2018. "A fast and robust TOUGH2 module to simulate geological CO_2 storage in saline aquifers," J. of Computers and Geosciences, (111), pp. 58-66.
https://doi.org/10.1016/j.cageo.2017.10.012

Paper 3: Shabani, B. and Vilcáez, J., 2019. "TOUGHREACT-CO2Bio - a new module to simulate GCS under biotic conditions (Part 1): the multiphase flow of CO_2-CH_4-H_2-H_2S gas mixtures," J. of Natural Gas Science and Eng., (63), pp. 85-94.

https://doi.org/10.1016/j.jngse.2019.01.013

In-preparation manuscript: Shabani, B., Vilcáez, J. and Pashin, J., 2019. "TOUGHREACT-CO2Bio – a new module to simulate GCS under biotic conditions (Part 2): the bio-geochemical reactive transport of CO_2-CH_4-H_2-H_2S gas mixtures," to be submitted to the International J. of Greenhouse Gas Control.

TABLE OF CONTENTS

LIST OF TABLES

Table Page

LIST OF FIGURES

Figure Page

CHAPTER I

INTRODUCTION

1.1. Background

Methanogenic biodegradation of crude oil (mostly n-alkanes) is a well-known process that occurs in oil reservoirs (Dolfing et al., 2008; Jones et al., 2008a; Larter and di Primio, 2005; Scott et al., 1994), and its stimulation has been seen as a pathway for a new enhanced oil recovery method (Cai et al., 2015a; Cai et al., 2015b; Jones et al., 2008b; Vilcáez, 2015b). Biodegradation of crude oil under anaerobic conditions generates acetate and H_2 as metabolic products (Eq. (1)). While the generated acetate is converted into CH_4 and CO_2 by acetoclastic methanogens via fermentation (Eq. (2)), the generated CO_2 is converted into CH_4 by hydrogenotrophic microbes via the reduction pathway with H_2 (Eq. (3)):

$$4C_{16}H_{34} + 64H_2O \rightarrow 32CH_3COO^- + 32H^+ + 68H_2 \quad (1)$$

$$32CH_3COO^- + 32H^+ \rightarrow 32CH_4 + 32CO_2 \quad (2)$$

$$196H_2 + 64CO_2 \rightarrow 49CH_4 + 15CO_2 + 98H_2O \quad (3)$$

H_2 is a key component for CH_4 production from CO_2 by hydrogenotrophic methanogens in oil reservoirs. The injection of CO_2 into depleted oil reservoirs increases its availability for CH_4 production and decreases the pH of the formation water to acidic pH (4-6) levels where the activity of H_2-forming fermentative microbes is highest. For this, the combined injection of CO_2 and

petroleum produced water supplied with nutrients such as protein-rich matter has been proposed to stimulate the microbial conversion of residual crude oil and CO_2 (substrates) to CH_4 in depleted oil reservoirs (Vilcáez, 2015a; Vilcáez, 2015b). The produced CH_4 in depleted oil reservoirs can be recovered more easily than residual crude oil. This highlights the promising potential of a shift towards a CH_4-based energy economy where microbially produced CH_4 in depleted oil reservoirs is commercialized as an energy source.

The stimulating effect of the combined injection of CO_2 and petroleum produced water supplied with nutrients such as protein-rich matter on the microbial conversion of crude oil (mostly n-alkanes) and CO_2 to CH_4 has been proven using formation water and crude oil collected from depleted oil reservoirs in Oklahoma (Vilcáez et al., 2018). The reported stimulating effect of CO_2 is in agreement with previous studies showing that CO_2 can be converted to CH_4 by indigenous anaerobic microbial communities in oil reservoirs (Jones et al., 2008a; Mayumi et al., 2011), and that CO_2 promotes the growth of H_2-forming microbes in depleted oil reservoirs (Liu et al., 2015; Sugai et al., 2012). The results of these studies highlight the need for simulation tools to not only predict the physical and chemical fate, but also the microbiological fate of CO_2 injected into depleted oil reservoirs. This can be considered for either geological storage of CO_2 or for enhanced oil recovery through the stimulation of microbial conversion of n-alkanes and CO_2 to CH_4.

1.2. Motivation

The motivation behind this dissertation is to numerically assess the feasibility of accelerating naturally occurring methanogenic crude oil biodegradation in-situ by combining the injection of supercritical CO_2 and produced water supplied with the protein-rich matter. In this method, CO_2 injection into depleted oil reservoirs is to increase the availability of CO_2 for CH_4 production and decreases the pH of the formation water to acidic pH (4-6) levels, where the activity of H_2-producing

microbes is highest; and the supply of protein-rich matter is to provide indigenous microbes with required key nutrients such as trace metals and aminoacid compounds, which stimulates the growth of methanogenic microbial communities (Vilcáez, 2015a; Vilcáez, 2015b). Fig. 1.1 shows a schematic representation of the proposed method to make a beneficial use of produced water and CO_2.

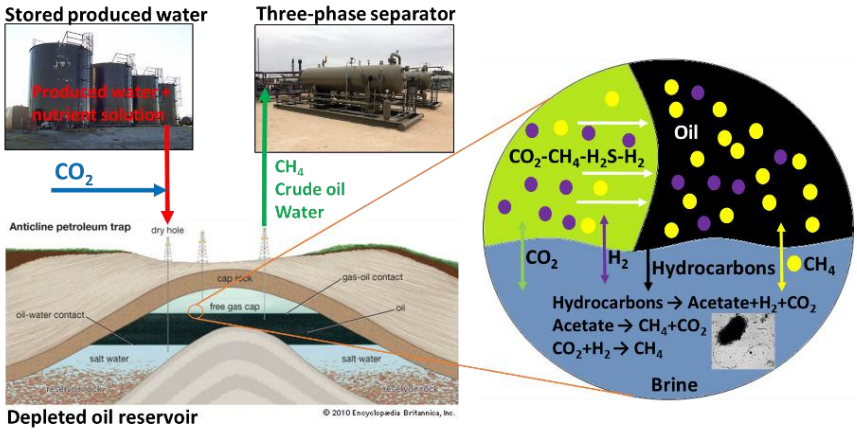

Fig. 1.1. Schematic representation of the proposed method and main interactions to make a beneficial use of produced water and CO_2 by stimulating the microbial conversion of crude oil to CH_4.

To the best of my knowledge, there is not any software to simulate the biogenic conversion of CO_2 to CH_4, and/or the biogenic formation of CO_2-CH_4-H_2S-H_2 gas mixtures from the biodegradation of organic substrates at reservoir pressure and temperature conditions. Accounting for this possibility is particularly important for depleted oil reservoirs where there is an ample source of organic substrates. Thus, the main objective of this dissertation is to develop a simulator to simulate the multiphase-multicomponent reactive transport of CO_2-CH_4-H_2-H_2S gas mixtures and brine in deep geological formations under biotic condition.

1.3. Significance

Oklahoma is one of the largest producers of natural gas and oil in the country. Thus, finding alternative ways not only to prevent the contamination of underground sources of drinking water, but

also to make a beneficial use of produced water is of paramount importance to the economy of Oklahoma. In this research, I proposed to make a beneficial use of produced water to enhance the recovery of oil from depleted oil reservoirs by using a novel method which consists of the in-situ stimulation of indigenous crude oil degrading and methanogenic microbial communities to convert residual crude oil to CH_4 gas. The concentration of saturated hydrocarbons (n-alkanes) in non-degraded and heavily biodegraded genetically related oils from Oklahoma was reported to be 55% and 20%, respectively (Mayer, 1987). A 55% of non-degraded oil constitutes a huge organic feedstock which can be recovered as CH_4 gas by the proposed method.

CHAPTER II

PREDICTION OF CO_2-CH_4-H_2S-N_2 GAS MIXTURES SOLUBILITY IN BRINE USING A NON-ITERATIVE FUGACITY-ACTIVITY MODEL RELEVANT TO CO_2-MEOR

Babak Shabani, Javier Vilcáez*

Boone Pickens School of Geology, Oklahoma State University, Stillwater, OK 74078, USA

2.1. Abstract

Numerical simulations of carbon dioxide-microbial enhanced oil recovery (CO_2-MEOR) would require computationally rigorous iterative methods to solve resulting system of flow, transport and kinetic reaction equations. This includes additional iterative procedures to account for the solubility of gas mixtures in the aqueous phase. This work proposes a new non-iterative fugacity-activity thermodynamic model to predict the solubility of CO_2-CH_4-H_2S-N_2 gas mixtures in brine. This model can readily be implemented in MEOR simulation programs to account for mass transfer and kinetics of microbial reactions in CO_2-MEOR operations. Fugacity coefficients (ϕ_i) in the proposed model were calculated using Predictive Peng-Robinson 78 (PPR78) and Peng-Robinson (PR) equation of state (EOS). The proposed model was successful in predicting CO_2 solubility in the aqueous phase with ϕ_i calculated either using PPR78 EOS or PR EOS. Comparison showed that at temperature and pressure conditions relevant to MEOR, using calibrated binary interaction parameters (PR EOS) leads to more accurate predictions than binary interaction parameters estimated from the group contribution expression (PPR78 EOS). Comparison of

predicted CO_2-CH_4-H_2S gas mixtures solubility in the aqueous phase obtained with the proposed non-iterative fugacity-activity model and an iterative fugacity-activity model, confirmed that proposed model with ϕ_i calculated using PR EOS can be used as substitute for iterative fugacity-activity models that relies on the solution of Rachford-Rice equation.

Key words: Geological CO_2 storage; MEOR; Gas mixtures solubility; Peng-Robinson EOS

*Corresponding author: vilcaez@okstate.edu (J. Vilcáez)

2.2. Introduction

Carbon dioxide capture and storage (CCS) operations involves capturing CO_2 produced from large power generation plants, compressing it for transportation and injecting into deep geological formations such as saline aquifers and depleted oil reservoirs. CCS is regarded as a potential effective method for reducing CO_2 emissions into the atmosphere. However, CCS is yet to become a standard of practice (Benson et al., 2012). One reason hindering the application of CCS to reduce the emissions of CO_2 into the atmosphere is the cost of CCS projects. Coupling CCS with enhanced oil recovery (EOR) projects has emerged as a promising method to reduce or compensate for the cost of CCS projects. CO_2 due to its low minimum miscibility pressure compared to other gases such as methane and nitrogen, has a swelling effect on oil enhancing its mobility. Another method to reduce or compensate for the cost of CCS projects is to couple it with microbial enhanced oil recovery (MEOR) projects. MEOR consists of injecting selected microbial nutrients into depleted oil reservoirs to stimulate the activity of indigenous microbes whose metabolic products enhance the oil recovery. A new method (CO_2-MEOR), which combines the injection of CO_2 and stimulating nutrients has been proposed to biogenically convert CO_2 and oil to CH_4 in depleted oil reservoirs (Vilcáez, 2015a, b). The formed CH_4 in depleted oil reservoirs can be recovered more easily than oil, and its commercialization as energy source might reduce or compensate for the cost of CCS projects. Preliminary experimental and numerical simulation studies have shown that a CO_2-MEOR method is possible in principle. However, this method would not be of general application because it depends on hydrogeological, geochemical, and microbiological

conditions that are different in each depleted oil reservoir. One way to screen potential of depleted oil reservoirs to implement CO_2-MEOR is to perform numerical simulation studies.

Most numerical simulation studies on MEOR have focused on the microbiological formation of biopolymers, biosurfactants, biomass (microbial cells), and fatty acids which enhance the mobility of oil by reducing the viscosity and interfacial tension of oil against water (Azadpour et al., 1996; Giangiacomo and Dennis, 1997; Nemati et al., 2001), and/or by increasing or reducing the porosity/permeability of target zones containing oil (Brown et al., 2000; Vilcáez et al., 2013). The biogenic formation of CO_2-CH_4-H_2S-N_2 gases mixtures, which can happen in depleted oil reservoirs inhabited by fermentative, sulfate reducing, methanogenic, and denitrifying microbes is usually neglected in numerical simulation studies of MEOR. Including the biogenic formation of CO_2-CH_4-H_2S-N_2 gas mixtures is particularly important in simulations of CO_2-MEOR to determine how much, how fast, and where valuable hydrocarbon gases (CH_4), and souring gases (H_2S) will accumulate in the reservoir (Hitzman et al., 2004). This is because the dissolution of the injected and the biogenically formed gases can significantly change the chemical composition and pH of the aqueous phase, which in turn can have a large impact on the activity of the targeted microbial species. MEOR methods that rely on biogenic formation of N_2 gas to restore pressure in depleted oil reservoirs have been proposed before (Nuryadi et al., 2011). Accounting for the solubility of CO_2-CH_4-H_2S-N_2 gas mixtures in brine will also allow to determine to which degree the biogenically formed gases can restore pressure.

Two thermodynamic models are widely employed to predict the solubility of gas mixtures in water and brine. They differ in the thermodynamic properties used to represent the equilibrium condition of each compound in the gas and aqueous phase. In the first model, called fugacity-activity model, the equilibrium condition of each compound is expressed in terms of gas phase fugacity coefficients and liquid phase activity coefficients. In this case, the fugacity coefficients are calculated using an equation of state (EOS), whereas activity coefficients are calculated using an activity model. In the second method, called fugacity-fugacity method, the equilibrium condition of each compound in

the gas and aqueous phase is expressed in terms of gas and liquid fugacity coefficients. In this case, both fugacity coefficients are calculated using an EOS that needs iterative estimation of K-value at each time step and at each grid. Because the fugacity-activity model can be solved using a non-iterative method, this thermodynamic model is preferred over the fugacity-fugacity model that requires an iterative method for its solution.

Numerous non-iterative fugacity-activity models have been proposed to predict the solubility of pure CO_2 in water and brine (Duan and Sun, 2003; Duan et al., 2006; Hou et al., 2013; Mao et al., 2013; Spycher and Pruess, 2005; Spycher et al., 2003; Yan et al., 2011; Zhao et al., 2015). This is not the case of CO_2-H_2S-CH_4-N_2 gas mixtures, for which very few non-iterative fugacity-activity models have been proposed. Zirrahi et al. (2010) developed a non-iterative fugacity-activity model to predict the phase equilibrium behavior of acid gas mixtures (CO_2-H_2S-CH_4), and water and brine. However, the method is not accurate in predicting CO_2 and H_2S solubility in the aqueous phase. Most proposed models to predict the solubility of gas mixtures are iterative models that requires solving Rachford-Rice equation (Eq. A1). For instance, Ziabakhsh-Ganji and Kooi (2012) developed an iterative fugacity-activity model to predict CO_2-N_2-H_2S-CH_4-SO_2 gas mixtures solubility in brine. In this model, fugacity coefficients in the gas phase are calculated using Peng-Robinson (PR) EOS, whereas activity coefficients in the aqueous phase are reproduced based on Pitzer formalism and Henry's law. Similarly, Li et al. (2015) presented an iterative fugacity-fugacity model to calculate the mutual solubility of a gas mixtures (CO_2-SO_2-H_2S-CH_4-N_2) in brine for a wide range of pressures, temperatures, and salinity conditions. These two models use Rachford-Rice equation whose iterative solution requires information on the initial feed of each compound including H_2O (z_i in Eq. A1) in the mixture. The use of Rachford-Rice equation makes models inefficient for implementation in reactive transport simulation programs because additional iterations would be required for its solution. Li et al. (2014) compared the performance of the fugacity-fugacity and fugacity-activity models in predicting the

solubility of CO_2-H_2S-CH_4 gas mixtures in brine. They confirmed that fugacity-activity models are more time efficient than fugacity-fugacity models.

Typical temperatures of conventional sandstone and carbonate oil reservoirs at depths shorter than 3000 m are within 50 – 95 °C (Millikan, 1941). Taking into account that successful field scale MEOR operations have been reported for reservoirs of temperatures as high as 92.2 °C (Strappa et al.), and that methanogenic microbes are capable of growing at temperatures ranging from 0 °C to 110 °C (Goodchild et al., 2004; Huber et al., 1989), the temperature range considered relevant to CO_2-MEOR in this work is within 0 – 100 °C.

Possible concentration ranges for individual gases in CO_2-CH_4-N_2-H_2S gas mixtures in depleted oil reservoirs subjected to CO_2-MEOR are expected to be highly variable depending on the geological, geochemical and microbiological condition of the depleted oil reservoir. Under appropriate conditions, CO_2 is expected to have the highest concentration, followed by CH_4 and H_2S. Therefore, the proposed non-iterative method in this work will be tested using experimental data of gas mixtures containing highest concentrations of CO_2.

This work introduces a new non-iterative fugacity-activity model to predict the solubility of CO_2-CH_4,-H_2S-N_2 gas mixtures in water and brine that does not require solving Rachford-Rice equation. This model is simple enough to be readily incorporated into multiphase and multicomponent reactive transport programs that account for kinetic microbial reactions taking place in the aqueous phase. The proposed model is solved using the Predictive-Peng-Robinson 1978 (PPR78) EOS and Peng-Robinson (PR) EOS to calculate fugacity coefficients in the gas phase. The use of the PPR78 EOS in an iterative fugacity-fugacity model resulted in accurate predictions of CO_2-CH_4-N_2-H_2S gas mixture solubilities in brine (Privat and Jaubert, 2014). This is attributed to the property that binary interaction parameters in PPR78 EOS is a function of temperature and can be estimated for any mixture containing alkanes, aromatics and naphthalenes using critical temperatures, critical pressures, and

acentric factors of pure compounds (Vitu et al., 2008). This approach greatly reduces the need for experimental data. The PPR78 EOS has not been used before in a non-iterative fugacity-activity model to predict the solubility of CO_2-CH_4-H_2S-N_2 gas mixtures in brine at temperatures, pressures and composition conditions relevant to MEOR.

For simplicity and comparison purposes, in this work the proposed non-iterative model solved using PPR78 EOS will be referred to as model 1 whereas the same model solved using PR EOS will be referred to as model 2. In both models activity coefficients of aqueous species are calculated based on Henry's law and Pitzer correlation.

In the following sections, first the proposed non-iterative fugacity-activity model for predicting the solubility of CO_2-CH_4-H_2S-N_2 gas mixtures in brine will be introduced. Then, the performance of the proposed model is evaluated using experimental data of solubility of pure CO_2 and CO_2-H_2S-CH_4, CO_2-H_2S, CO_2-CH_4, and CO_2-N_2 gas mixtures in water and brine. The performance of the proposed models will also be evaluated in comparison with the performance of an iterative fugacity-activity model that uses Rachford-Rice equation. This later model will be referred to as model 3.

2.3. Thermodynamic model

In a system with gas and liquid phases at equilibrium, the fugacity of each compound in the gas phase (f_i^g) is equal to the fugacity of that compound in the liquid phase (f_i^l):

$$f_i^g = f_i^l \tag{1}$$

For the gas phase, f_i^g can be expressed as:

$$f_i^g = P\phi_i y_i \tag{2}$$

where P is the total pressure in the system, and ϕ_i and y_i are the fugacity coefficient and molar fraction of each compound in the gas phase, respectively. For the liquid phase (because of the relatively low solubility of CO_2 ,H_2S, CH_4 and N_2 gases and its nonionic character in the aqueous phase and considering the effect of salinity in the solubility of gases) f_i^l can be expressed as (Spycher and Pruess, 2005):

$$f_i^l = h_i \gamma_i x_i \tag{3}$$

where h_i is Henry's constant, γ_i is the activity coefficient, and x_i is the molar fraction of each compound in the liquid phase. Equating fugacities gives:

$$h_i \gamma_i x_i = P \phi_i y_i \tag{4}$$

which can be rearranged to obtain K_i as follows:

$$K_i = \frac{y_i}{x_i} = \frac{h_i \gamma_i}{P \phi_i} \tag{5}$$

where K_i is the phase equilibrium constant of compound i in Rachford-Rice equation. In the proposed model, except for H_2O, K_i values of CO_2, H_2S, CH_4 and N_2 in the system are calculated using Eq. (5). K_i for H_2O is calculated using the relation proposed by Spycher et al. (2003):

$$K_{H2O} = \frac{y_{H2O}}{x_{H2O}} = \frac{K_{H2O}^0}{f_{H2O} P} \exp\left[\frac{(P-1)\times 18.18}{RT}\right] \tag{6}$$

where K_{H2O}^0 is the equilibrium constant of H_2O at the reference pressure of 1 bar, R is gas constant, and T is temperature in Kelvin. The approach of Spycher et al. (2003) is used to calculate K_{H2O}^0:

$$\log\left(K^{0}_{H2O}\right) = -2.209 + 3.097\times10^{-2}\theta - 1.098\times10^{-4}\theta^{2} + 2.048\times10^{-7}\theta^{3} \quad (7)$$

where θ is temperature in Celsius.

In the proposed model, the molar fraction of H_2O in the gas phase (y_{H2O}) is calculated using the following equation:

$$y_{H2O} = \frac{1 - \sum \frac{y_i}{K_i}}{\frac{1}{K_{H2O}} - \sum \frac{y_i}{K_i}} \quad (8)$$

This equation is similar to that proposed by Spycher et al. (2003) to predict the solubility of pure CO_2 in brine:

$$y_{H2O} = \frac{1 - \frac{1}{K_{CO2}}}{\frac{1}{K_{H2O}} - \frac{1}{K_{CO2}}} \quad (9)$$

Note that the application of Eq. (8) to a pure CO_2-brine system produces Eq. 9 of Spycher et al. (2003). In the proposed equation in this work (Eq. (8)), y_i is the initial molar fraction of CO_2, H_2S, CH_4 and N_2 in the gas phase. The calculated y_{H2O} (Eq. (8)) is used to correct the molar fractions of CO_2, H_2S, CH_4 and N_2 in the gas phase using the following normalization equation:

$$y_i^n = \frac{y_i}{1 + y_{H_2O}} \quad (10)$$

where y_i^n is the normalized molar fractions of CO_2, H_2S, CH_4, and N_2 in the gas phase. This simplification has not been used before and might result in loss of accuracy due to the lack of inclusion

of the binary interactions parameters for H_2O-CO_2, H_2O-H_2S, H_2O-CH_4 and H_2O-N_2. However, because temperature and pressure conditions relevant to MEOR do not result in high H_2O solubility in the gas phase, it is safe to assume that the omission of the effect of H_2O in the calculation of gas fugacity coefficients will not result in a significant loss of accuracy in predicting the solubility of CO_2-H_2S-CH_4-N_2 gas mixtures in brine. Following this procedure, the equilibrium molar fractions of all compounds including H_2O in brine can be directly calculated from the equation:

$$x_i = \frac{y_i^n}{K_i} \tag{11}$$

where x_i is the molar fraction of dissolved compounds in the aqueous phase, and y_i^n calculated from Eq. (10) is the molar fraction of each compound in the existing or injected mixture of gases. Activity coefficients of dissolved gases in the aqueous phase are calculated following the approach of Ziabakhsh-Ganji and Kooi (2012) who proposed to use the correlation of Pitzer (1973):

$$\ln\gamma_i = \sum_c 2m_c\lambda_{i\text{-}Na} + \sum_a 2m_a\lambda_{i\text{-}Cl} + \sum_c\sum_a 2m_a m_c\xi_{i\text{-}Na\text{-}Cl} \tag{12}$$

where m_c and m_a are anion and cation molalities, respectively, $\lambda_{i\text{-}Na}$ and $\xi_{i\text{-}Na\text{-}Cl}$ are second and third order interaction parameters that depend on pressure and temperature, $\lambda_{i\text{-}Cl}$ is assumed to equal zero in most previous studies (Duan and Sun, 2003; Li et al., 2014; Ziabakhsh-Ganji and Kooi, 2012), and $\lambda_{i\text{-}Na}$ and $\xi_{i\text{-}Na\text{-}Cl}$ are calculated using the following equation:

$$Par(T,P) = c_1 + c_2T + \frac{c_3}{T} + c_4P + \frac{c_5}{P} + c_6\frac{P}{T} + c_7\frac{T}{P^2} + \frac{c_8P}{630-T} + c_9T\ln(P) + c_{10}\frac{P}{T^2} \tag{13}$$

where Par (T, P) is either $\lambda_{i\text{-}Na}$ or $\xi_{i\text{-}Na\text{-}Cl}$, T is temperature in Kelvin, and P is pressure in bar. Values of c_1 through c_{10} for $\lambda_{i\text{-}Na}$ and or $\xi_{i\text{-}Na\text{-}Cl}$ are presented in Table 2.1 and 2.2, respectively.

Table 2.1. Second order interaction parameters (Ziabakhsh-Ganji and Kooi, 2012)

Constant	$\lambda_{CO2\text{-}Na}$	$\lambda_{H2S\text{-}Na}$	$\lambda_{N2\text{-}Na}$	$\lambda_{CH4\text{-}Na}$
c_1	−0.0652869	1.03658689	−2.0939363	−5.7066455E−01
c_2	1.6790636E−04	−1.1784797E−03	3.1445269E−03	7.2997588E−04
c_3	40.838951	−1.7754826E+02	3.91E+02	1.52E+02
c_4	0	−4.5313285E−04	−2.9973977E−07	3.1927112E−05
c_5	0	0	0	0
c_6	−3.9266518E−02	0	−1.5918098E−05	−1.6426510E−05
c_7	0	0	0	0
c_8	2.1157167E−02	0	0	0
c_9	6.5486487E−06	0	0	0
c_{10}	0	0.47751650E+02	0	0

Table 2.2. Third order interaction parameters (Ziabakhsh-Ganji and Kooi, 2012)

Constant	$\xi_{CO2\text{-}Na\text{-}Cl}$	$\xi_{H2S\text{-}Na\text{-}Cl}$	$\xi_{N2\text{-}Na\text{-}Cl}$	$\xi_{CH4\text{-}Na\text{-}Cl}$
c_1	−1.144624E−02	−0.010274152	−6.3981858E−03	−2.9990084E−03
c_2	2.8274958E−05	0	0	0
c_3	0	0	0	0
c_4	0	0	0	0
c_5	0	0	0	0
c_6	1.3980876E−02	0	0	0
c_7	0	0	0	0
c_8	−1.4349005E−02	0	0	0
c_9	0	0	0	0
c_{10}	0	0	0	0

Henry's constant (h_i) of dissolved gases in the aqueous phase are calculated using the correlation of Akinfiev and Diamond (2003) which was subsequently employed by Ziabakhsh-Ganji and Kooi (2012). It is noteworthy that this correlation is valid for infinite dilution as expressed by:

$$\ln h_i = (1-\eta)\ln f^0_{H2O} + \eta \ln\left(\frac{RT}{Mw_{H2O}}\rho^0_{H2O}\right) + 2\rho^0_{H2O}\Delta B \tag{14}$$

where T is temperature in Kelvin, η is a constant for each gas dissolved in water, Mw_{H2O} is molecular mass of water, $f_{H2O}{}^0$ is the fugacity, and $\rho_{H2O}{}^0$ is the density of pure water which are calculated using Fine and Millero (1973) correlation (Eqs. (A4 – A8)), and ΔB represents the difference in interaction

between dissimilar molecules and that between identical solvent molecules. ΔB is determined from the following equation:

$$\Delta B=\tau+\beta\left(\frac{10^3}{T}\right)^{0.5} \tag{15}$$

where τ (cm^3g^{-1}) and β ($cm^3K^{0.5}g^{-1}$) are adjustable parameters. The values of η, τ and β are listed in Table 2.3.

Table 2.3. Parameters for Henry's constant (Ziabakhsh-Ganji and Kooi, 2012)

Gas	**H**	**τ**	**β**
CO_2	−0.114535	−5.279063	6.187967
H_2S	0.77357854	0.270494	0.275434
CH_4	−0.092248	−5.779280	7.26273
N_2	−0.008194	−5.175337	6.906469

Fugacity coefficients (ϕ_i) in both PPR78 EOS and PR EOS are calculated from the following fugacity equation:

$$\ln\phi_i=\frac{b_i}{b}(Z-1)-\ln(Z-B)-\frac{A}{B(\delta_2-\delta_1)}\left(\frac{\left(2\sum_{j=1}^{N}y_j a_{ij}\right)}{a}-\frac{b_i}{b}\right)\ln\left(\frac{Z+\delta_2 B}{Z+\delta_1 B}\right) \tag{16}$$

where δ_1 is $1+\sqrt{2}$, δ_2 is $1-\sqrt{2}$. The a_i, b_i and m_i parameters of pure components in the mixture are calculated from:

$$\begin{cases} a_i(T)=0.457236\dfrac{R^2T_{c,i}^2}{P_{c,i}}\left[1+m_i\left(1-\sqrt{\dfrac{T}{T_{c,i}}}\right)\right]^2 \\ b_i=0.077796\dfrac{RT_{c,i}}{P_{c,i}} \\ m_i=0.37464+1.54226\omega_i-0.26992\omega_i^2 \end{cases} \tag{17}$$

here P_c, T_c and ω_i are the critical pressure, critical temperature and acentric factor of pure compounds, respectively.

The *a* and b parameters of the mixture gas are obtained by applying classic mixing rules widely employed in oil reservoir simulation software:

$$\begin{cases} a=\sum_{i=1}^{N}\sum_{j=1}^{N}y_i y_j a_{ij} \\ b=\sum_{i=1}^{N}y_i b_i \\ a_{ij}=\sqrt{a_i a_j}\left(1-k_{ij}\right) \end{cases} \tag{18}$$

where N denotes the number of compounds in the mixture, and k_{ij} the binary interaction parameter between binary pairs in the mixture. The difference between PPR78 EOS and PR EOS is in the way the binary interaction parameters (k_{ij}) between the binary pairs i and j is calculated. Binary interaction parameters are the single most important parameter in both PPR78 EOS and PR EOS that affects phase equilibrium predictions of multicomponent systems.

In PPR78 EOS, k_{ij} is temperature dependent through the application of the following group contribution expression:

$$k_{ij}(T)=\frac{A_{ij}\left(\frac{298.15}{T}\right)^{\left(\frac{B_{ij}}{A_{ij}}-1\right)}-\left(\frac{\sqrt{a_i(T)}}{b_i}-\frac{\sqrt{a_j(T)}}{b_j}\right)^2}{2\left(\frac{\sqrt{a_i(T).a_j(T)}}{b_i.b_i}\right)} \quad (19)$$

where T is temperature in Kelvin. A_{ij} and B_{ij} are group interaction parameters. Their estimated values for mixed CO_2, CH_4, H_2S, N_2 and H_2O gases are listed in Table 2.4.

Table 2.4. Group interaction parameters for PPR78 EOS in bar ($A_{ij}=A_{ji}$, and $B_{ij}=B_{ji}$) (Privat and Jaubert, 2014)

Gas	**CO_2**	**H_2S**	**N_2**	**CH_4**	**H_2O**
CO_2	0	-	-	-	-
H_2S	A=1349	0	-	-	-
	B=2014				
N_2	A=984.2	A=3195	0	-	-
	B=2214	B=5501			
CH_4	A=1373	A=1812	A=379	0	-
	B=1942	B=2889	B=372		
H_2O	A=5593	A=6039	A=25740	A=22650	0
	B=2779	B=5991	B=54900	B=47220	

In PR EOS, k_{ij} are constant values determined directly by minimizing the difference between predicted and experimental data. k_{ij} values for mixed CO_2, CH_4, H_2S, N_2 and H_2O gases are listed in Table 2.5.

Table 2.5. Binary interaction parameters for PR EOS ($k_{ij}=k_{ji}$)

Gas	**CO_2**	**H_2S**	**N_2**	**CH_4**	**H_2O**
CO_2	0	-	-	-	-
H_2S	0.099[a]	0		-	-
N_2	-0.007[a]	0	0	-	-
CH_4	0.1[a]	0.084[b]	0	0	-
H_2O	0.19014[c]	0.105[c]	0.32547[c]	0.47893[c]	0

[a] extracted from Li and Yan (2009)
[b] extracted from Kontogeorgis et al. (2006)

[c] extracted from Ziabakhsh-Ganji and Kooi (2012)

Finally, Z in Eq. (16) is the compressibility factor calculated from the following cubic equation:

$$Z^3-(1-B)Z^2+\left(A-2B-3B^2\right)Z-\left(AB-B^2-B^3\right)=0 \tag{20}$$

which is derived from the general form of Peng-Robinson EOS for mixtures:

$$P(T,v)=\frac{RT}{v-b_i}-\frac{a_i(T)}{v(v+b_i)+b_i(v-b_i)} \tag{21}$$

where the dimensionless parameters A and B are defined as:

$$A=\frac{aP}{(RT)^2} \tag{22}$$

$$B=\frac{bP}{RT} \tag{23}$$

Z can be can be easily determined from Eq. (20) either analytically or numerically. It may have three roots, in which case the intermediate root is ignored and the one that gives the lowest Gibbs energy difference is selected as the correct root. The Gibbs energy difference at two roots Z_g and Z_l is determined from (Danesh, 1998):

$$\frac{\left(G_g - G_l\right)}{RT} = \left(Z_g - Z_l + \ln\left(\frac{Z_l - B}{Z_g - B}\right) - \frac{A}{B\left(\delta - \delta_1\right)} \ln\left[\left(\frac{Z_l + \delta_1 B}{Z_l + \delta_2 B}\right)\left(\frac{Z_g + \delta_2 B}{Z_g + \delta_1 B}\right)\right]\right) \quad (24)$$

where Z_g and Z_l are the maximum and minimum roots, respectively. If Gibbs energy difference is positive, Z_l is selected, otherwise, Z_g is considered the correct root that should be used in Eq. (16).

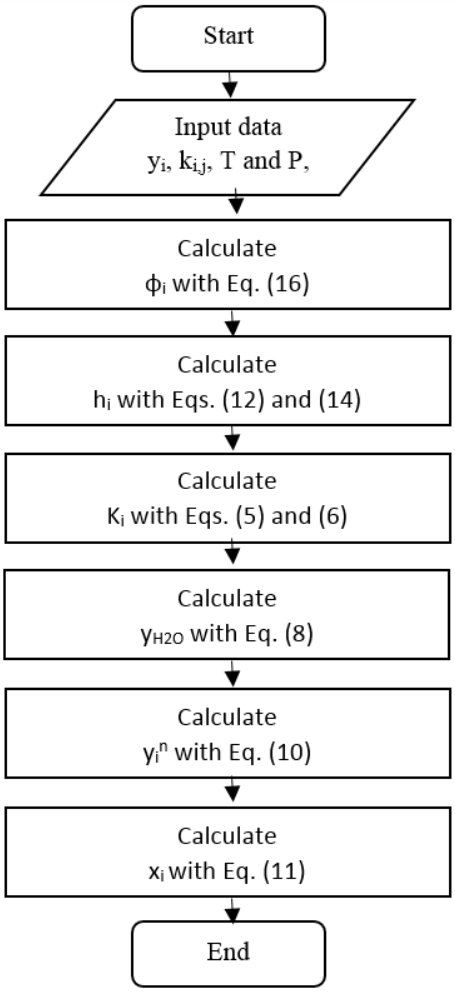

Fig. 2.1. Flow chart of calculation procedure

The calculation of gas fugacity coefficients using PPR78 EOS and PR EOS is accomplished assuming that the mole fraction of H_2O in the gas phase (y_{H2O}) is zero. This assumption yields a non-iterative procedure which is time efficient compared with iterative procedures that relay on Rachford-

Rice equation (Spycher and Pruess, 2005; Spycher et al., 2003). The proposed calculation procedure is outlined in Fig. 2.1.

2.4. Results and discussion

Experimental data used to test the performance of models 1 and 2 correspond to temperatures from 35 to 120°C and pressures from 30 and 300 bar. These temperature and pressure ranges correspond to oil reservoir conditions where microbial activity can be used to enhance the recovery of oil.

Deviations between calculated and measured values are expressed in terms of the absolute relative deviation percentage (ARD%):

$$\text{ARD\%}=\left(\frac{\left|x_{exp}-x_{cal}\right|}{x_{exp}}\right)\times 100 \tag{25}$$

and in terms of the average absolute relative deviation percentage (AARD%):

$$\text{AARD\%}=\frac{1}{N^{exp}}\sum\left(\frac{\left|x_{exp}-x_{cal}\right|}{x_{exp}}\right)\times 100 \tag{26}$$

where x_{exp} and x_{cal} are the experimental and calculated molar fractions of the gas, respectively, and N^{exp} is the number of data points.

Pure CO_2

Table 2.A2 contains ARD% between experimental and predicted solubility values of CO_2 in water. Experimental solubility values were collected from 29 references and correspond to CO_2-poor gas phase in equilibrium with pure water. The AARD% between experimental and predicted solubility values for models 1 and 2 are 4.08 and 3.98, respectively. These were calculated using 306 data points. These values indicate that both models 1 and 2 achieve good predictions for the solubility of a CO_2-poor gas phase in water at temperature and pressure ranges relevant to MEOR.

Table 2.A3 contains ARD% between experimental and predicted solubility values of H_2O in CO_2-rich gas phase. Experimental data were collected from 12 references and correspond to pure CO_2 gas phase in equilibrium with pure water. It is found that model 2 is capable of reproducing experimental data of H_2O solubility in pure CO_2 with good precision as indicated by the AARD% of 6.14. Model 1 was successful in the regeneration of experimental data of H_2O solubility in pure CO_2 for pressures lower than 50 bar. However, this model overestimated H_2O solubility in the gas phase for higher pressures. The AARD% of H_2O solubility in the gas phase for model 1 is 137.09.

Table 2.A4 contains ARD% between experimental and predicted solubility values of CO_2 in brine with NaCl molality of 0.0172-6 m. Predicted solubility values with models 1 and 2 are in good agreement with experimental data for temperature and pressure conditions relevant to MEOR. For instance, for a NaCl molality of 0.0172, the AARD% for models 1 and 2 are 4.47 and 5.56, respectively, and for a higher NaCl molality of 0.172 the AARD% for models 1 and 2 are 3.86 and 4.49, respectively. The AARD% for both models increases with increasing temperature. For instance, for a NaCl molality of 0.0172, the ARD% between experimental and predicted solubility values at 60°C and 80°C for model 1 increases from 0.42 to 1.45, whereas for model 2 it increases from 6.93 and 8.0. At higher NaCl molalities, ARD% between experimental and predicted solubility values generally decreases with increasing temperature.

Models 1 and 2 have been proven to have acceptable accuracy in reproducing experimental solubility values of CO_2 in water and brine. Subsequently, this work tests the validity of the proposed model in predicting the solubility of CO_2-CH_4-H_2S-N_2 gas mixtures in water and brine. For this, the solubility predictions obtained with models 1 and 2 are compared against experimental data on the solubility CO_2-H_2S-CH_4, CO_2-H_2S, CO_2-CH_4, and CO_2-N_2 gas mixtures in water and brine. It is also compared with solubility predictions obtained with the model proposed by Ziabakhsh-Ganji and Kooi (2012) which is referred to as model 3 in this work. Model 3 uses the Rachford-Rice equation that requires an iterative approach to be solved.

Table 2.6. Absolute Average Relative Deviation (AARD %) between experimental and calculated solubilities in the aqueous phase

Reference	**Component**	**AARD%**		
		Model 2	Model 1	Model 3
Huang et al. (1985)	CO_2	4.17	3.94	4.18
	H_2S	26.60	27.89	24.04
	CH_4	11.35	10.80	10.12
	H_2O	15.54	57.71	6.77
Dhima et al. (1999)	CO_2	6.28	7.50	-
	CH_4	4.70	4.49	-
Al Ghafri et al. (2014)	CO_2	6.48	6.40	-
	CH_4	34.79	34.81	-
	H_2O	33.06	32.72	-
Foltran et al. (2015)	H_2O	11.40	161.14	-
Savary et al. (2012)	H_2S	6.36	6.50	-

CO_2-CH_4-H_2S

Published experimental data of CO_2-CH_4-H_2S-N_2 gas mixtures solubility in brine is scarce. Hence, experimental data of CO_2-CH_4-H_2S gas mixtures solubility in water reported by Huang et al. (1985) is used to test models 1, 2 and 3. This experimental data includes information on the initial feed of each compound, including H_2O in the mixture, which is needed to solve Rachford-Rice equation used by model 3. Fig. 2.2 compares experimental and predicted solubility values of CO_2, H_2S and CH_4 in water at 37.8-107°C and 40-180 bar. The AARD% between experimental and predicted solubility values for models 1, 2 and 3 are summarized in Table 2.6. All three models predicted similar solubility values for CO_2, H_2S and CH_4 in water, confirming the feasibility of using a non-iterative approach instead of an iterative approach to predict the solubility of gas mixtures in water at temperature and pressure conditions relevant to MEOR. Because it uses iterative approach, model 3 gives slightly better results than models 1 and 2, which use a non-iterative approach. However, the difference is insignificant given the exhausting computational requirement of model 3.

A comparison between the performance of model 1 and 2 shows that model 1 better predicts the solubility of gas mixtures in water than model 2. The AARD%s of CH_4 and H_2S in water for model 1 are 9.45 and 15.79 at 37.8 °C, and 12.15 and 39.98 at 107.2 °C, respectively. Differently, the AARD% of CH_4 and H_2S in water with model 2 are 10.04 and 13.36 at 37.8 °C, and 12.67 and 39.84 at 107.2 °C, respectively. Both models underestimated the solubility of CH_4 and overestimated the solubility of H_2S in pure water. Comparisons show that as temperature increases, the accuracy of both models in predicting CH_4 and H_2S solubility in pure water decreases.

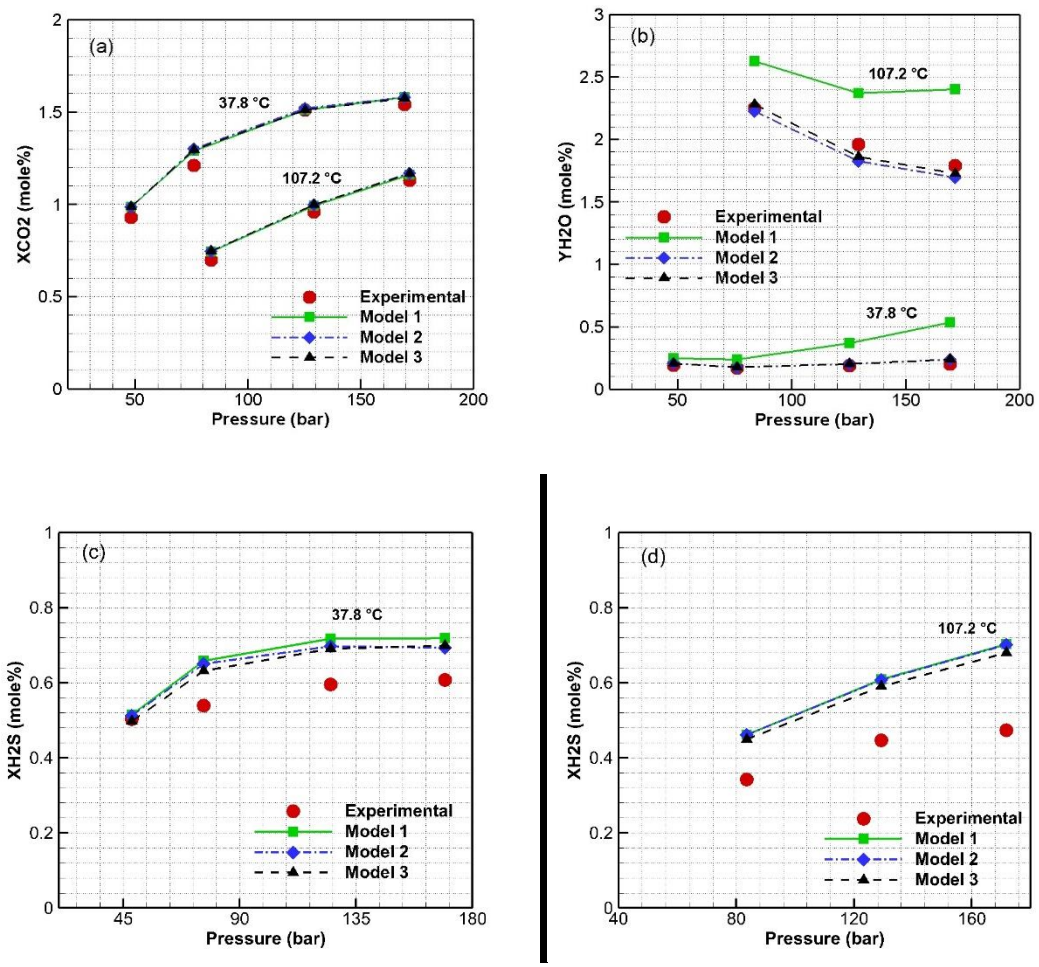

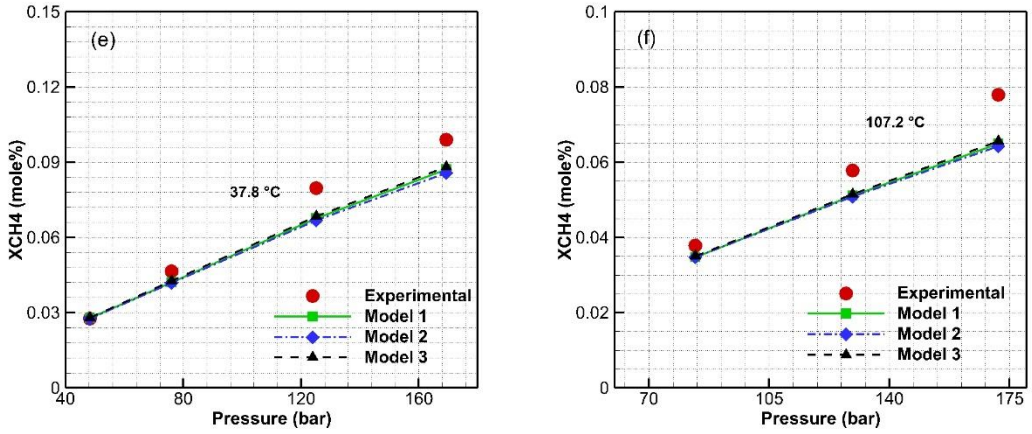

Fig. 2.2. Comparison between experimental (Huang et al., 1985) and predicted CO_2-H_2S-CH_4 gas mixture solubility in water. (a) CO_2 solubility in the aqueous phase at 37.8°C and 107.2°C; (b) H_2O solubility in the gas phase at 37.8°C and 107.2°C; (c) H_2S solubility in the aqueous phase at 37.8°C; (d) H_2S solubility in the aqueous phase at 107.2 °C; (e) CH_4 solubility in aqueous phase at 37.8 °C; (f) CH_4 solubility in aqueous phase at 107.2 °C.

CO_2-CH_4

The experimental solubility values of CO_2-CH_4 gas mixtures in water at 71°C and 100-1000 bar reported by Dhima et al. (1999), and at 50-100°C and 19-180 bar reported by Al Ghafri et al. (2014) are compared with solubility values of CO_2-CH_4 gas mixtures predicted with models 1 and 2.

Figs. 2.3a and 2.3b compare experimental and predicted solubility values of CO_2 and CH_4 in water at 71°C and 100-1000 bar. Within this high pressure range, predicted solubility values obtained with models 1 and 2 are almost identical and showed high accuracy. Model 1 predicted the solubility of CO_2 and CH_4 in water with an AARD% of 7.50 and 4.49, respectively, and model 2 predicted the solubility of CO_2 and CH_4 in water with an AARD% of 6.28 and 4.70, respectively.

Figs. 2.3c-f compare experimental and predicted solubility values of CO_2-CH_4 gas mixtures in water at 50-100°C and 19-180 bar. A comparison between experimental and predicted solubility values of CO_2 in water obtained with models 1 and 2 within this low pressure range, shows a high accuracy of

both models to predict the solubility of CO_2 in water. Models 1 and 2 predicted CO_2 solubility in water with an AARD% of 6.19 and 6.43, respectively. However, the accuracy of both models to predict the solubility of CH_4 in water decreased for this low pressure range. Both model 1 and 2 predicted CH_4 solubility in water with an AARD% of 29.3. The AARD% for H_2O solubility in the gas phase for models 1 and 2 within this low pressure range are 42.49 and 32.64, respectively.

Because pressure conditions in depleted oil reservoirs fall within the high pressure range (up to 1000 bar), it is expected that the proposed model will be suitable to predict the solubility of CO_2-CH_4-H_2S-N_2 gas mixtures in brine in reactive transport simulations of MEOR.

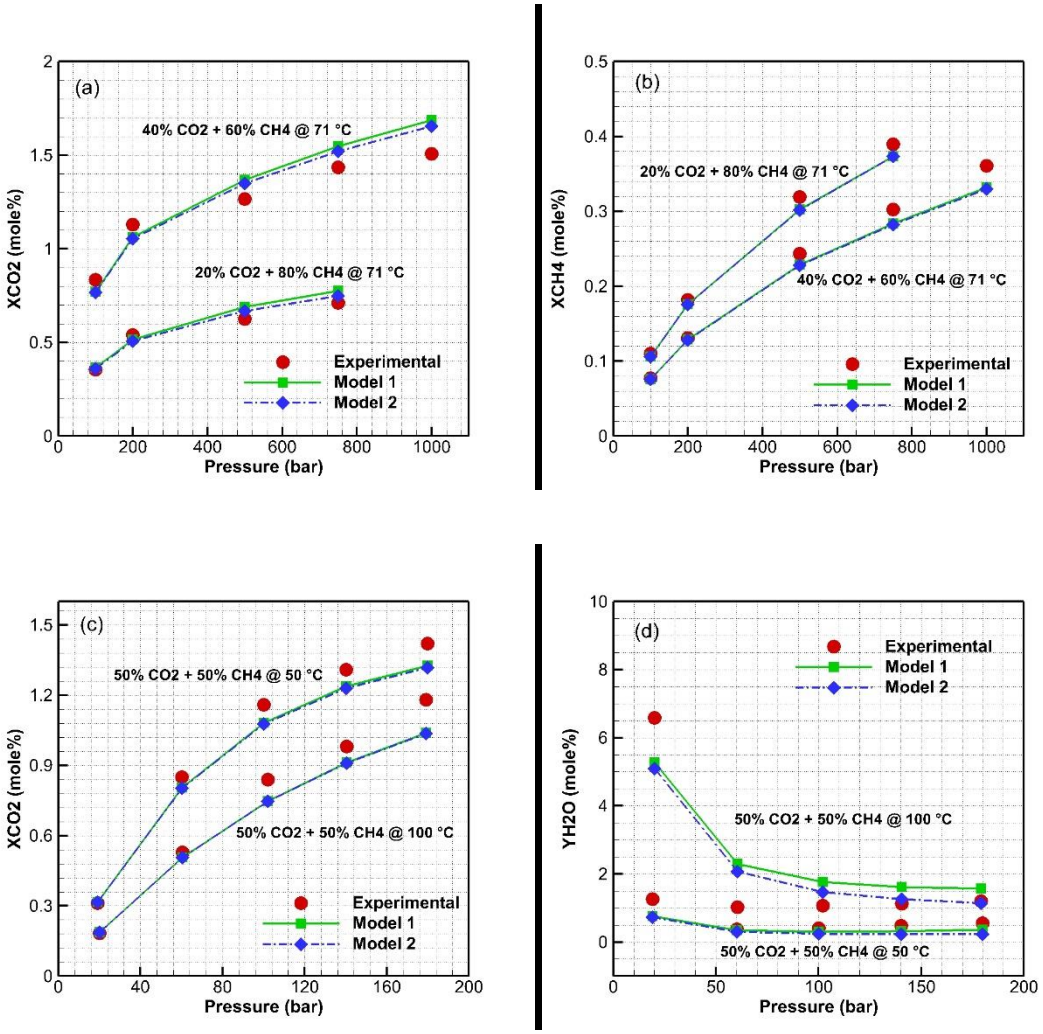

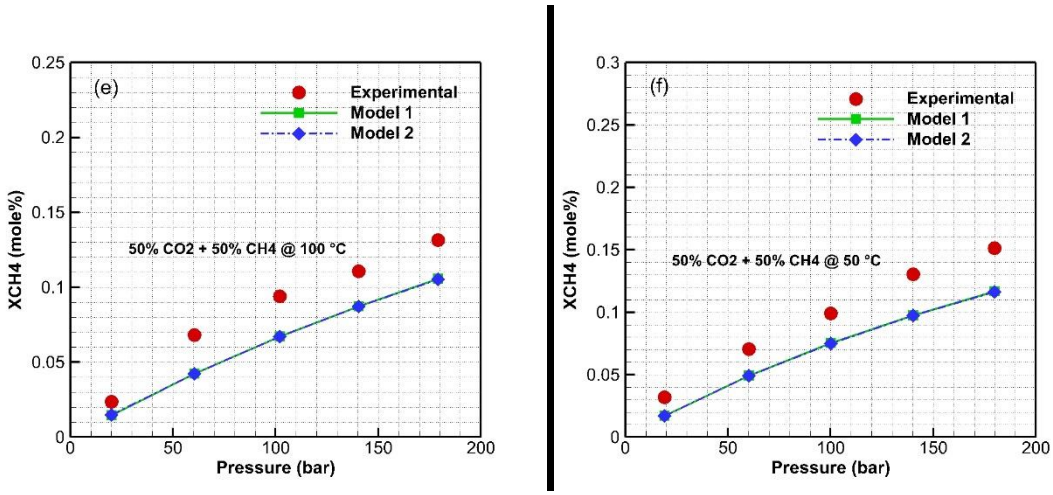

Fig. 2.3. Comparison between experimental and predicted CO_2-CH_4 gas mixtures solubility in water. (a) and (c) CO_2 solubility in aqueous phase; (d) H_2O Solubility in the gas phase; (b), (e) and (f) CH_4 solubility in water. Experimental data for (a) and (b) are from Dhima et al. (1999), other experimental data are from Al Ghafri et al. (2014).

CO_2-N_2

Experimental data of H_2O solubility in CO_2-N_2 gas mixtures at 41°C and 80-190 bar was reported by Foltran et al. (2015). Fig. 2.4 compares experimental and predicted H_2O solubility values at two different CO_2-N_2 gas mixture compositions. Model 2 reproduced H_2O solubility data with an AARD% between the calculated and experimental solubilities of 11.40. Model 1 overestimated the solubility of H_2O in the gas phase. These results confirm that the proposed model solved using PPR78 EOS to calculate fugacity coefficients in the gas phase (model 1) is not suitable to predict the solubility of H_2O in CO_2-CH_4-H_2S-N_2 gas mixtures.

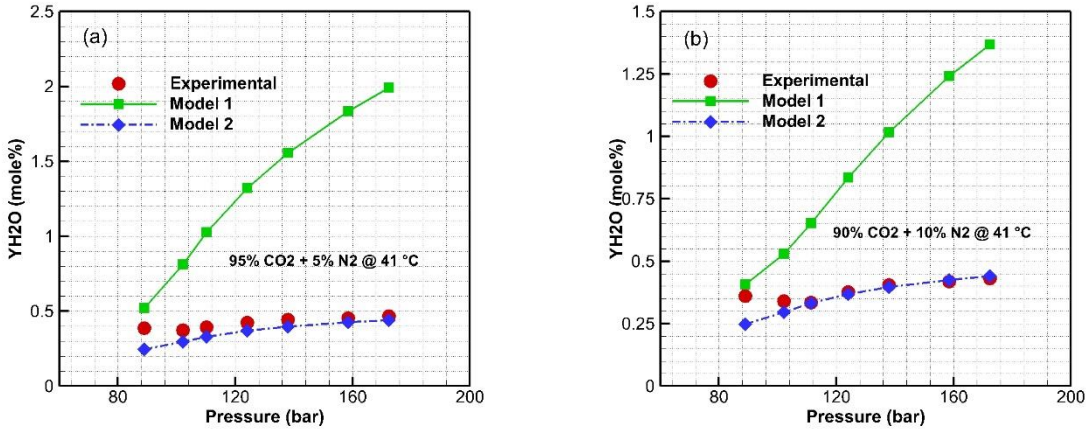

Fig. 2.4. Comparison between experimental (Foltran et al., 2015) and predicted H_2O solubility in a CO_2-N_2 gas mixture phase.

CO_2-H_2S

Experimental solubility values of CO_2-H_2S gas mixtures in water at 120°C, 86-350 bar, were reported by Savary et al. (2012). These experimental solubility values are compared with solubility values predicted with models 1 and 2 (Fig. 2.5). A very good agreement between experimental and predicted solubility values of CO_2 in water were obtained with both models. The AARD% between experimental and calculated solubility values for both models is 6.4% (Table 2.6). Both models predicted the solubility of H_2S in water with an AARD% of around 30. This indicates the lack of accuracy of both models to predict the solubility of H_2S in water at high H_2S concentration conditions.

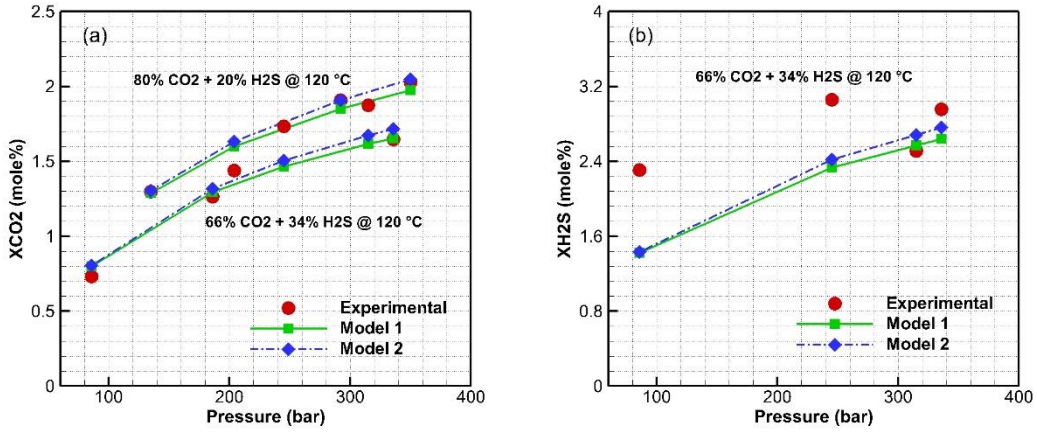

Fig. 2.5. Comparison between experimental (Savary et al., 2012) and predicted CO_2-H_2S gas mixtures solubility in water. (a) CO_2 solubility in aqueous phase; (b) H_2S solubility in aqueous phase

2.5. Conclusions

A new non-iterative fugacity-activity thermodynamic model to predict the solubility of CO_2-CH_4-H_2S-N_2 gas mixtures in water and brine has been proposed. Gas phase fugacity coefficients (ϕ_i) in the proposed model were calculated using PPR78 EOS (model 1) and PR EOS (model 2). Comparisons between experimental and predicted solubility values at temperature and pressure conditions relevant to MEOR have shown that:

- The proposed model predicts the solubility of pure CO_2 in water and brine of salinity up to 2.5 m NaCl. Up to this salinity level, predictions of CO_2 solubility with the proposed model are accurate using either PPR78 EOS or PR EOS to calculate ϕ_i. The proposed model using PR EOS to calculate ϕ_i accurately predicts H_2O solubility in CO_2-rich phases. However, the proposed model using PPR78 EOS to calculate ϕ_i leads to inaccurate predictions of H_2O solubility in CO_2-rich phases. Inaccuracy increases with increasing temperature, pressure and salinity.
- The proposed model's predictions of CO_2-CH_4-H_2S gas mixtures solubility in water are good and are almost identical using either PPR78 EOS or PR EOS to calculate ϕ_i. However, similar to the

predictions of pure CO_2 solubility in water, the proposed model using PPR78 EOS to calculate ϕ_i (model 1) overestimates H_2O solubility in CO_2-CH_4-H_2S gas mixtures.

- Comparisons of the proposed model's predictions of CO_2-CH_4-H_2S gas mixtures solubility in water against predictions obtained with an iterative fugacity-activity model have shown that the proposed non-iterative model using PR EOS to calculate ϕ_i can be used as substitute for iterative fugacity-activity models that relies on the solution of Rachford-Rice equation.
- PR EOS that uses calibrated constant binary interaction parameters to calculate ϕ_i in the proposed model leads to better predictions of CO_2-CH_4-H_2S, CO_2-CH_4, CO_2-N_2, and CO_2-H_2S gas mixtures solubility in water than PPR78 EOS that used temperature and composition dependent binary interaction parameters to calculate ϕ_i. As such, it is recommended that the proposed model be used with ϕ_i calculated using PR EOS.
- Most experimental data used in this work are for pure gas and gas mixtures solubility in water. Nonetheless, it is expected that the proposed model will be equally suitable in reproducing experimental data of CO_2-CH_4-H_2S-N_2 gas mixtures solubility in brine. This is because the activity correlations used in the proposed model include the effect of salinity, and binary interaction parameters of PR EOS can always be recalibrated using new experimental data if necessary.

The injected and biogenically formed gases in depleted oil reservoirs can dissolve in both the aqueous and oil phases. The partitioning of gases between the aqueous and oil phases can be included in a simulation program by including one additional experimental or empirical correlation describing the solubility of each individual gas in the oil phase. However, this correlation would need to be solved simultaneously with the thermodynamic model describing the solubility of gases in the aqueous phase.

2.6. Appendix A

Flash calculations using PR EOS are performed to predict gas-liquid equilibrium conditions. These calculations relays on the solution of Rachford-Rice equation (Eq. A1) where the total mole fraction (z_i) of each compound must be known beforehand:

$$\sum_{i=1}^{N} \frac{z_i(K_i - 1)}{1+(K_i - 1)n^V} = 0 \tag{A1}$$

The solution of Rachford-Rice equation yields the mole fraction of the gas phase (n^V) in equilibrium with the liquid phase. Equilibrium constant of compound i in Rachford-Rice equation are calculated from Eqs. (5) and (6) at given temperature and pressure conditions. Then, the mole fraction of each compound in the liquid and gas phases is determined using following equations:

$$x_i = \frac{z_i}{1+(K_i - 1)n^V} \tag{A2}$$

$$y_i = \frac{K_i z_i}{1+(K_i - 1)n^V} \tag{A3}$$

In the proposed model, Fine and Millero (1973) correlation is used to determine the fugacity and density of pure water:

$$\frac{1}{\rho} = V^0 - \frac{V^0 P}{B + A_1 P + A_2 P^2} \tag{A4}$$

$$V^0 = \frac{1+18.1597\times10^{-3}\theta}{0.9998+18.2249\times10^{-3}\theta-7.9222\times10^{-6}\theta^2-55.4485\times10^{-9}\theta^3+149.7562\times10^{-12}\theta^4-393.2952\times10^{-15}\theta^5} \tag{A5}$$

$$B = 19654.32 + 147.037\theta - 2.2155\theta^2 + 1.0478\times10^{-2}\theta^3 - 2.2789\times10^{-5}\theta^4 \tag{A6}$$

$$A_1 = 3.2891 - 2.391\times10^{-3}\theta + 2.8446\times10^{-4}\theta^2 - 2.82\times10^{-6}\theta^3 + 8.477\times10^{-9}\theta^4 \quad \text{(A7)}$$

$$A_2 = 6.245\times10^{-5} - 3.913\times10^{-6}\theta - 3.499\times10^{-8}\theta^2 + 7.942\times10^{-10}\theta^3 - 3.299\times10^{-12}\theta^4 \quad \text{(A8)}$$

where θ is temperature in Celsius, and ρ is the density of pure water in cm^3g^{-1}. The fugacity of H_2O is calculated using the approach proposed by King et al. (1992):

$$f^0_{H_2O} = P_s \exp\left[\frac{18.0152\times(P - P_s)}{\rho RT}\right] \quad \text{(A9)}$$

where P_s is obtained using the correlation of Shibue (2003):

$$\ln\left(\frac{P_s}{P_c}\right) = \frac{T_c}{T}\left[a_1\left(1-\frac{T}{T_c}\right) + a_2\left(1-\frac{T}{T_c}\right)^{1.5} + a_3\left(1-\frac{T}{T_c}\right)^{3} + a_4\left(1-\frac{T}{T_c}\right)^{3.5} + a_5\left(1-\frac{T}{T_c}\right)^{4} + a_6\left(1-\frac{T}{T_c}\right)^{7.5}\right]$$

(A10)

Values of a_1 to a_6 is reported in Table 2.A1.

Table 2.A1. Constants for Equation A10

Constant	a_1	a_2	a_3	a_4	a_5	a_6
	−7.8595178	1.8440825	−11.786649	22.680741	−15.9618719	1.8012250

Table 2.A2. Experimental data of CO_2 solubility in pure water and calculated ARD% values

Temp °C	**Pressure (bar)**	**X_{CO2} Mole%**	**ARD% Model-2**	**ARD% Model-1**	**Reference**
35.00	50.70	1.754	0.582	0.498	Wiebe and Gaddy (1940)
35.00	76.00	2.189	0.511	0.766	Wiebe and Gaddy (1940)
35.00	101.30	2.288	0.072	1.352	Wiebe and Gaddy (1940)
35.00	152.00	2.394	0.849	1.445	Wiebe and Gaddy (1940)
35.00	202.70	2.495	0.714	2.125	Wiebe and Gaddy (1940)
35.00	39.20	1.083	36.418	36.332	Sander (1912)
35.00	39.20	1.306	13.124	13.054	Sander (1912)

35.00	49.00	1.381	24.960	24.860	Sander (1912)
35.00	49.00	1.604	7.587	7.501	Sander (1912)
35.00	58.80	1.663	16.031	15.907	Sander (1912)
35.00	58.80	1.430	34.936	34.793	Sander (1912)
35.00	68.60	1.968	6.159	5.992	Sander (1912)
35.00	68.60	1.824	14.540	14.360	Sander (1912)
35.00	78.50	2.127	3.426	3.065	Sander (1912)
35.00	40.90	1.574	3.201	3.264	Liu et al. (2011)
35.00	60.80	2.035	3.409	3.520	Liu et al. (2011)
35.00	80.90	2.240	1.082	1.642	Liu et al. (2011)
35.00	100.80	2.314	1.112	2.507	Liu et al. (2011)
35.00	120.50	2.375	1.400	3.187	Liu et al. (2011)
35.00	140.10	2.454	2.677	4.737	Liu et al. (2011)
35.00	158.30	2.494	2.648	4.937	Liu et al. (2011)
35.01	35.46	0.810	69.182	69.084	Vilcu and Gainar (1967)
35.01	40.53	0.990	52.876	52.777	Vilcu and Gainar (1967)
35.01	45.60	1.120	46.816	46.709	Vilcu and Gainar (1967)
35.01	50.66	1.310	34.581	34.469	Vilcu and Gainar (1967)
35.01	55.73	1.480	26.359	26.237	Vilcu and Gainar (1967)
35.01	60.80	1.630	20.582	20.444	Vilcu and Gainar (1967)
35.01	65.86	1.810	13.195	13.038	Vilcu and Gainar (1967)
35.01	70.93	1.960	8.164	7.971	Vilcu and Gainar (1967)
35.01	75.99	2.140	1.748	1.487	Vilcu and Gainar (1967)
35.05	30.29	1.259	3.845	3.895	Valtz et al. (2004)
35.05	40.05	1.563	4.075	4.136	Valtz et al. (2004)
35.05	49.85	1.837	5.088	5.165	Valtz et al. (2004)
35.05	59.49	2.033	4.543	4.647	Valtz et al. (2004)
35.05	60.77	2.066	4.956	5.064	Valtz et al. (2004)
35.05	69.72	2.229	5.659	5.816	Valtz et al. (2004)
35.05	69.86	2.152	2.196	2.360	Valtz et al. (2004)
35.05	70.29	2.221	4.979	5.142	Valtz et al. (2004)
35.05	79.63	2.304	4.229	4.637	Valtz et al. (2004)
37.71	73.09	2.017	2.232	2.031	Chapoy et al. (2004)
40.00	50.70	1.609	0.575	0.478	Wiebe and Gaddy (1940)
40.00	76.00	2.032	0.120	0.344	Wiebe and Gaddy (1940)
40.00	101.30	2.186	0.290	0.840	Wiebe and Gaddy (1940)
40.00	126.70	2.256	0.610	1.131	Wiebe and Gaddy (1940)
40.00	152.00	2.308	1.048	1.113	Wiebe and Gaddy (1940)
40.00	202.70	2.488	2.044	4.724	Wiebe and Gaddy (1940)
40.00	100.00	2.070	5.680	4.535	Bando et al. (2003)
40.00	150.00	2.230	4.375	2.173	Bando et al. (2003)
40.00	200.00	2.340	3.932	1.117	Bando et al. (2003)
40.05	46.67	1.639	6.735	6.817	Kiepe et al. (2002)

40.05	56.64	1.902	8.753	8.856	Kiepe et al. (2002)
40.05	66.44	2.123	10.427	10.564	Kiepe et al. (2002)
40.05	92.32	2.481	13.138	13.804	Kiepe et al. (2002)
40.21	41.19	1.420	1.812	1.889	Chapoy et al. (2004)
45.00	41.00	1.305	1.703	1.793	Liu et al. (2011)
45.00	60.90	1.711	1.722	1.862	Liu et al. (2011)
45.00	81.10	2.022	3.356	3.623	Liu et al. (2011)
45.00	100.80	2.170	3.380	4.155	Liu et al. (2011)
45.00	120.60	2.231	2.648	4.008	Liu et al. (2011)
45.00	141.10	2.266	1.512	3.299	Liu et al. (2011)
45.00	158.60	2.296	0.897	2.974	Liu et al. (2011)
45.08	30.01	1.018	1.570	1.644	Valtz et al. (2004)
45.08	39.69	1.293	3.287	3.374	Valtz et al. (2004)
45.08	39.77	1.259	0.524	0.613	Valtz et al. (2004)
45.08	49.52	1.508	2.619	2.726	Valtz et al. (2004)
45.08	49.82	1.532	3.745	3.851	Valtz et al. (2004)
45.08	59.78	1.720	3.428	3.563	Valtz et al. (2004)
45.08	59.92	1.726	3.626	3.760	Valtz et al. (2004)
45.08	69.23	1.895	4.590	4.763	Valtz et al. (2004)
45.08	69.84	1.905	4.644	4.820	Valtz et al. (2004)
45.08	79.33	2.031	4.791	5.035	Valtz et al. (2004)
48.82	52.16	1.420	1.399	1.268	Chapoy et al. (2004)
48.99	93.33	2.017	2.165	2.605	Chapoy et al. (2004)
49.95	51.00	1.420	1.754	1.882	Koschel et al. (2006)
49.95	105.30	2.000	1.514	0.761	Koschel et al. (2006)
49.95	142.00	2.140	1.278	0.411	Koschel et al. (2006)
49.95	202.00	2.270	1.973	0.632	Koschel et al. (2006)
50.00	50.70	1.367	1.563	1.432	Wiebe and Gaddy (1939)
50.00	76.00	1.779	0.183	0.055	Wiebe and Gaddy (1939)
50.00	101.30	2.018	0.538	1.160	Wiebe and Gaddy (1939)
50.00	126.70	2.106	0.582	0.763	Wiebe and Gaddy (1939)
50.00	152.00	2.174	0.966	0.902	Wiebe and Gaddy (1939)
50.00	202.70	2.289	1.169	1.422	Wiebe and Gaddy (1939)
50.00	200.00	2.300	0.434	2.107	Tödheide and Franck (1963)
50.00	68.20	1.651	1.738	1.542	Briones et al. (1987)
50.00	75.30	1.750	1.355	1.119	Briones et al. (1987)
50.00	87.20	1.768	7.550	7.179	Briones et al. (1987)
50.00	101.30	2.081	3.549	4.152	Briones et al. (1987)
50.00	122.10	2.096	0.283	0.944	Briones et al. (1987)
50.00	147.50	2.215	1.466	3.210	Briones et al. (1987)
50.00	147.50	2.207	1.109	2.859	Briones et al. (1987)
50.00	176.80	2.262	0.188	2.417	Briones et al. (1987)
50.00	101.33	1.980	1.380	0.745	D'souza et al. (1988)

50.00	152.00	2.100	4.523	2.590	D'souza et al. (1988)
50.00	101.00	2.075	3.357	3.953	Dohrn et al. (1993)
50.00	201.00	2.347	1.486	3.989	Dohrn et al. (1993)
50.00	100.00	1.970	1.486	0.887	Bando et al. (2003)
50.00	150.00	2.090	4.761	2.860	Bando et al. (2003)
50.00	200.00	2.290	0.872	1.679	Bando et al. (2003)
50.00	80.00	1.601	14.233	13.926	Portier and Rochelle (2005)
50.00	80.00	1.658	10.270	9.974	Portier and Rochelle (2005)
50.00	100.00	1.693	18.083	17.386	Portier and Rochelle (2005)
50.00	120.00	1.952	7.290	6.036	Portier and Rochelle (2005)
50.00	120.00	1.917	9.229	7.952	Portier and Rochelle (2005)
50.00	100.00	1.999	0.013	0.577	Shagiakhmetov and Tarzimanov (1981)
50.00	200.00	2.293	0.740	1.808	Shagiakhmetov and Tarzimanov (1981)
50.00	35.00	1.029	2.024	1.926	Oleinik (cited in Namiot and Bondareva (1991))
50.00	50.00	1.357	1.318	1.189	Oleinik (cited in Namiot and Bondareva (1991))
50.00	75.00	1.773	0.140	0.371	Oleinik (cited in Namiot and Bondareva (1991))
50.00	100.00	2.014	0.732	1.317	Oleinik (cited in Namiot and Bondareva (1991))
50.00	130.00	2.130	0.047	1.462	Oleinik (cited in Namiot and Bondareva (1991))
50.00	160.00	2.216	0.028	1.955	Oleinik (cited in Namiot and Bondareva (1991))
50.00	33.00	0.996	0.516	0.422	Zel’vinskii (1937)
50.00	33.01	0.977	2.506	2.410	Zel’vinskii (1937)
50.00	33.21	1.016	0.944	1.037	Zel’vinskii (1937)
50.00	33.23	0.986	2.141	2.045	Zel’vinskii (1937)
50.00	47.42	1.273	4.000	3.873	Zel’vinskii (1937)
50.00	47.50	1.282	3.419	3.294	Zel’vinskii (1937)
50.00	47.50	1.326	0.021	0.142	Zel’vinskii (1937)
50.00	57.76	1.523	0.455	0.605	Zel’vinskii (1937)
50.00	61.10	1.597	1.570	1.729	Zel’vinskii (1937)
50.00	61.73	1.617	2.137	2.298	Zel’vinskii (1937)
50.00	61.91	1.624	2.382	2.543	Zel’vinskii (1937)
50.00	62.82	1.634	2.111	2.276	Zel’vinskii (1937)
50.00	74.19	1.796	1.994	2.215	Zel’vinskii (1937)
50.00	74.80	1.849	4.390	4.610	Zel’vinskii (1937)
50.00	75.49	1.828	2.826	3.054	Zel’vinskii (1937)
50.00	90.79	2.061	6.221	6.592	Zel’vinskii (1937)
50.00	92.71	2.036	4.318	4.729	Zel’vinskii (1937)
50.00	93.22	2.050	4.779	5.196	Zel’vinskii (1937)
50.00	49.55	1.366	0.005	0.131	Malinin and Saveleva (1972)

50.00	49.55	1.372	0.406	0.532	Malinin and Saveleva (1972)
50.00	49.55	1.372	0.420	0.546	Malinin and Saveleva (1972)
50.00	49.55	1.373	0.529	0.655	Malinin and Saveleva (1972)
50.00	39.01	1.210	5.457	5.555	Matouš et al. (1969)
50.00	33.32	1.003	0.610	0.515	Al Ghafri et al. (2014)
50.00	44.15	1.269	0.991	1.104	Al Ghafri et al. (2014)
50.00	55.85	1.561	4.986	5.123	Al Ghafri et al. (2014)
50.00	69.53	1.758	3.394	3.586	Al Ghafri et al. (2014)
50.00	90.62	2.004	3.619	3.999	Al Ghafri et al. (2014)
50.00	135.21	2.173	1.236	2.747	Al Ghafri et al. (2014)
50.00	186.83	2.280	0.042	2.326	Al Ghafri et al. (2014)
50.00	74.06	1.829	3.867	4.084	Hou et al. (2013)
50.00	100.21	2.054	2.602	3.182	Hou et al. (2013)
50.00	129.73	2.141	0.584	1.985	Hou et al. (2013)
50.00	175.33	2.255	0.033	2.245	Hou et al. (2013)
50.00	41.10	1.170	1.782	1.673	Liu et al. (2011)
50.00	61.20	1.570	0.237	0.075	Liu et al. (2011)
50.00	81.00	1.815	1.368	1.087	Liu et al. (2011)
50.00	101.00	2.001	0.242	0.377	Liu et al. (2011)
50.00	120.40	2.087	0.400	0.784	Liu et al. (2011)
50.00	159.90	2.161	2.534	0.502	Liu et al. (2011)
50.05	40.50	1.090	7.921	7.806	Bamberger et al. (2000)
50.05	50.60	1.370	1.129	0.998	Bamberger et al. (2000)
50.05	60.60	1.610	2.934	3.090	Bamberger et al. (2000)
50.05	70.80	1.760	2.579	2.780	Bamberger et al. (2000)
50.05	80.80	1.900	3.354	3.621	Bamberger et al. (2000)
50.05	90.90	2.000	3.361	3.745	Bamberger et al. (2000)
50.05	100.90	2.050	2.252	2.851	Bamberger et al. (2000)
50.05	111.00	2.100	2.082	2.974	Bamberger et al. (2000)
50.05	121.00	2.140	2.003	3.172	Bamberger et al. (2000)
50.05	141.10	2.170	0.303	1.946	Bamberger et al. (2000)
50.05	50.00	1.473	6.727	6.847	Yan et al. (2011)
50.05	100.00	2.137	6.489	7.039	Yan et al. (2011)
50.05	150.00	2.206	0.776	2.575	Yan et al. (2011)
50.05	200.00	2.285	1.070	1.486	Yan et al. (2011)
50.05	300.00	2.492	0.175	3.280	Yan et al. (2011)
55.00	43.70	1.187	2.017	2.146	Liu et al. (2011)
55.00	61.10	1.501	1.813	1.992	Liu et al. (2011)
55.00	84.80	1.797	1.000	1.320	Liu et al. (2011)
55.00	99.90	1.918	0.445	0.963	Liu et al. (2011)
55.00	122.00	2.057	1.245	2.277	Liu et al. (2011)
55.00	131.90	2.105	1.626	2.892	Liu et al. (2011)
55.00	152.30	2.131	0.324	1.394	Liu et al. (2011)

60.00	100.00	1.850	1.135	1.632	Bando et al. (2003)
60.00	150.00	2.040	1.821	0.258	Bando et al. (2003)
60.00	200.00	2.250	1.409	3.723	Bando et al. (2003)
60.00	41.00	1.020	1.699	1.551	Mohammadian et al. (2015)
60.00	83.00	1.646	1.621	1.291	Mohammadian et al. (2015)
60.00	103.00	1.839	0.670	0.120	Mohammadian et al. (2015)
60.00	138.00	2.019	0.731	0.564	Mohammadian et al. (2015)
60.00	158.00	2.071	1.543	0.172	Mohammadian et al. (2015)
60.00	172.00	2.104	1.942	0.029	Mohammadian et al. (2015)
60.00	193.00	2.152	2.258	0.045	Mohammadian et al. (2015)
60.05	40.50	0.960	6.944	6.789	Bamberger et al. (2000)
60.05	50.60	1.210	0.541	0.369	Bamberger et al. (2000)
60.05	60.60	1.380	0.079	0.126	Bamberger et al. (2000)
60.05	70.80	1.570	2.783	3.025	Bamberger et al. (2000)
60.05	80.80	1.660	0.733	1.040	Bamberger et al. (2000)
60.05	90.90	1.790	2.181	2.567	Bamberger et al. (2000)
60.05	100.90	1.860	1.337	1.846	Bamberger et al. (2000)
60.05	111.00	1.950	2.356	3.026	Bamberger et al. (2000)
60.05	121.00	2.010	2.519	3.395	Bamberger et al. (2000)
60.05	141.10	2.080	1.672	3.000	Bamberger et al. (2000)
70.00	35.00	0.773	4.933	4.746	Oleinik (cited in Namiot and Bondareva (1991))
70.00	50.00	1.037	4.199	3.970	Oleinik (cited in Namiot and Bondareva (1991))
70.00	75.00	1.404	2.245	1.911	Oleinik (cited in Namiot and Bondareva (1991))
70.00	100.00	1.673	0.995	0.469	Oleinik (cited in Namiot and Bondareva (1991))
70.00	130.00	1.885	0.318	0.642	Oleinik (cited in Namiot and Bondareva (1991))
70.00	160.00	2.014	0.389	1.141	Oleinik (cited in Namiot and Bondareva (1991))
71.00	100.00	1.660	1.067	0.536	Dhima et al. (1999)
71.00	125.00	1.820	1.811	0.932	Dhima et al. (1999)
71.00	150.00	1.970	0.231	1.093	Dhima et al. (1999)
71.00	200.00	2.130	0.611	1.567	Dhima et al. (1999)
75.00	50.70	1.002	3.839	3.578	Wiebe and Gaddy (1939)
75.00	76.00	1.351	2.756	2.382	Wiebe and Gaddy (1939)
75.00	101.30	1.630	0.775	0.214	Wiebe and Gaddy (1939)
75.00	152.00	1.937	0.708	0.613	Wiebe and Gaddy (1939)
75.00	202.70	2.098	1.474	0.706	Wiebe and Gaddy (1939)
75.00	101.33	1.560	5.313	4.727	D'souza et al. (1988)
75.00	152.00	1.880	3.761	2.400	D'souza et al. (1988)
75.00	35.91	0.760	3.543	3.329	Zawisza and Malesinska (1981)

75.00	50.70	1.013	2.762	2.504	Gillespie et al. (1982)
75.00	101.40	1.626	1.056	0.493	Gillespie et al. (1982)
75.00	202.70	2.104	1.184	0.989	Gillespie et al. (1982)
75.00	32.63	0.717	1.171	0.971	Zel'vinskii (1937)
75.00	32.71	0.723	0.487	0.288	Zel'vinskii (1937)
75.00	33.11	0.727	0.984	0.783	Zel'vinskii (1937)
75.00	47.22	0.985	0.066	0.305	Zel'vinskii (1937)
75.00	47.24	0.971	1.409	1.166	Zel'vinskii (1937)
75.00	61.07	1.219	1.894	2.180	Zel'vinskii (1937)
75.00	61.73	1.204	0.031	0.262	Zel'vinskii (1937)
75.00	61.84	1.208	0.173	0.466	Zel'vinskii (1937)
75.00	62.03	1.219	0.856	1.148	Zel'vinskii (1937)
75.00	76.70	1.406	0.694	1.059	Zel'vinskii (1937)
75.00	76.94	1.436	2.560	2.920	Zel'vinskii (1937)
75.00	77.36	1.423	1.306	1.673	Zel'vinskii (1937)
75.00	93.27	1.606	2.208	2.681	Zel'vinskii (1937)
75.00	94.46	1.611	1.803	2.288	Zel'vinskii (1937)
75.00	49.55	0.988	3.489	3.233	Malinin and Saveleva (1972)
75.00	49.55	0.994	2.874	2.620	Malinin and Saveleva (1972)
75.00	49.55	0.996	2.616	2.362	Malinin and Saveleva (1972)
75.00	49.55	0.997	2.523	2.270	Malinin and Saveleva (1972)
75.00	71.23	1.267	4.999	4.644	Hou et al. (2013)
75.00	101.67	1.593	3.312	2.733	Hou et al. (2013)
75.00	132.82	1.856	0.094	0.884	Hou et al. (2013)
75.00	169.18	1.993	1.315	0.322	Hou et al. (2013)
75.15	153.10	1.920	1.787	0.434	Sako et al. (1991)
79.70	101.80	1.660	3.719	4.285	Nighswander et al. (1989)
79.95	40.50	0.800	3.811	3.553	Bamberger et al. (2000)
79.95	60.60	1.140	0.025	0.296	Bamberger et al. (2000)
79.95	70.80	1.280	0.472	0.841	Bamberger et al. (2000)
79.95	80.80	1.400	0.646	1.071	Bamberger et al. (2000)
79.95	90.90	1.510	0.926	1.419	Bamberger et al. (2000)
79.95	100.90	1.600	0.745	1.321	Bamberger et al. (2000)
79.95	111.00	1.720	2.903	3.566	Bamberger et al. (2000)
79.95	121.00	1.760	1.052	1.846	Bamberger et al. (2000)
79.95	131.00	1.840	1.934	2.857	Bamberger et al. (2000)
79.96	49.39	1.111	12.207	12.451	Kiepe et al. (2002)
79.96	67.00	1.437	14.698	14.997	Kiepe et al. (2002)
79.96	85.50	1.734	16.877	17.258	Kiepe et al. (2002)
80.00	100.00	1.323	19.444	18.759	Portier and Rochelle (2005)
80.00	100.00	1.445	9.308	8.681	Portier and Rochelle (2005)
80.00	38.81	0.799	0.259	0.015	Matouš et al. (1969)
80.00	41.00	0.813	3.147	2.889	Mohammadian et al. (2015)

80.00	62.00	1.122	3.283	2.944	Mohammadian et al. (2015)
80.00	83.00	1.333	6.098	5.630	Mohammadian et al. (2015)
80.00	103.00	1.568	2.420	1.805	Mohammadian et al. (2015)
80.00	138.00	1.782	3.471	2.389	Mohammadian et al. (2015)
80.00	158.00	1.903	1.986	0.585	Mohammadian et al. (2015)
80.00	172.00	1.938	3.134	1.476	Mohammadian et al. (2015)
80.00	193.00	2.012	3.054	1.052	Mohammadian et al. (2015)
80.00	213.00	2.064	3.506	1.194	Mohammadian et al. (2015)
80.20	43.10	0.850	2.625	2.360	Nighswander et al. (1989)
80.30	101.60	1.640	3.004	3.577	Nighswander et al. (1989)
80.50	61.10	1.120	1.979	1.645	Nighswander et al. (1989)
80.50	77.60	1.370	1.490	1.895	Nighswander et al. (1989)
80.50	78.40	1.380	1.543	1.953	Nighswander et al. (1989)
80.60	43.40	0.840	4.072	3.800	Nighswander et al. (1989)
93.30	50.70	0.851	5.710	5.310	Gillespie et al. (1982)
93.30	101.40	1.459	1.559	0.865	Gillespie et al. (1982)
93.30	202.70	2.074	0.749	2.718	Gillespie et al. (1982)
99.95	50.50	0.790	8.852	8.383	Koschel et al. (2006)
99.95	100.80	1.360	5.440	4.664	Koschel et al. (2006)
99.95	194.70	2.010	0.008	1.845	Koschel et al. (2006)
100.00	50.70	0.812	6.218	5.759	Wiebe and Gaddy (1939)
100.00	76.00	1.135	4.180	3.594	Wiebe and Gaddy (1939)
100.00	101.30	1.400	2.729	1.967	Wiebe and Gaddy (1939)
100.00	152.00	1.794	0.504	0.780	Wiebe and Gaddy (1939)
100.00	202.70	2.023	0.962	1.018	Wiebe and Gaddy (1939)
100.00	200.00	2.000	1.585	0.371	Tödheide and Franck (1963)
100.00	45.60	0.760	3.842	3.416	Zawisza and Malesinska (1981)
100.00	100.00	1.444	1.216	1.937	Shagiakhmetov and Tarzimanov (1981)
100.00	200.00	2.030	0.084	1.843	Shagiakhmetov and Tarzimanov (1981)
100.00	32.49	0.574	2.123	1.756	Zel’vinskii (1937)
100.00	33.01	0.590	0.791	0.427	Zel’vinskii (1937)
100.00	33.10	0.583	2.287	1.918	Zel’vinskii (1937)
100.00	33.13	0.581	2.653	2.282	Zel’vinskii (1937)
100.00	33.21	0.578	3.447	3.073	Zel’vinskii (1937)
100.00	46.71	0.801	0.514	0.097	Zel’vinskii (1937)
100.00	47.36	0.812	0.388	0.032	Zel’vinskii (1937)
100.00	47.39	0.815	0.047	0.372	Zel’vinskii (1937)
100.00	47.51	0.794	2.873	2.442	Zel’vinskii (1937)
100.00	61.71	1.083	6.734	7.185	Zel’vinskii (1937)
100.00	61.76	0.981	3.058	2.558	Zel’vinskii (1937)
100.00	61.81	1.046	3.285	3.754	Zel’vinskii (1937)
100.00	62.11	1.083	6.192	6.649	Zel’vinskii (1937)
100.00	75.99	1.240	4.651	5.187	Zel’vinskii (1937)

100.00	91.19	1.448	7.253	7.868	Zel'vinskii (1937)
100.00	49.55	0.801	5.621	5.170	Malinin and Saveleva (1972)
100.00	49.55	0.805	5.175	4.726	Malinin and Saveleva (1972)
100.00	49.55	0.805	5.123	4.674	Malinin and Saveleva (1972)
100.00	70.88	1.085	3.525	2.973	Hou et al. (2013)
100.00	102.35	1.365	6.051	5.256	Hou et al. (2013)
100.00	133.52	1.626	3.869	2.773	Hou et al. (2013)
100.00	170.70	1.872	1.594	0.046	Hou et al. (2013)

Table 2.A3. Experimental data of H_2O solubility in CO_2-rich phase and calculated AARD% values

Temp °C	**Pressure bar**	**Y_{H2O} Mole%**	**ARD % Model-2**	**ARD % Model-1**	**Reference**
35.00	91.20	0.384	9.199	284.703	King et al. (1992)
35.00	101.30	0.407	6.788	340.803	King et al. (1992)
35.00	111.50	0.414	3.333	391.785	King et al. (1992)
35.00	126.70	0.435	2.840	434.700	King et al. (1992)
35.00	136.80	0.440	1.306	465.885	King et al. (1992)
35.00	152.00	0.457	1.845	492.501	King et al. (1992)
35.00	202.70	0.498	3.465	558.673	King et al. (1992)
35.06	30.29	0.230	8.791	31.231	Valtz et al. (2004)
35.06	40.05	0.200	5.675	37.510	Valtz et al. (2004)
35.06	49.85	0.170	13.025	60.789	Valtz et al. (2004)
35.06	59.49	0.160	15.879	83.740	Valtz et al. (2004)
35.06	70.56	0.170	13.613	115.602	Valtz et al. (2004)
35.06	79.30	0.230	4.147	175.917	Valtz et al. (2004)
35.06	79.63	0.250	2.078	166.815	Valtz et al. (2004)
40.00	101.30	0.428	7.464	254.119	King et al. (1992)
40.00	111.50	0.440	2.371	315.955	King et al. (1992)
40.00	126.70	0.467	1.012	367.090	King et al. (1992)
40.00	152.00	0.507	1.879	416.954	King et al. (1992)
40.00	177.30	0.543	4.006	446.203	King et al. (1992)
40.00	202.70	0.580	7.096	461.219	King et al. (1992)
40.00	89.00	0.392	19.211	132.493	Foltran et al. (2015)
40.00	102.10	0.445	10.274	247.000	Foltran et al. (2015)
40.00	111.40	0.454	5.441	302.539	Foltran et al. (2015)
40.00	124.10	0.481	4.874	342.332	Foltran et al. (2015)
40.00	91.19	0.320	5.204	227.307	Springer et al. (2012)
45.07	30.01	0.440	4.993	11.924	Valtz et al. (2004)
45.07	39.80	0.380	8.450	15.033	Valtz et al. (2004)
45.07	49.56	0.350	11.212	19.938	Valtz et al. (2004)
45.07	59.92	0.330	11.713	30.406	Valtz et al. (2004)

45.07	69.30	0.290	1.101	61.062	Valtz et al. (2004)
50.00	50.70	0.383	0.539	34.192	Wiebe and Gaddy (1941)
50.00	60.80	0.357	0.810	45.628	Wiebe and Gaddy (1941)
50.00	76.00	0.350	0.414	68.018	Wiebe and Gaddy (1941)
50.00	101.30	0.449	5.519	132.811	Wiebe and Gaddy (1941)
50.00	152.00	0.610	1.138	299.754	Wiebe and Gaddy (1941)
50.00	202.70	0.677	1.140	374.029	Wiebe and Gaddy (1941)
50.00	200.00	1.000	33.325	217.534	Tödheide and Franck (1963)
50.00	101.33	0.550	22.840	90.236	D'souza et al. (1988)
50.00	152.00	0.790	23.664	208.671	D'souza et al. (1988)
50.00	101.00	0.547	22.741	89.317	Dohrn et al. (1993)
50.00	201.00	0.682	2.097	367.441	Dohrn et al. (1993)
50.00	36.38	0.466	0.438	20.709	King Jr and Coan (1971)
50.00	36.38	0.463	0.207	21.491	King Jr and Coan (1971)
50.00	46.31	0.396	1.639	31.492	King Jr and Coan (1971)
50.00	74.06	0.350	0.206	64.141	Hou et al. (2013)
50.00	100.21	0.403	3.826	150.701	Hou et al. (2013)
50.00	129.73	0.533	3.275	265.658	Hou et al. (2013)
50.00	175.33	0.614	4.127	361.564	Hou et al. (2013)
50.05	40.50	0.460	5.461	17.634	Bamberger et al. (2000)
50.05	50.60	0.360	7.299	43.081	Bamberger et al. (2000)
50.05	60.60	0.370	2.432	40.666	Bamberger et al. (2000)
50.05	70.80	0.340	3.356	63.597	Bamberger et al. (2000)
50.05	80.80	0.340	4.804	85.498	Bamberger et al. (2000)
50.05	90.90	0.410	7.664	88.744	Bamberger et al. (2000)
50.05	100.90	0.450	6.127	129.223	Bamberger et al. (2000)
50.05	111.00	0.500	4.610	176.388	Bamberger et al. (2000)
50.05	121.00	0.550	5.228	210.199	Bamberger et al. (2000)
50.05	141.10	0.610	4.769	263.271	Bamberger et al. (2000)
60.05	40.50	0.660	2.742	24.560	Bamberger et al. (2000)
60.05	50.60	0.550	8.261	39.161	Bamberger et al. (2000)
60.05	60.60	0.550	0.318	36.583	Bamberger et al. (2000)
60.05	70.80	0.510	2.470	51.000	Bamberger et al. (2000)
60.05	80.80	0.500	2.785	64.208	Bamberger et al. (2000)
60.05	90.90	0.470	10.577	93.945	Bamberger et al. (2000)
60.05	100.90	0.490	10.119	114.627	Bamberger et al. (2000)
60.05	111.00	0.530	8.102	136.684	Bamberger et al. (2000)
60.05	121.00	0.580	5.848	159.532	Bamberger et al. (2000)
60.05	141.10	0.780	11.361	160.307	Bamberger et al. (2000)
75.00	101.30	0.829	2.955	69.456	Wiebe and Gaddy (1941)
75.00	126.70	0.855	4.772	106.590	Wiebe and Gaddy (1941)
75.00	152.00	0.956	1.812	137.522	Wiebe and Gaddy (1941)
75.00	202.70	1.130	2.408	185.347	Wiebe and Gaddy (1941)

75.00	50.70	1.087	0.880	21.977	Gillespie et al. (1982)
75.00	101.40	0.727	17.405	93.370	Gillespie et al. (1982)
75.00	202.70	0.938	17.568	243.755	Gillespie et al. (1982)
75.00	101.33	0.740	15.339	89.877	D'souza et al. (1988)
75.00	152.00	0.900	8.147	152.301	D'souza et al. (1988)
75.00	37.39	1.250	5.271	21.886	King Jr and Coan (1971)
75.00	37.49	1.260	4.235	20.740	King Jr and Coan (1971)
75.00	51.27	1.040	2.919	26.998	King Jr and Coan (1971)
75.00	51.47	1.020	4.695	29.315	King Jr and Coan (1971)
75.00	91.19	0.850	0.787	55.184	Springer et al. (2012)
75.00	71.23	0.845	7.844	47.468	Hou et al. (2013)
75.00	101.67	0.805	6.042	74.976	Hou et al. (2013)
75.00	132.82	0.836	9.238	124.946	Hou et al. (2013)
75.00	169.18	0.996	2.849	163.135	Hou et al. (2013)
79.95	40.50	1.430	4.906	22.012	Bamberger et al. (2000)
79.95	60.60	1.090	7.321	36.475	Bamberger et al. (2000)
79.95	70.80	1.040	4.559	39.730	Bamberger et al. (2000)
79.95	80.80	0.970	6.877	50.430	Bamberger et al. (2000)
79.95	90.90	0.920	9.486	62.936	Bamberger et al. (2000)
79.95	100.90	0.930	6.969	68.772	Bamberger et al. (2000)
79.95	111.00	0.900	10.644	85.718	Bamberger et al. (2000)
79.95	121.00	0.960	4.960	87.660	Bamberger et al. (2000)
79.95	131.00	1.000	2.767	95.767	Bamberger et al. (2000)
93.30	50.70	1.970	4.523	23.324	Gillespie et al. (1982)
93.30	101.40	1.374	8.097	57.071	Gillespie et al. (1982)
93.30	202.70	1.432	10.450	146.630	Gillespie et al. (1982)
100.00	36.78	3.280	1.841	9.230	King Jr and Coan (1971)
100.00	37.19	3.230	1.142	10.150	King Jr and Coan (1971)
100.00	44.79	2.770	0.612	14.897	King Jr and Coan (1971)
100.00	44.79	2.740	1.714	16.155	King Jr and Coan (1971)
100.00	51.47	2.480	2.137	19.263	King Jr and Coan (1971)
100.00	51.47	2.510	0.916	17.837	King Jr and Coan (1971)
100.00	91.19	1.610	15.842	56.247	Springer et al. (2012)
100.00	70.88	2.102	0.565	24.263	Hou et al. (2013)
100.00	102.35	1.747	2.840	44.948	Hou et al. (2013)
100.00	133.52	1.675	2.845	64.666	Hou et al. (2013)
100.00	170.70	1.712	2.336	89.733	Hou et al. (2013)

Table 2.A4. Experimental data of CO_2 solubility in NaCl brine and calculated AARD% values

Temp °C	**Pressure bar**	**X_{CO2} Mole%**	**ARD% Model-2**	**ARD% Model-1**	**NaCl Molality mole/kg_{H2O}**	**Reference**
`60.00	83.00	1.637	1.775	1.445	0.0172	Mohammadian et al. (2015)
60.00	103.00	1.833	0.576	0.026	0.0172	Mohammadian et al. (2015)
60.00	138.00	2.012	0.700	0.594	0.0172	Mohammadian et al. (2015)
60.00	172.00	2.096	1.899	0.070	0.0172	Mohammadian et al. (2015)
60.00	193.00	2.143	2.292	0.011	0.0172	Mohammadian et al. (2015)
80.00	41.00	0.719	16.203	15.912	0.0172	Mohammadian et al. (2015)
80.00	83.00	1.263	11.580	11.088	0.0172	Mohammadian et al. (2015)
80.00	103.00	1.475	8.447	7.795	0.0172	Mohammadian et al. (2015)
80.00	138.00	1.722	6.628	5.512	0.0172	Mohammadian et al. (2015)
80.00	158.00	1.839	5.158	3.713	0.0172	Mohammadian et al. (2015)
80.00	172.00	1.872	6.371	4.661	0.0172	Mohammadian et al. (2015)
80.00	213.00	2.024	5.156	2.806	0.0172	Mohammadian et al. (2015)
80.00	94.90	1.410	4.496	3.942	0.171	Nighswander et al. (1989)
80.10	99.40	1.540	1.841	2.399	0.171	Nighswander et al. (1989)
80.20	41.30	0.760	6.456	6.188	0.171	Nighswander et al. (1989)
80.20	60.20	1.010	7.707	7.361	0.171	Nighswander et al. (1989)
80.20	60.70	1.080	1.342	1.014	0.171	Nighswander et al. (1989)
80.30	40.40	0.740	7.257	6.988	0.171	Nighswander et al. (1989)
80.30	80.40	1.350	1.584	2.004	0.171	Nighswander et al. (1989)
80.50	80.50	1.340	0.909	1.335	0.171	Nighswander et al. (1989)
60.00	41.00	0.976	1.972	1.823	0.172	Mohammadian et al. (2015)
60.00	83.00	1.531	4.850	4.509	0.172	Mohammadian et al. (2015)
60.00	138.00	1.944	0.485	0.807	0.172	Mohammadian et al. (2015)
60.00	158.00	1.956	3.278	1.532	0.172	Mohammadian et al. (2015)
60.00	172.00	2.025	1.754	0.215	0.172	Mohammadian et al. (2015)
60.00	193.00	2.065	2.435	0.127	0.172	Mohammadian et al. (2015)
80.00	41.00	0.703	14.658	14.371	0.172	Mohammadian et al. (2015)
80.00	83.00	1.231	10.372	9.884	0.172	Mohammadian et al. (2015)
80.00	138.00	1.697	4.415	3.322	0.172	Mohammadian et al. (2015)
80.00	172.00	1.835	4.670	2.986	0.172	Mohammadian et al. (2015)
80.00	213.00	1.958	4.916	2.570	0.172	Mohammadian et al. (2015)
100.00	48.00	0.635	3.286	2.850	1	Zhao et al. (2015)
49.95	51.00	1.110	1.086	1.215	1	Koschel et al. (2006)
49.95	100.30	1.640	3.687	4.267	1	Koschel et al. (2006)
49.95	143.80	1.770	2.848	4.509	1	Koschel et al. (2006)
50.05	50.00	1.167	7.363	7.482	1	Yan et al. (2011)
50.05	100.00	1.672	5.725	6.283	1	Yan et al. (2011)
50.00	150.00	1.766	1.832	3.622	1	Zhao et al. (2015)
50.05	150.00	1.772	2.161	3.943	1	Yan et al. (2011)

50.05	200.00	1.909	3.808	6.252	1	Yan et al. (2011)
50.05	300.00	2.011	0.353	3.806	1	Yan et al. (2011)
99.95	50.70	0.600	14.394	13.899	1	Koschel et al. (2006)
99.95	104.00	1.120	3.871	3.076	1	Koschel et al. (2006)
99.95	191.40	1.610	1.108	2.902	1	Koschel et al. (2006)
100.05	50.00	0.753	9.889	10.277	1	Yan et al. (2011)
100.05	100.00	1.195	5.050	5.746	1	Yan et al. (2011)
100.05	150.00	1.444	1.230	2.471	1	Yan et al. (2011)
100.00	150.00	1.458	2.132	3.362	1	Zhao et al. (2015)
100.05	200.00	1.682	3.649	5.510	1	Yan et al. (2011)
100.05	300.00	1.864	1.083	2.057	1	Yan et al. (2011)
40.16	38.44	0.861	15.357	15.420	2.5	Kiepe et al. (2002)
40.16	51.37	1.089	17.734	17.816	2.5	Kiepe et al. (2002)
40.16	63.73	1.272	19.581	19.694	2.5	Kiepe et al. (2002)
40.16	77.89	1.431	21.049	21.246	2.5	Kiepe et al. (2002)
40.16	91.29	1.517	21.628	22.187	2.5	Kiepe et al. (2002)
50.00	57.39	0.875	4.228	4.372	2.5	Hou et al. (2013)
50.00	87.30	1.146	7.499	7.821	2.5	Hou et al. (2013)
50.00	117.73	1.238	5.622	6.676	2.5	Hou et al. (2013)
50.00	150.20	1.293	4.466	6.219	2.5	Hou et al. (2013)
50.00	182.11	1.335	3.409	5.657	2.5	Hou et al. (2013)
79.92	40.82	0.532	11.277	11.499	2.5	Kiepe et al. (2002)
79.92	52.21	0.660	12.848	13.100	2.5	Kiepe et al. (2002)
79.92	64.70	0.789	14.376	14.669	2.5	Kiepe et al. (2002)
79.92	76.79	0.902	15.632	15.974	2.5	Kiepe et al. (2002)
79.92	100.61	1.091	17.578	18.058	2.5	Kiepe et al. (2002)
100.00	57.42	0.545	0.459	0.922	2.5	Hou et al. (2013)
100.00	87.89	0.745	0.125	0.519	2.5	Hou et al. (2013)
100.00	118.67	0.911	0.747	1.644	2.5	Hou et al. (2013)
100.00	149.21	1.039	1.320	2.554	2.5	Hou et al. (2013)
100.00	180.13	1.139	1.476	3.117	2.5	Hou et al. (2013)
40.23	40.27	0.657	18.607	18.670	4	Kiepe et al. (2002)
40.23	59.78	0.898	22.111	22.208	4	Kiepe et al. (2002)
40.23	73.78	1.029	23.823	23.980	4	Kiepe et al. (2002)
40.23	81.22	1.080	24.365	24.596	4	Kiepe et al. (2002)
40.23	90.61	1.120	24.545	25.054	4	Kiepe et al. (2002)
50.00	150.00	1.036	14.019	15.599	4	Zhao et al. (2015)
50.00	59.54	0.697	12.175	12.313	4	Hou et al. (2013)
50.00	89.53	0.875	12.393	12.727	4	Hou et al. (2013)
50.00	120.17	0.956	11.777	12.825	4	Hou et al. (2013)
50.00	149.59	0.997	10.710	12.344	4	Hou et al. (2013)
50.00	179.54	1.025	9.130	11.220	4	Hou et al. (2013)
100.00	150.00	0.878	14.214	15.299	4	Zhao et al. (2015)

100.00	60.68	0.466	12.272	12.695	4	Hou et al. (2013)
100.00	89.16	0.620	11.995	12.570	4	Hou et al. (2013)
100.00	120.03	0.752	11.846	12.656	4	Hou et al. (2013)
100.00	149.24	0.857	12.370	13.470	4	Hou et al. (2013)
100.00	181.62	0.924	10.130	11.650	4	Hou et al. (2013)
50.00	150.00	0.902	20.033	21.505	5	Zhao et al. (2015)
50.05	50.00	0.553	21.098	21.200	5	Yan et al. (2011)
50.05	100.00	0.804	19.883	20.361	5	Yan et al. (2011)
50.05	150.00	0.906	20.384	21.848	5	Yan et al. (2011)
50.05	200.00	0.915	14.775	16.961	5	Yan et al. (2011)
50.05	300.00	0.989	10.110	13.257	5	Yan et al. (2011)
100.00	150.00	0.769	19.710	20.727	5	Zhao et al. (2015)
100.05	50.00	0.351	19.838	20.184	5	Yan et al. (2011)
100.05	100.00	0.598	19.841	20.433	5	Yan et al. (2011)
100.05	150.00	0.789	21.697	22.689	5	Yan et al. (2011)
100.05	200.00	0.947	23.968	25.450	5	Yan et al. (2011)
100.05	300.00	1.047	15.594	18.239	5	Yan et al. (2011)
50.00	150.00	0.803	26.802	28.151	6	Zhao et al. (2015)
100.00	150.00	0.689	26.006	26.944	6	Zhao et al. (2015)

2.7. References

Akinfiev, N. N., and Diamond, L. W., 2003, Thermodynamic description of aqueous nonelectrolytes at infinite dilution over a wide range of state parameters: Geochimica et Cosmochimica Acta, v. 67, no. 4, p. 613-629.

Al Ghafri, S. Z., Forte, E., Maitland, G. C., Rodriguez-Henríquez, J. J., and Trusler, J. M., 2014, Experimental and Modeling Study of the Phase Behavior of (Methane+ CO2+ Water) Mixtures: The Journal of Physical Chemistry B, v. 118, no. 49, p. 14461-14478.

Azadpour, A., Brown, L., and Vadie, A., 1996, Examination of thirteen petroliferous formations for hydrocarbon-utilizing sulfate-reducing microorganisms: Journal of industrial microbiology, v. 16, no. 5, p. 263-266.

Bamberger, A., Sieder, G., and Maurer, G., 2000, High-pressure (vapor+ liquid) equilibrium in binary mixtures of (carbon dioxide+ water or acetic acid) at temperatures from 313 to 353 K: The Journal of Supercritical Fluids, v. 17, no. 2, p. 97-110.

Bando, S., Takemura, F., Nishio, M., Hihara, E., and Akai, M., 2003, Solubility of CO2 in aqueous solutions of NaCl at (30 to 60) C and (10 to 20) MPa: Journal of Chemical & Engineering Data, v. 48, no. 3, p. 576-579.

Benson, S., Bennaceur, K., Cook, P., Davison, J., Coninck, H. d., Farhat, K., Ramirez, C., Simbeck, D., Surles, T., and Verma, P., 2012, Carbon capture and storage.

Briones, J., Mullins, J., Thies, M. C., and Kim, B.-U., 1987, Ternary phase equilibria for acetic acid-water mixtures with supercritical carbon dioxide: Fluid Phase Equilibria, v. 36, p. 235-246.

Brown, L., Vadie, A., and Stephens, J., Slowing production decline and extending the economic life of an oil field: new MEOR technology, *in* Proceedings SPE/DOE Improved Oil Recovery Symposium2000, Society of Petroleum Engineers.

Chapoy, A., Mohammadi, A., Chareton, A., Tohidi, B., and Richon, D., 2004, Measurement and modeling of gas solubility and literature review of the properties for the carbon dioxide-water system: Industrial & engineering chemistry research, v. 43, no. 7, p. 1794-1802.

D'souza, R., Patrick, J. R., and Teja, A. S., 1988, High pressure phase equilibria in the carbon dioxide-n-Hexadecane and carbon dioxide—water systems: The Canadian Journal of Chemical Engineering, v. 66, no. 2, p. 319-323.

Danesh, A., 1998, PVT and phase behaviour of petroleum reservoir fluids, Elsevier.

Dhima, A., de Hemptinne, J.-C., and Jose, J., 1999, Solubility of hydrocarbons and CO2 mixtures in water under high pressure: Industrial & engineering chemistry research, v. 38, no. 8, p. 3144-3161.

Dohrn, R., Bünz, A., Devlieghere, F., and Thelen, D., 1993, Experimental measurements of phase equilibria for ternary and quaternary systems of glucose, water, CO 2 and ethanol with a novel apparatus: Fluid Phase Equilibria, v. 83, p. 149-158.

Duan, Z., and Sun, R., 2003, An improved model calculating CO 2 solubility in pure water and aqueous NaCl solutions from 273 to 533 K and from 0 to 2000 bar: Chemical geology, v. 193, no. 3, p. 257-271.

Duan, Z., Sun, R., Zhu, C., and Chou, I.-M., 2006, An improved model for the calculation of CO 2 solubility in aqueous solutions containing Na+, K+, Ca 2+, Mg 2+, Cl−, and SO 4 2−: Marine Chemistry, v. 98, no. 2, p. 131-139.

Fine, R. A., and Millero, F. J., 1973, Compressibility of water as a function of temperature and pressure: The Journal of Chemical Physics, v. 59, no. 10, p. 5529-5536.

Foltran, S., Vosper, M. E., Suleiman, N. B., Wriglesworth, A., Ke, J., Drage, T. C., Poliakoff, M., and George, M. W., 2015, Understanding the solubility of water in carbon capture and storage mixtures: An FTIR spectroscopic study of H 2 O+ CO 2+ N 2 ternary mixtures: International Journal of Greenhouse Gas Control, v. 35, p. 131-137.

Giangiacomo, L. A., and Dennis, D. M., Field testing of the biocompetitive exclusion process for control of iron and hydrogen sulfides, *in* Proceedings SPE Rocky Mountain Regional Meeting1997, Society of Petroleum Engineers.

Gillespie, P. C., Wilson, G. M., and Association, G. P., 1982, Vapor-liquid and liquid-liquid equilibria: water-methane, water-carbon dioxide, water-hydrogen sulfide, water-npentane, water-methane-npentane, Gas Processors Association.

Goodchild, A., Raftery, M., Saunders, N. F. W., Guilhaus, M., and Cavicchioli, R., 2004, Biology of the Cold Adapted Archaeon, Methanococcoides burtonii Determined by Proteomics Using Liquid Chromatography-Tandem Mass Spectrometry: Journal of Proteome Research, v. 3, no. 6, p. 1164-1176.

Hitzman, D. O., Dennis, M., and Hitzman, D. C., Recent successes: MEOR using synergistic H2S prevention and increased oil recovery systems, *in* Proceedings SPE/DOE Symposium on Improved Oil Recovery2004, Society of Petroleum Engineers.

Hou, S.-X., Maitland, G. C., and Trusler, J. M., 2013, Measurement and modeling of the phase behavior of the (carbon dioxide+ water) mixture at temperatures from 298.15 K to 448.15 K: The Journal of Supercritical Fluids, v. 73, p. 87-96.

Huang, S. S.-S., Leu, A.-D., Ng, H.-J., and Robinson, D. B., 1985, The phase behavior of two mixtures of methane, carbon dioxide, hydrogen sulfide, and water: Fluid Phase Equilibria, v. 19, no. 1, p. 21-32.

Huber, R., Kurr, M., Jannasch, H. W., and Stetter, K. O., 1989, A novel group of abyssal methanogenic archaebacteria (Methanopyrus) growing at 110 [deg]C: Nature, v. 342, no. 6251, p. 833-834.

Kiepe, J., Horstmann, S., Fischer, K., and Gmehling, J., 2002, Experimental determination and prediction of gas solubility data for CO2+ H2O mixtures containing NaCl or KCl at temperatures between 313 and 393 K and pressures up to 10 MPa: Industrial & engineering chemistry research, v. 41, no. 17, p. 4393-4398.

King Jr, A. D., and Coan, C., 1971, Solubility of water in compressed carbon dioxide, nitrous oxide, and ethane. Evidence for hydration of carbon dioxide and nitrous oxide in the gas phase: Journal of the American Chemical Society, v. 93, no. 8, p. 1857-1862.

King, M., Mubarak, A., Kim, J., and Bott, T., 1992, The mutual solubilities of water with supercritical and liquid carbon dioxides: The Journal of Supercritical Fluids, v. 5, no. 4, p. 296-302.

Kontogeorgis, G. M., Michelsen, M. L., Folas, G. K., Derawi, S., von Solms, N., and Stenby, E. H., 2006, Ten years with the CPA (Cubic-Plus-Association) equation of state. Part 1. Pure compounds and self-associating systems: Industrial & engineering chemistry research, v. 45, no. 14, p. 4855-4868.

Koschel, D., Coxam, J.-Y., Rodier, L., and Majer, V., 2006, Enthalpy and solubility data of CO 2 in water and NaCl (aq) at conditions of interest for geological sequestration: Fluid Phase Equilibria, v. 247, no. 1, p. 107-120.

Li, H., and Yan, J., 2009, Evaluating cubic equations of state for calculation of vapor–liquid equilibrium of CO 2 and CO 2-mixtures for CO 2 capture and storage processes: Applied Energy, v. 86, no. 6, p. 826-836.

Li, J., Wei, L., and Li, X., 2014, Modeling of CO 2-CH 4-H 2 S-brine based on cubic EOS and fugacity-activity approach and their comparisons: Energy Procedia, v. 63, p. 3598-3607.

-, 2015, An improved cubic model for the mutual solubilities of CO 2–CH 4–H 2 S–brine systems to high temperature, pressure and salinity: Applied Geochemistry, v. 54, p. 1-12.

Liu, Y., Hou, M., Yang, G., and Han, B., 2011, Solubility of CO 2 in aqueous solutions of NaCl, KCl, CaCl 2 and their mixed salts at different temperatures and pressures: The Journal of Supercritical Fluids, v. 56, no. 2, p. 125-129.

Malinin, S., and Saveleva, N., 1972, Experimental investigations of CO2 solubility in NaCl and CaCl2 solutions at temperatures of 25, 50 and 75 degrees and elevated CO2 pressure: Geokhimiya, no. 6, p. 643-&.

Mao, S., Zhang, D., Li, Y., and Liu, N., 2013, An improved model for calculating CO 2 solubility in aqueous NaCl solutions and the application to CO 2–H 2 O–NaCl fluid inclusions: Chemical Geology, v. 347, p. 43-58.

Matouš, J., Šobr, J., Novak, J., and Pick, J., 1969, Solubility of carbon dioxide in water at pressures up to 40 atm: Collection of Czechoslovak Chemical Communications, v. 34, no. 12, p. 3982-3985.

Millikan, C. V., 1941, Temperature Surveys in Oil Wells: SPE Journal, p. 15-23.

Mohammadian, E., Hamidi, H., Asadullah, M., Azdarpour, A., Motamedi, S., and Junin, R., 2015, Measurement of CO2 Solubility in NaCl Brine Solutions at Different Temperatures and Pressures Using the Potentiometric Titration Method: Journal of Chemical & Engineering Data, v. 60, no. 7, p. 2042-2049.

Namiot, A. Y., and Bondareva, M., 1991, Solubility of gases in water: Nedra, Moscow.

Nemati, M., Jenneman, G. E., and Voordouw, G., 2001, Impact of Nitrate-Mediated Microbial Control of Souring in Oil Reservoirs on the Extent of Corrosion: Biotechnology progress, v. 17, no. 5, p. 852-859.

Nighswander, J. A., Kalogerakis, N., and Mehrotra, A. K., 1989, Solubilities of carbon dioxide in water and 1 wt.% sodium chloride solution at pressures up to 10 MPa and temperatures from 80 to 200. degree. C: Journal of Chemical and Engineering Data, v. 34, no. 3, p. 355-360.

Nuryadi, A., Kishita, A., Watanabe, N., Vilcaez Perez, J., and Kawai, N., 2011, EOR Simulation by in situ Nitrogen Production via Denitrifying Bacteria and Performance Improvement by Nitrogen Alternating Surfactant Injection, Society of Petroleum Engineers.

Pitzer, K. S., 1973, Thermodynamics of electrolytes. I. Theoretical basis and general equations: The Journal of Physical Chemistry, v. 77, no. 2, p. 268-277.

Portier, S., and Rochelle, C., 2005, Modelling CO 2 solubility in pure water and NaCl-type waters from 0 to 300 C and from 1 to 300 bar: Application to the Utsira Formation at Sleipner: Chemical Geology, v. 217, no. 3, p. 187-199.

Privat, R., and Jaubert, J.-N., 2014, Predicting the Phase Equilibria of Carbon Dioxide Containing Mixtures Involved in CCS Processes Using the PPR78 Model.

Sako, T., Sugeta, T., Nakazawa, N., Okubo, T., Sato, M., Taguchi, T., and Hiaki, T., 1991, Phase equilibrium study of extraction and concentration of furfural produced in reactor using supercritical carbon dioxide: Journal of chemical engineering of Japan, v. 24, no. 4, p. 449-455.

Sander, W., 1912, The solubility of carbon dioxide in water: Z. Phys. Chem., Stochiom. Verwandtsch, v. 78, p. 513-549.

Savary, V., Berger, G., Dubois, M., Lacharpagne, J.-C., Pages, A., Thibeau, S., and Lescanne, M., 2012, The solubility of CO 2+ H 2 S mixtures in water and 2M NaCl at 120° C and pressures up to 35MPa: International Journal of Greenhouse Gas Control, v. 10, p. 123-133.

Shagiakhmetov, R., and Tarzimanov, A., 1981, Measurements of CO2 solubility in water up to 60 MPa: Deposited Document SPSTL 200khp-D81-1982.

Shibue, Y., 2003, Vapor pressures of aqueous NaCl and CaCl 2 solutions at elevated temperatures: Fluid phase equilibria, v. 213, no. 1, p. 39-51.

Springer, R. D., Wang, Z., Anderko, A., Wang, P., and Felmy, A. R., 2012, A thermodynamic model for predicting mineral reactivity in supercritical carbon dioxide: I. Phase behavior of carbon dioxide–water–chloride salt systems across the H 2 O-rich to the CO 2-rich regions: Chemical Geology, v. 322, p. 151-171.

Spycher, N., and Pruess, K., 2005, CO2–H2O mixtures in the geological sequestration of CO2. II: Partitioning in chloride brines at, p. 12-100.

Spycher, N., Pruess, K., and Ennis-King, J., 2003, CO 2-H 2 O mixtures in the geological sequestration of CO 2. I. Assessment and calculation of mutual solubilities from 12 to 100 C and up to 600 bar: Geochimica et cosmochimica acta, v. 67, no. 16, p. 3015-3031.

Strappa, L. A., De Lucia, J. P., Maure, M. A., and Llopiz, M. L. L., A Novel and Successful MEOR Pilot Project in a Strong Water-Drive Reservoir Vizcacheras Field, Argentina, Society of Petroleum Engineers.

Tödheide, K., and Franck, E., 1963, Das Zweiphasengebiet und die kritische Kurve im System Kohlendioxid–Wasser bis zu Drucken von 3500 bar: Zeitschrift für Physikalische Chemie, v. 37, no. 5_6, p. 387-401.

Valtz, A., Chapoy, A., Coquelet, C., Paricaud, P., and Richon, D., 2004, Vapour–liquid equilibria in the carbon dioxide–water system, measurement and modelling from 278.2 to 318.2 K: Fluid phase equilibria, v. 226, p. 333-344.

Vilcáez, J., 2015a, Numerical modeling and simulation of microbial methanogenesis in geological CO 2 storage sites: Journal of Petroleum Science and Engineering, v. 135, p. 583-595.

-, 2015b, Stimulating effect of protein-rich matter on the biogenic conversion of CO 2 to CH 4: Journal of CO2 Utilization, v. 10, p. 60-66.

Vilcáez, J., Li, L., Wu, D., and Hubbard, S. S., 2013, Reactive Transport Modeling of Induced Selective Plugging by Leuconostoc Mesenteroides in Carbonate Formations: Geomicrobiology Journal, v. 30, no. 9, p. 813-828.

Vilcu, R., and Gainar, I., 1967, Loslichkeit der gase unter druck in flussigkeiten. i. das system kohlendioxid-wasser: Revue Roumaine de Chimie, v. 12, no. 2, p. 181-&.

Vitu, S., Privat, R., Jaubert, J.-N., and Mutelet, F., 2008, Predicting the phase equilibria of CO2 + hydrocarbon systems with the PPR78 model (PR EOS and kij calculated through a group contribution method): The Journal of Supercritical Fluids, v. 45, no. 1, p. 1-26.

Wiebe, R., and Gaddy, V., 1939, The solubility in water of carbon dioxide at 50, 75 and 100, at pressures to 700 atmospheres: Journal of the American Chemical Society, v. 61, no. 2, p. 315-318.

Wiebe, R., and Gaddy, V., 1940, The solubility of carbon dioxide in water at various temperatures from 12 to 40 and at pressures to 500 atmospheres. Critical phenomena*: Journal of the American Chemical Society, v. 62, no. 4, p. 815-817.

Wiebe, R., and Gaddy, V., 1941, Vapor phase composition of carbon dioxide-water mixtures at various temperatures and at pressures to 700 atmospheres: Journal of the American Chemical Society, v. 63, no. 2, p. 475-477.

Yan, W., Huang, S., and Stenby, E. H., 2011, Measurement and modeling of CO 2 solubility in NaCl brine and CO 2–saturated NaCl brine density: International Journal of Greenhouse Gas Control, v. 5, no. 6, p. 1460-1477.

Zawisza, A., and Malesinska, B., 1981, Solubility of carbon dioxide in liquid water and of water in gaseous carbon dioxide in the range 0.2-5 MPa and at temperatures up to 473 K: Journal of Chemical and Engineering Data, v. 26, no. 4, p. 388-391.

Zel'vinskii, Y., 1937, Measurements of carbon dioxide solubility in water: Zhurn. Khim. Prom, v. 14, p. 1250-1257.

Zhao, H., Fedkin, M. V., Dilmore, R. M., and Lvov, S. N., 2015, Carbon dioxide solubility in aqueous solutions of sodium chloride at geological conditions: Experimental results at 323.15, 373.15, and 423.15 K and 150bar and modeling up to 573.15 K and 2000bar: Geochimica et Cosmochimica Acta, v. 149, p. 165-189.

Ziabakhsh-Ganji, Z., and Kooi, H., 2012, An equation of state for thermodynamic equilibrium of gas mixtures and brines to allow simulation of the effects of impurities in subsurface CO 2 storage: International Journal of Greenhouse Gas Control, v. 11, p. S21-S34.

Zirrahi, M., Azin, R., Hassanzadeh, H., and Moshfeghian, M., 2010, Prediction of water content of sour and acid gases: Fluid Phase Equilibria, v. 299, no. 2, p. 171-179.

CHAPTER III

A FAST AND ROBUST TOUGH2 MODULE TO SIMULATE GEOLOGICAL CO_2 STORAGE IN SALINE AQUIFERS

Babak Shabani, Javier Vilcáez*

Boone Pickens School of Geology, Oklahoma State University, Stillwater, OK 74078, USA

3.1. Abstract

A new TOUGH2 module to simulate geological CO_2 storage (GCS) in saline aquifers is developed based on the widely employed ECO2N module of TOUGH2. The newly developed TOUGH2 module uses a new non-iterative fugacity-activity thermodynamic model to obtain the partitioning of CO_2 and H_2O between the aqueous and gas phases. Simple but robust thermophysical correlations are used to obtain density, viscosity, and enthalpy of the gas phase. The implementation and accuracy of the employed thermophysical correlations are verified by comparisons against the national institute of standards and technology (NIST) online thermophysical database. To assess the computation accuracy and efficiency, simulation results obtained with the new TOUGH2 module for a one-dimensional non-isothermal radial and a three-dimensional isothermal system are compared against the simulation results obtained with the ECO2N module. Treating salt mass fraction in the aqueous phase as a constant, along with the inclusion of a non-iterative fugacity-activity thermodynamic model, and simple thermophysical correlations, resulted in simulations much faster than simulations with ECO2N module, without losing numerical accuracy. Both modules yield virtually identical results. Additional field-scale simulations of CO_2 injection into an

actual non-isothermal and heterogeneous geological formation confirmed that the new module is much faster than the ECO2N module in simulating complex field-scale conditions. Owing to its capability to handle CO_2-CH_4-H_2S-N_2 gas mixtures and its compatibility with TOUGHREACT, this new TOUGH2 module offers the possibility of developing a fast and robust TOUGHREACT module to predict the fate of CO_2 in GCS sites under biotic conditions where CO_2, CH_4, H_2S, and N_2 gases can be formed.

Keywords: Geological CO_2 storage; Saline aquifers; Non-iterative thermodynamic model; TOUGH2

*Corresponding author: vilcaez@okstate.edu (J. Vilcáez)

3.2. Introduction

Geological carbon storage (GCS) in deep underground geological formations is a promising method to mitigate emissions of CO_2 into the atmosphere. Among potential geological formations for CO_2 storage, depleted oil reservoirs and deep saline aquifers are of special interest because they provide pore space and trapping conditions for long term storage of CO_2. Four trapping mechanisms keep injected CO_2 underground, namely the structural, residual, solubility, and mineral trapping mechanisms. In the structural trapping mechanism, an impermeable cap rock prevents the upward migration of CO_2 due to buoyancy, in the residual trapping mechanism, disconnected CO_2 droplets are held permanently in small pore sizes by capillary forces, in the solubility trapping mechanism, CO_2 dissolves in the formation water and hydrocarbons, and in the mineral trapping mechanism, CO_2 reacts directly or indirectly with native minerals and organic matter forming immobile carbonate minerals (Hitchon, 1996; Zhang and Song, 2014).

Recent studies on the impact of CO_2 injection on the microbial community of saline aquifers using molecular biology techniques (Basso et al., 2009; Itavaara et al., 2011; Kotelnikova, 2002; Morozova et al., 2010; Mu et al., 2014) , have shown that methanogenic microbes and sulfate reducing bacteria (SRB) are capable of adapting to the extreme conditions of GCS. A metabolic shift occurs avoiding the complete inhibition of the microbial community. Similar responses have been observed in

oil reservoirs (pH<5, temperature > 50°C, salinity > 1.0 mol/L) flooded with CO_2, where the concentration of H_2-forming microbes either increased or remained unchanged (Fujiwara et al., 2006; Liu et al., 2015a; Liu et al., 2015b; Sugai et al., 2012), which imply that in depleted oil reservoirs and deep saline aquifers used for long term storage of CO_2, the fate and trapping of CO_2 may be affected by the activity of indigenous microbial communities (Peet et al., 2015).

Estimations of the long term effect of microbial activity on the fate and trapping of CO_2 in depleted oil reservoirs and deep saline aquifers used for CO_2 storage can be obtained by conducting numerical simulations. Several commercial and open source software exist to model and simulate GCS in depleted oil reservoirs and deep saline aquifers (e.g., ECLIPSE© (Schlumberger), GEM© (CMG), VIP-Comp© (Halliburton), and TOUGH2 family of codes (Lawrence Berkeley National Laboratory)). The capabilities of these software can be expanded to account for the transport and kinetic growth of indigenous microbes. This can allow predicting the fate and transport of bioproducts (e.g., CH_4, H_2S and N_2), and organic substrates (e.g., fatty acids, alkanes). However, incorporating microbial kinetic models and increasing the number of independent variables (microbes, bioproducts and substrates) would substantially increase the calculation time of these software. Coupling of reactive and multiphase flow processes is usually done through the application of sequential or iterative methods where kinetic and equilibrium reaction equations along with mass and heat conservation equations are solved for each independent variable iteratively (Vilcáez et al., 2013; Vilcáez et al., 2017; Vilcáez et al., 2008).

To the best of our knowledge, there is not any software to simulate the biogenic conversion of CO_2 to CH_4, and/or the biogenic formation of CO_2-CH_4-H_2S-N_2 gas mixtures from the biodegradation of organic substrates at GCS conditions. Accounting for this possibility is particularly important for depleted oil reservoirs where there is an ample source of organic substrates. In depleted oil reservoirs, microbial activity stimulated by the injection of CO_2 and/or nutrients can affect the fate and trapping of not only CO_2 but also the remaining oil in depleted oil reservoirs. For instance, methanogenic biodegradation of alkanes is a well-known process to occur in oil reservoirs (Dolfing et al., 2008; Jones

et al., 2008; Larter and di Primio, 2005; Scott et al., 1994), and its stimulation can be seen as a pathway for a new enhanced oil recovery method (Cai et al., 2015a; Cai et al., 2015b; Jones et al., 2008; Vilcáez, 2015a, b). A new TOUGHREACT module with expanded capabilities accounting for the activity of microbes and transport of their metabolic substrates and products, would be advantageous to assess the fate and trapping of CO_2 under biotic conditions as well as the economic value of stimulating methanogenic biodegradation of alkanes in depleted oil reservoirs.

TOUGHREACT is a numerical simulation program for chemically reactive non-isothermal flows of multiphase fluids in porous and fractured media. It was developed by introducing reactive chemistry into the multiphase flow code TOUGH2 (Xu et al., 2006). Hence, several TOUGHREACT modules could be derived from available TOUGH2 modules to simulate a variety of multiphase and multicomponent reactive transport processes (Pruess, 1991). ECO2N module of TOUGHREACT allows for the simulation of not only the dissolution but also the mineral trapping of CO_2 in deep saline aquifers. The latest version of TOUGHREACT includes microbial capabilities (Xu et al., 2014). However, ECO2N module of TOUGH2 can only handle pure CO_2 (Pruess and Spycher, 2007), limiting the applicability of TOUGHREACT-ECO2N to simulate the fate and trapping of CO_2 under biotic conditions. Accounting for the biogenic formation of CO_2, CH_4, H_2S, and N_2 is important because they can affect the trapping and conversion of both the injected CO_2 and available organic substrates (e.g., alkanes).

Because of the complex numerical schemes needed to couple bio-geochemical and multiphase processes and the large number of independent variables which would substantially increase the calculation time of a new TOUGHREACT-ECO2N module, the aim of this research is to reduce the calculation time of the ECO2N module of TOUGH2 and expand its capabilities to simulate the multiphase flow of CO_2-CH_4-H_2S-N_2 gas mixtures. The approach consists of using simple correlations to obtain the thermophysical (density, viscosity and enthalpy) properties of gas mixtures along with a

new non-iterative fugacity-activity thermodynamic model which can predict the mutual solubility of CO_2-CH_4-H_2S-N_2 gas mixtures in brine (Shabani and Vilcáez, 2017).

Similar to this research but with different objectives, other TOUGH2 modules have been developed based on other TOUGH2 modules. EOS7Cm was developed based on EOS7C module (Oldenburg et al., 2004) to simulate the flow of CO_2-CH_4-H_2S gas mixtures under high temperature, pressure, and salinity conditions (Lei et al., 2016). EOS7Cm uses an iterative thermodynamic model to solve the mutual solubility of CO_2-CH_4-H_2S gas mixtures in brine. TMGAS is another TOUGH2 module developed based on the TMVOC module to simulate the injection of gas mixtures into deep geological sites (Battistelli and Marcolini, 2009). TMGAS also uses an iterative thermodynamic model to solve the mutual solubility of acid gases (CO_2 and H_2S) in brine. The inclusion of iterative thermodynamic models in simulating the flow of gas mixtures has been proven to result in long calculation times (Battistelli and Marcolini, 2009). Thus, the necessity of using non-iterative thermodynamic models to reduce the calculation time of GCS is evident.

Prior to its coupling to TOUGHREACT, the efficiency of the new module developed based on the ECO2N module of TOUGH2 is verified by conducting simulations of CO_2 injection using synthetic and real one-dimensional (1D) and three-dimensional (3D) geological models.

3.3. Methodology

In the newly developed module, possible thermodynamic states include a single aqueous phase with or without dissolved CO_2, a single CO_2-rich phase that might be either gas or liquid CO_2 with dissolved H_2O, and a two-phase aqueous-CO_2 rich state. Supercritical CO_2 is treated as a gas phase, and salt (NaCl) is treated as component whose concertation in the aqueous phase remains unchanged over time and space. The possibility of a separate solid salt phase forming due to the precipitation of halite (NaCl) is not considered. This simplification is valid for the co-injection of CO_2 and brine, or the injection of CO_2 into a geological formation containing relatively low salinity formation waters, where

microbial activity is relevant and the formation of a solid separate salt phase is not possible and/or can be neglected. This simplification is made based on CO_2 storage capacity enhancements obtained through co-injecting CO_2 and brine into saline aquifers (Rathnaweera et al., 2016), as well as on proposed methods to stimulate microbial methanogenesis in depleted oil reservoirs that involves the co-injection of CO_2 and brine amended with nutrients (Vilcáez, 2015b).

Keeping the approach used in the ECO2N module of TOUGH2, the thermodynamic state of a single-phase system is defined by pressure, CO_2 mass fraction in the aqueous phase, and temperature, whereas the thermodynamic state of a two-phase system is defined by pressure, gas saturation, and temperature. For single-phase isothermal systems, the list of primary thermodynamic variables reduces pressure and CO_2 mass fraction in the aqueous phase, whereas, for two-phase isothermal systems, the list of primary thermodynamic variables reduces to pressure and gas saturation. The equilibrium gas and liquid CO_2 mass fractions at the specified temperature and pressure conditions are calculated using the non-iterative fugacity-activity thermodynamic model of Shabani and Vilcáez (2017).

3.3.1. Governing equations

TOUGH2 uses the integral finite difference method (IFDM) to solve the mass and heat balance equations for a system with NK components and NPH phases in equilibrium:

$$\frac{d}{dt}\int_{V_n} M^{(i)} \cdot dV = \int_{\Gamma_n} F^{(i)} \cdot n \, d\Gamma + \int_{V_n} Q^{(i)} \, dV$$

(1)

where subscript *i* is the index for the NK components in the system, M is the mass or energy accumulation term, F is the mass or energy flow term, and Q is the sink/source term of mass or energy.

The mass accumulation per volume of component *i* is given by:

$$M^{(i)} = \varphi \sum_{\beta=1}^{NPH} S_\beta \rho_\beta X_\beta^{(i)},\ i = 1, NK;\ \beta = 1, NPH$$

(2)

where β is the phase index, φ is porosity, S_β is saturation of phase β, ρ_β is density of phase β, and X_β^i is the mass fraction of component *i* in phase β.

The heat accumulation per volume of component *i* = NK + 1 (heat), in a multiphase system is calculated according to:

$$M^{(NK+1)} = \phi \sum_{\beta=1}^{NPH} S_\beta \rho_\beta u_\beta + (1-\phi)\rho_R C_R T \quad (3)$$

where u_β is the specific internal energy of phase β, ρ_R and C_R are grain density and specific heat of the rock respectively, and T is temperature.

The advective mass flux of component *i* is a sum over all phases in equilibrium:

$$F^{(i)} = \sum_{\beta=1}^{NPH} X_\beta^{(i)} F_\beta$$

(4)

where individual phase fluxes are given by a multi-phase version of Darcy's law:

$$F_\beta = -k \frac{k_{r\beta}}{\mu_\beta} \rho_\beta \left(\nabla P_\beta - \rho_\beta g\right)$$

(5)

where k is absolute permeability, $k_{r\beta}$ is relative permeability of phase β, μ_β is viscosity of phase β, and P_β is the fluid pressure in phase β, and g is the vector of gravitational acceleration.

Conductive and convective heat flux of component *i* = NK + 1 (heat) is given by:

$$F^{(NK+1)} = \sum_{\beta=1}^{NPH} H_\beta F_\beta + \lambda \nabla T$$

(6)

where H_β is specific enthalpy of phase β, and λ is thermal conductivity (Pruess, 1991).

In addition to the total sum of mass fractions (X_β^i) which must equal 1.0, capillary pressure and relative permeability equations are required to complete the solution of the resulting system of equations. The new TOUGH2 module uses the relative permeability and capillary pressure equations already available to all TOUGH2 modules. The difference between the ECO2N module and the new module is on the approach used to calculate X_β^i and the thermophysical properties including density, viscosity and enthalpy of the gas phase. While ECO2N module obtains the thermophysical properties of pure CO_2 by means of interpolation from tabular data extracted from the correlation of Altunin (1975), the new module uses correlations to obtain the thermophysical properties of pure CO_2. These correlations are implemented directly in the code. Also, different from the ECO2N module that uses the correlation of Spycher and Pruess (2005) to obtain the mutual solubility of CO_2 in brine, the new module uses a new non-iterative thermodynamic model capable of predicting the mutual solubility of CO_2-CH_4-H_2S-N_2 gas mixtures in brine. Details on this new non- iterative thermodynamic model, as well as a description of the correlations used to obtain thermophysical properties of the mixture of gases and brine are given below.

3.3.2. Mutual solubility of CO_2-CH_4-H_2S-N_2 gas mixture in brine

The new non-iterative activity-fugacity thermodynamic model of Shabani and Vilcáez (2017) is implemented into TOUGH2 source code as a set of new subroutines to consider the mutual solubility of CO_2-CH_4-H_2S-N_2 gas mixtures in brine. This thermodynamic model was developed by equating the chemical potential of each component in the gas and liquid phase at equilibrium:

$$h_i \gamma_i x_i = P \emptyset_i y_i \tag{7}$$

which can be rearranged to obtain K_i as follows:

$$K_i = \frac{y_i}{x_i} = \frac{h_i \gamma_i}{P \emptyset_i} \tag{8}$$

where K_i is the phase equilibrium constant of component *i*, h_i is Henry's constant of component *i*, γ_i is activity of component *i* in liquid phase, P is pressure, φ_i is fugacity of component *i* in gas phase, and y_i and x_i, respectively, are mole fractions of component *i* in gas and liquid phases.

Fugacity coefficients are calculated using Peng-Robinson (PR) EOS (Peng and Robinson, 1976) and activity coefficients are calculated using Pitzer formalism and Henry's law (Pitzer, 1973). Henry's constant of dissolved gases in the aqueous phase is calculated using the correlation of Akinfiev and Diamond (2003). Both PR EOS and correlations account for the effect of salt (NaCl) mass fraction in the calculations. Hence, the application of the non-iterative activity-fugacity thermodynamic model (Shabani and Vilcáez, 2017) to pure CO_2 gas, is equivalent to the thermodynamic model of Ziabakhsh-Ganji and Kooi (2012) who used a similar approach. Details on the calculation of the activity and fugacity coefficients and Henry's constant can be found in Shabani and Vilcáez (2017).

The molar fraction of H_2O in the gas phase (y_{H2O}) is calculated using the following equation:

$$y_{H2O} = \frac{1-\sum\frac{y_i}{K_i}}{\frac{1}{K_{H2O}}-\sum\frac{y_i}{K_i}}$$

(9)

where y_i is the initial molar fraction of CO_2, H_2S, CH_4, and N_2 in the gas phase. Application of Eq. (9) to pure CO_2-brine systems gives the equation proposed by Spycher et al. (2003). The calculated y_{H2O} is used to correct the molar fractions of CO_2, H_2S, CH_4, and N_2 in the gas phase using the following normalization equation:

$$y_i^n = \frac{y_i}{1+y_{H2O}}$$

(10)

where y_i^n is the normalized molar fractions of CO_2, H_2S, CH_4, and N_2 in the gas phase. By applying this simplification, the equilibrium molar fractions of all components including H_2O in brine is directly calculated from the following equation:

$$x_i = \frac{y_i^n}{K_i}$$

(11)

where x_i is the molar fraction of dissolved compounds in the aqueous phase, and y_i^n calculated from Eq. (10) is the molar fraction of each compound in the existing or injected mixture of gases. The mass fraction (X_β^i) of component *i* in the liquid (β = l) and gas (β = 2) phase is required to solve the mass accumulation and flow equations (Eqs. (2) and (4)), are obtained from the following equations:

$$X_l^i = x_i \times \frac{MW_i}{MW_l}$$

(12)

$$X_g^i = y_i^n \times \frac{MW_i}{MW_g}$$

(13)

where MW_i is molecular weight of component *i*, and MW_l and MW_g are average molecular weights of liquid and gas mixtures:

$$MW_g = \sum y_i^n MW_i$$

(14)

$$MW_l = \sum x_i MW_i$$

(15)

The effect of salt (NaCl) mass fraction on the molecular weight of the aqueous phase is taken into account by using the following equation:

$$MW_{brine} = \frac{MW_{H_2O}}{1-X_S+X_S(\frac{MW_{H_2O}}{MW_{NaCl}})}$$

(16)

where X_S is the mass fraction of NaCl in brine.

3.3.3. Thermophysical properties of the gas phase

Since at temperatures relevant for GCS under biotic condition (<100 °C), the concentration of H_2O in the CO_2-reach phase is very small (typically less than 1 mol%), thermophysical properties of pure CO_2 are used to represent the thermophysical properties of the gas phase.

3.3.3.1. Density

Density of CO_2 in the gas phase is calculated from PR EOS as follows (Shabani and Vilcáez, 2017):

$$v_g = \frac{Z_g RT}{P}$$

(17)

$$\rho = \frac{Mw_g}{v_g+c}$$

(18)

$$c = T_r^{6.27844} * (-8.18682 * P_r^{-0.94163} + 0.94612) + 2.49642$$

(19)

where v_g is the molar volume, Z_g is the gas compressibility factor, R is the gas constant, T is temperature, P is pressure, MW_g and ρ are the molecular weight and gas density of pure CO_2, respectively, and c is the volume shift parameter. We have found that calculated density values of pure CO_2 are more accurate if c is calculated as a function of both reduced temperature (T_r) and reduced pressure (P_r) rather than as a function of only T_r, or by using a constant c value (Al-Khoury and

Bundschuh, 2014). Compared to the online NIST database (NIST, 2017), the calculated density of pure CO_2 gas using the derived correlation for c (Eq. 19) has less than 1% error (Fig. 3.1).

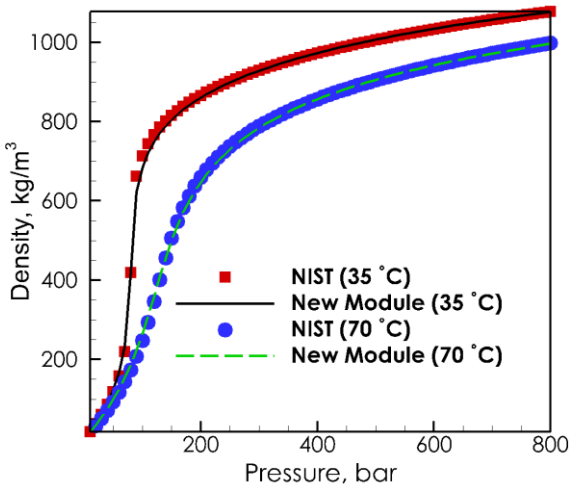

Fig. 3.1. Comparison of CO_2 density at 35 and 70 ˚C obtained with NIST database and the new module applying Peng-Robinson (PR) EOS.

3.3.3.2. Viscosity

Viscosity of the gas phase is estimated from the correlation developed from the one-parameter friction theory (Quiñones-Cisneros et al., 2000, 2001b). This general and simple correlation can be applied to hydrocarbon and acidic gases. This correlation in conjunction with the PR EOS has been shown to provide accurate viscosity estimations (Quiñones-Cisneros et al., 2001a; Schmidt et al., 2008). According to the one-parameter friction theory, the total fluid viscosity (η) can be estimated from:

$$\eta = \eta_o + \eta_f$$

(20)

where η_f is the friction viscosity that can be calculated from:

$$\eta_f = k_r p_r + k_a p_a$$

(21)

where p_r and p_a are the repulsive and attractive pressures that are calculated using PR EOS, k_r and k_a are the repulsive and attractive viscous friction coefficients. η_o in Eq. (20) is the diluted gas viscosity and can be calculated from:

$$\eta_o = 40.785 \frac{\sqrt{MW\,T}}{v_c^{2/3}\,\Omega^*} F_c$$

(22)

where MW is the molecular weight of the fluid (CO_2), T is the temperature, v_c is the critical volume, and F_c for non-polar gases such as CO_2 is:

$$F_c = 1 - 0.2756\,\omega$$

(23)

where ω is the acentric factor. The reduced collision integral (Ω*) in Eq. (22) is estimated from the following empirical equation:

$$\Omega^* = \frac{1.16145}{T^{*0.14874}} + \frac{0.52487}{\exp(0.7732\,T^*)} + \frac{2.16178}{\exp(2.43787\,T^*)} - 6.435\times10^{-4} T^{*0.14874} \sin\left(18.0323 T^{*-0.7683} - 7.27371\right)$$

(24)

with

$$T^* = \frac{1.2593 T}{T_c}$$

(25)

where T_c is the critical temperature. More details on the viscosity calculation procedure can be found at Quiñones-Cisneros et al. (2001a). Fig. 3.2 compares calculated and NIST values of CO_2 dynamic viscosity. The average error over a wide range of temperature and pressure conditions is around 5%.

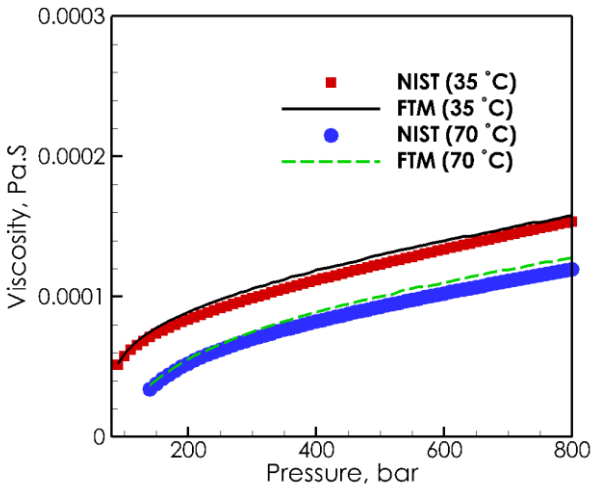

Fig. 3.2. Comparison of CO_2 dynamic viscosity at 35 and 70 ˚C obtained with NIST database and the new module applying the friction theory model (FTM).

3.3.3.3. Enthalpy

Enthalpy of the gas phase (H_g) is calculated as the sum of the departure enthalpy and ideal gas mixture enthalpy (Battistelli and Marcolini, 2009; Guide, 2015):

$$H_g = \sum_{i=1}^{n_c} y_i . H_{gi}^{ideal} + H_g^{departure}$$

(26)

This approach can be applied to both pure and mixture gases. The ideal enthalpy of gas component *i* (H_{gi}^{ideal}) is calculated by integrating the specific heat capacity (C_{pg}):

$$H_{gi}^{ideal} - H_{gi}^{reference} = \int_{T_1}^{T_2} C_{pg} dT$$

(27)

where the C_{pg} is a function of temperature according to the following fourth order polynomial equation:

$$C_{pg} = C_{pg1} + C_{pg2} T + C_{pg3} T^2 + C_{pg4} T^3 + C_{pg5} T^4$$

(28)

where C_{pg1} to C_{pg5} are coefficients (Poling et al., 2001). The temperature of the triple point of water (273.16 °K) is considered as the reference state.

The departure enthalpy of the gas phase ($H_g^{departure}$) can be calculated using either Lee-Kesler (LK) (Lee and Kesler (1975)) or PR EOS:

$$\mathrm{H}_g^{departure} = \mathrm{RT}\left(\left(\mathrm{Z}_g - 1\right) - \frac{\mathrm{A}}{2\sqrt{2}\mathrm{B}}\left(1 + \left(0.37646 + 1.5422\omega_i - 0.26992\omega_i^2\right)\sqrt{\frac{\mathrm{T}}{T_{c,i}\alpha_i}}\right)\ln\left(\frac{\mathrm{Z}_g + (1+\sqrt{2})B}{\mathrm{Z}_g + (1-\sqrt{2})B}\right)\right) \quad (29)$$

$$\alpha_i = 1 + \left(0.37464 + 1.5422\omega_i - 0.26992\omega_i^2\right)\left(1 - \sqrt{\frac{T}{T_{c,i}}}\right) \quad (30)$$

where R is the gas constant, T is temperature, ω is acentric factor, T_c is critical temperature, Z_g is gas compressibility factor obtained from PR EOS. Details on the calculation of A and B can be found in Shabani and Vilcáez (2017).

Both LK and PR EOS reproduce departure enthalpy very well, however, LK EOS provides more accurate results (1.5% AARD) than PR EOS (2.13% AARD). Fig. 3.3 compares calculated enthalpies of CO_2 using the LK and PR EOS against NIST data of CO_2 enthalpies.

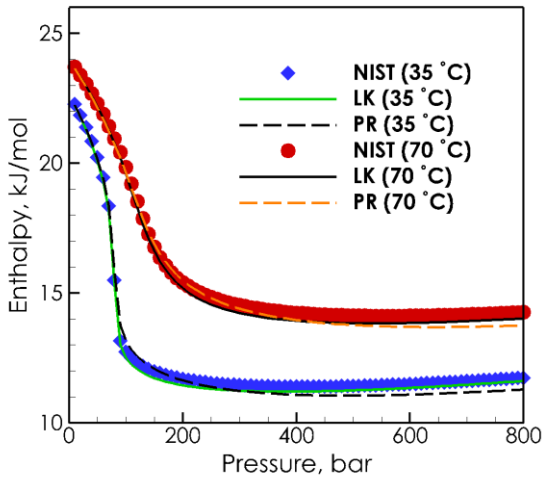

Fig. 3.3. Comparison of CO_2 enthalpy at 35 and 70 ˚C obtained with NIST database and the new module applying Lee-Kesler (LK) and Peng-Robinson (PR) EOSs.

3.3.4. Thermophysical properties of the liquid phase

Because deep geological formation waters are generally brine, thermophysical properties of the aqueous phase are calculated using correlations for pure brine in which corrections are made to account for the effect of CO_2 and other gases dissolution. This approach which has been already implemented in the ECO2N module is also used in the new TOUGH2 module. Briefly, the aqueous phase density is first calculated for pure H_2O using the correlation given by the International Formulation Committee (Committee, 1967), then corrections are made to account for the effect of temperature, pressure, and salinity using correlations of Haas Jr (1976) and Andersen et al. (1992), finally the effect of CO_2 dissolution into the aqueous phase is taken into account using Garcia (2001) correlation.

The viscosity of the aqueous phase is calculated from the correlation developed by Phillips (1981) which is valid for a wide range of temperature, pressure and salinity conditions, and the specific enthalpy of the aqueous phase is calculated using the correlation of Lorenz et al. (2000).

3.4. Verification, evaluation and application

To verify the accuracy and applicability of the new TOUGH2 module, simulation results obtained with the new TOUGH2 module are compared against the simulation results obtained with the ECO2N module.

3.4.1. Verification: 1D non-isothermal radial flow of CO_2 in a saline aquifer

To verify the accuracy of the new module, the 1D simulation example included in the manual of ECO2N module (Pruess, 2005) is rerun using both the new module and ECO2N module. In this 1D radial model of infinite extent, CO_2 is injected for 5 years at a constant rate of 100 kg/s. The saline aquifer is homogeneous and has a thickness of 100 m. The initial pressure of the aquifer is 120 bar, the initial temperature is 45 °C, and salt (NaCl) mass fraction is 0.15. Fig. 3.4 compares the pressure, gas saturation, mass fraction of CO_2 in brine, and mass fraction of H_2O in the gas phase obtained with both modules. The new module yields practically the same results as the ECO2N module. Since the new module does not treat solid salt as a separate phase, but rather its concentration in the aqueous phase is assumed to remain constant, and the approach to calculate the thermophysical properties (density, enthalpy, and dynamic viscosity) of the gas phase in both modules are different, a slight difference in predicting the mutual solubility of CO_2 in brine is inevitable.

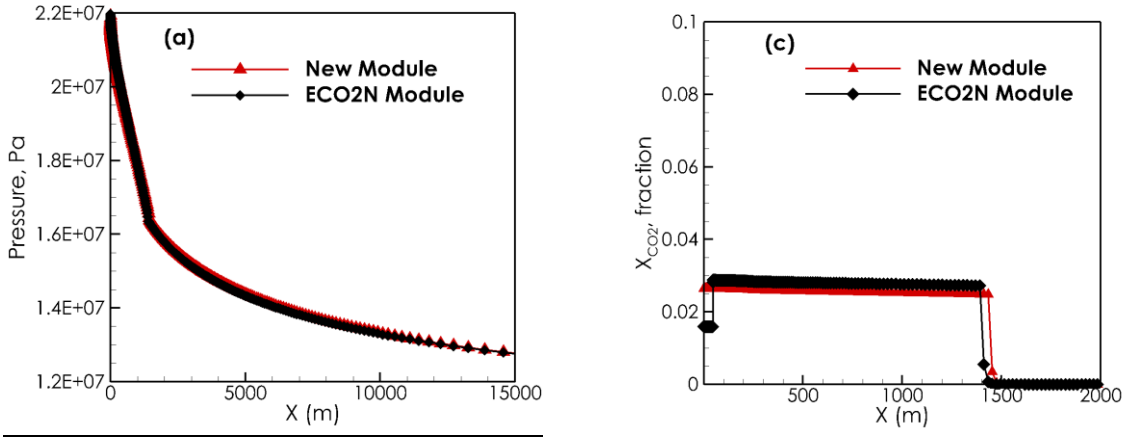

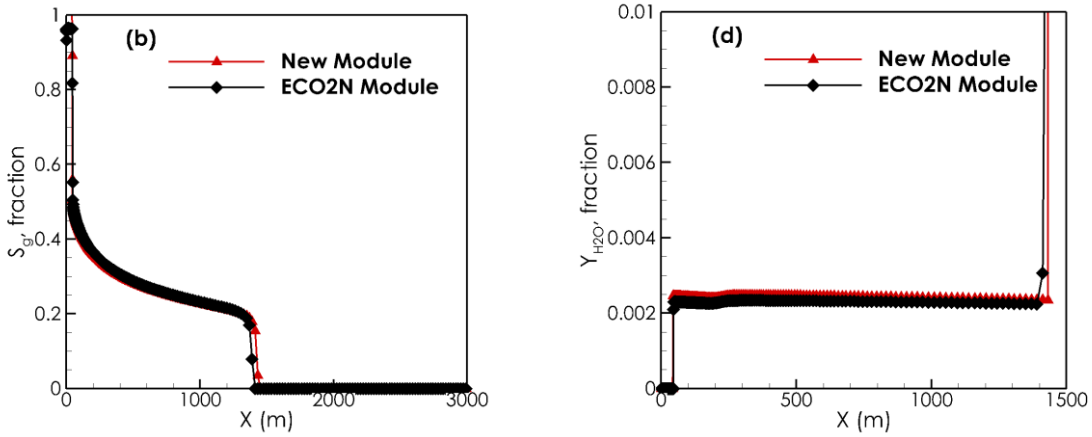

Fig. 3.4. Comparison of simulation results of CO_2 injection into a 1D non- isothermal saline aquifer obtained with the new module and ECO2N module. (a) Reservoir pressure, (b) Gas saturation (S_g), (c) CO_2 mass fraction in the aqueous phase (X_{CO2}), and (d) H_2O mass fraction in the gas phase (Y_{H2O}). Simulation time is 5 years.

3.4.2. Evaluation: CO_2 injection into a synthetic saline aquifer

To evaluate the computational efficiency of the new module, simulations of CO_2 injection into a large 3D rectangular (1000×1000×100 m^3) synthetic saline aquifer are conducted at three different grid cell resolutions (Table 3.1). Initial temperature and pressure conditions are 200 kPa and 40 °C, respectively. Salt (NaCl) mass fraction is 0.05, porosity is 0.1, and permeability in the three directions is 10^{-13} m^2. CO_2 is injected at 0.5 kg/s at the center of the model for 9 years.

Table 3.1. Grid cell resolutions used to evaluate the efficiency of the new module.

Grid cell resolution	**X-direction No. cells × size (m)**	**Y-direction No. cells × size (m)**	**Z-direction No. cells × size (m)**	**No. of grid cells**
1	5×91+3×30+5×91	5×91+3×30+5×91	5×20	845
2	9×50+5×20+9×50	9×50+5×20+9×50	5×20	2880
3	18×25+10×10+18×25	18×25+10×10+18×25	5×20	10580

Table 3.2 shows the total number of time steps, total calculation time, and the CPU times used by the EOS (solves the non-iterative EOS and thermophysical correlations), MULTI (sets up the system

of linear equations), and LINEQ (solves the linear system of equations) subroutines, with both ECO2N and new modules, at different grid cell resolutions (Table 3.1).

Shorter total calculation times obtained with the new model than with the ECO2N module reveals an enhancement in the computational efficiency of ECO2N. This enhancement increases with increasing the number of discretization grid cells. Apparently, the faster convergence achieved with the new module, reflected by the shorter total number of time steps needed to complete the simulation, is amplified by increasing the number of grid cells. In TOUGH2, time steps can be automatically adjusted during a simulation run, depending on the convergence rate of the iteration process.

A comparison between the CPU times used by the LINEQ, MULTI, and EOS subroutines, shows that most efficiency with the new module, is gained due to shorter CPU times used by the LINEQ and MULTI subroutines, rather than due to the shorter CPU time used by the EOS subroutine. This is attributed to the reduction of the number of primary variables from four (temperature, pressure, CO_2 mass fraction or gas saturation, and salt mass fraction) to three (temperature, pressure, and CO_2 mass fraction or gas saturation) by treating salt (NaCl) mass fraction as a constant. However, it is noteworthy that the new EOS subroutine where the new non-iterative EOS and the thermophysical correlations are solved, does contribute to the efficiency gained with the new module. This contribution is particularly evident when simulating larger and more complex scenarios (Fig. 3.6), as shown in the following section.

Table 3.2. Comparison of new module's efficiency against ECO2N module's efficiency.

Grid cell resolution	LINEQ, sec	MULTI, sec	EOS, sec	Total No. of time steps	Total time, sec	Memory usage, MB
ECO2N module						
1	28.3	3.2	1.2	71	69.8	1111
2	176.3	12.8	4.8	83	326.7	1110
3	3374.7	102.5	36.3	162	4340.9	1111
4*	5363.9	839.5	277.3	805	12888.8	1110
New module						
1	9.7	1.6	1.3	64	50.6	1120

2	49.4	6.6	4.6	80	193.5	1120
3	798.0	57.6	35.4	157	1828.6	1120
4*	928.8	87.1	45.0	316	3020.9	1120

*Cushing oil field

Fig. 3.5 compares the pressure, gas saturation, mass fraction of CO_2 in brine, and mass fraction of H_2O in the gas phase obtained with the new and ECO2N modules in a grid cell located at a horizontal distance of 56.5 and a vertical distance of 50 m from the injection point. Simulation results obtained with both modules are virtually the same, confirming that accuracy with the new module is preserved. Salt mass fraction in the aqueous phase predicted by the ECO2N module did decrease from 0.05 to 0.047 (results not shown), however this did not result in a substantial difference between CO_2 mass fractions in the aqueous phase predicted by both modules, confirming that at salinity levels where microbial activity is relevant, salt mass fraction in the aqueous phase can be assumed to remain constant.

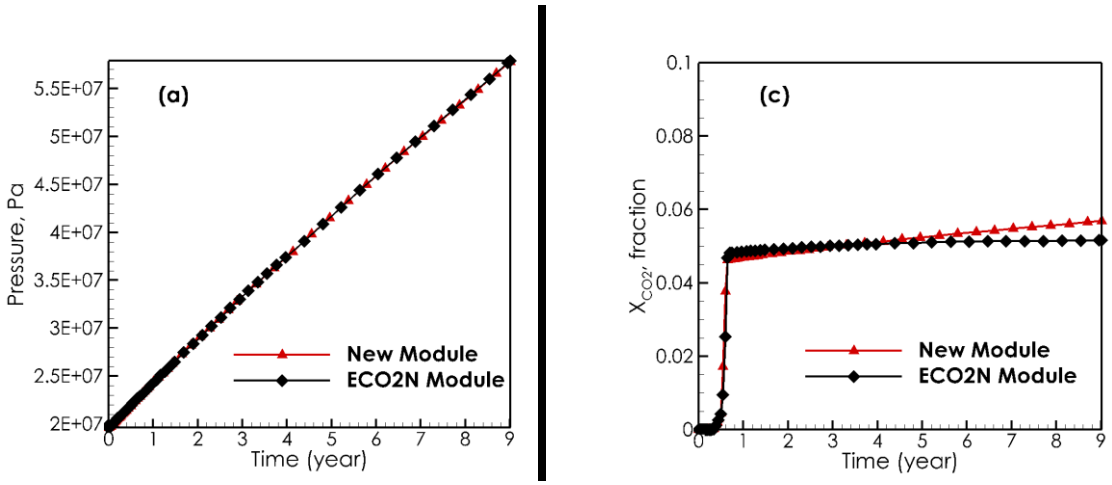

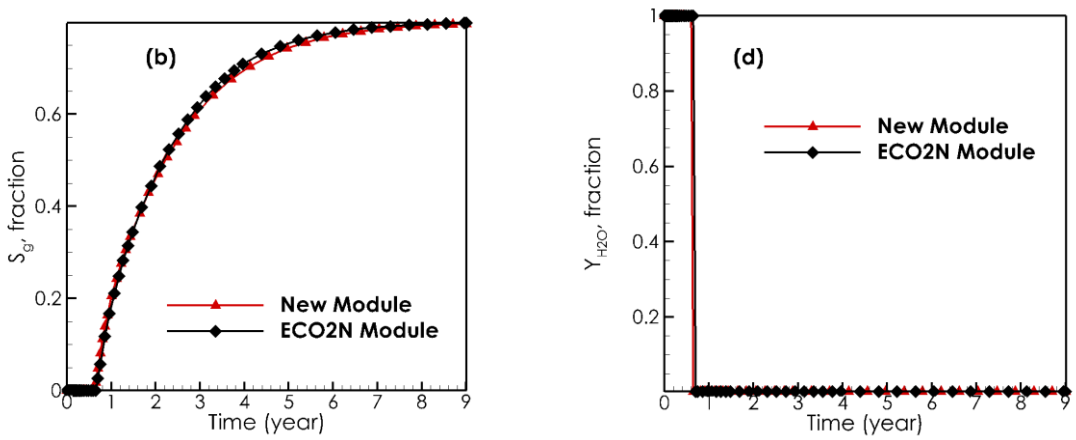

Fig. 3.5. Comparison of simulation results of CO_2 injection into a synthetic saline aquifer (1000×1000×100 m^3) obtained with the new module and ECO2N module. (a) Reservoir pressure, (b) Gas saturation (S_g), (c) CO_2 mass fraction in the aqueous phase (X_{CO2}), and (d) H_2O mass fraction in the gas phase (Y_{H2O}). Results correspond to a grid cell located at a horizontal distance of 56.5 and a vertical distance of 50 m from the injection point. Total number of grid cells is 2880.

3.4.3. Application: Injection of CO_2 into the Cushing oil field

To evaluate the applicability of the new module to real scenario conditions, simulation of CO_2 injection are conducted for the Cushing oil field. The Cushing oil field is roughly ten miles long (N-S) by three miles wide (E-W). It is located in northwestern part of Creek County, Oklahoma, USA. The initial vertical pressure and temperature distributions are determined using typical pressure and temperature gradients of 0.00875 MPa/m and 0.025 °C/m, respectively. The employed 3D model for this simulation has been generated based on log data available for 48 wells. At a depth of 1054 m (reservoir bottom), pressure and temperature are 9.22 MPa and 46.35°C, respectively. This reservoir consists of 15 different layers of porosities ranging from 0.01 to 0.2, and permeabilities ranging from 9.87×10^{-12} m^2 to 1.88×10^{-10} m^2 (Fig. 3.6). CO_2 is injected at the bottom of the geological formation at 6.5 kg/s, and salt (NaCl) mass fraction is 0.01. The remaining oil in the reservoir is assumed to be immobile.

Figs. 3.7 and 3.8 show the distribution of gas saturation, and CO_2 mass fraction in the aqueous phase obtained with both the new and ECO2N modules after 10 years of simulation. A comparison

between the simulation results obtained with both modules probes that the new module reproduces simulation results obtained with the ECO2N module. Moreover, the contribution of the new EOS subroutine to the computational efficiency gained with the new module, is much larger than when simulating simpler scenarios (Fig. 3.5). Table 3.2 shows that the CPU time used by the EOS subroutine decreases from 277.3 to 45.0 seconds, and that the total number of time steps decreases from 805 to 316. Meaning that the CPU time used by the EOS subroutine in the ECO2N module for each time step is 2.41 times larger than the CPU time used by the EOS subroutine in the new module. This is reflected by a reduction in the total calculation time from 12888.8 to 3020.9 seconds.

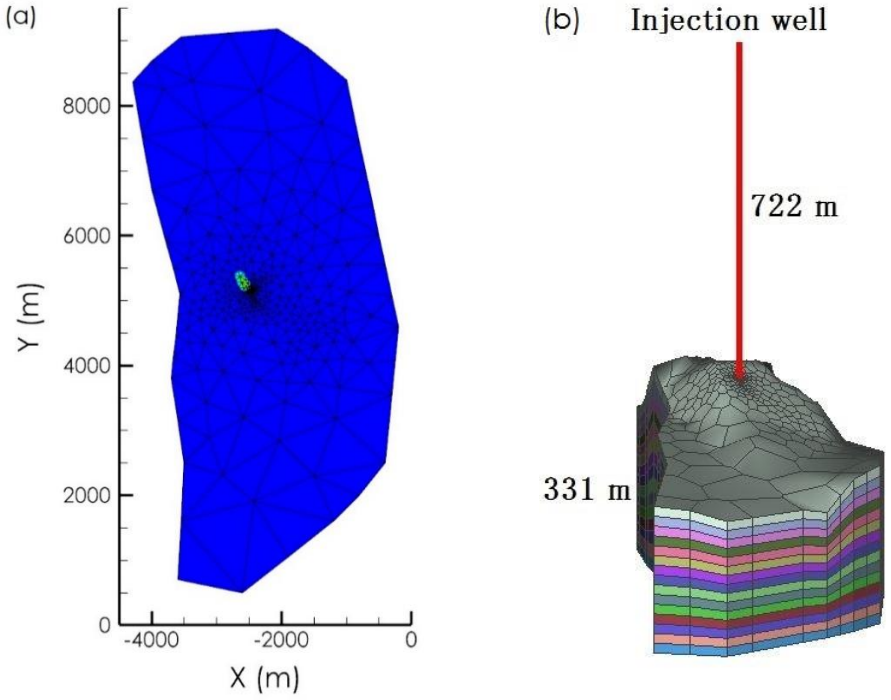

Fig. 3.6. Geological model of the Cushing oil field. (a) top view, (b) vertical view.

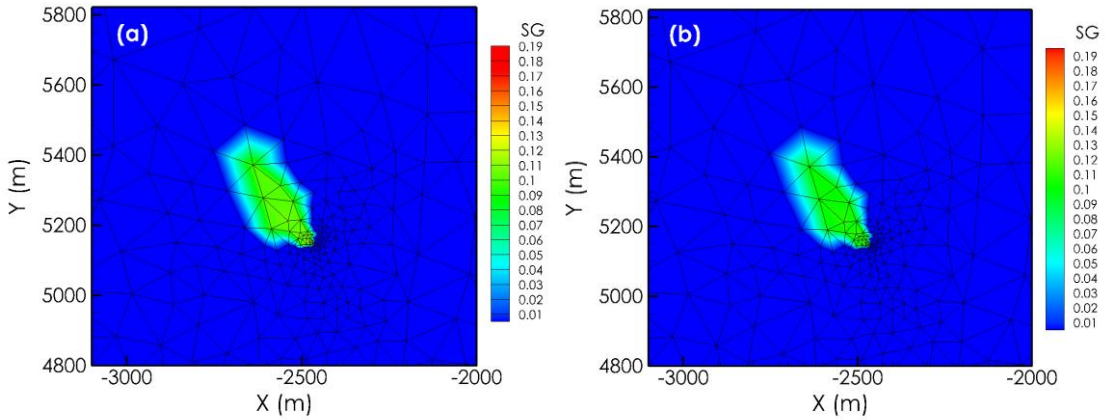

Fig. 3.7. Comparison of CO_2 gas saturation (Sg) in the Cushing oil field predicted with the (a) New module and (b) ECO2N module. Simulation time is 10 years.

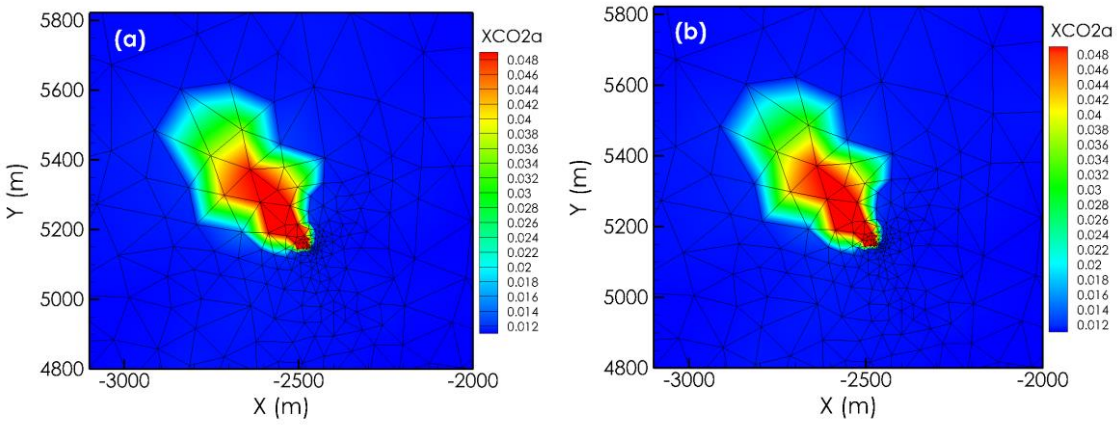

Fig. 3.8. Comparison of CO_2 mass fraction in the aqueous phase (X_{CO2}) in the Cushing oil field predicted with the (a) New module and (b) ECO2N module. Simulation time is 10 years.

3.5. Conclusions

A simple and robust TOUGH2 module has been developed to simulate geological CO_2 storage in deep saline aquifers. Not including salt mass fraction as a variable but as a constant, along with the utilization of a new non-iterative activity-fugacity thermodynamic model and simple thermophysical

correlations have been found significantly reduces the simulation time of the ECO2N module of TOUGH2.

Minor differences between the simulated results obtained with the new and ECO2N modules is attributed to the intrinsic differences between the approaches uses to calculate the thermophysical properties of the gas phase in both modules, and to the fact that the new module does not treat salt (NaCl) as a separate solid phase, but rather its concentration in the aqueous phase is assumed to remain constant.

Estimated thermophysical (density, viscosity, and enthalpy) properties of the gas phase using the selected thermophysical correlations are in good agreement with NIST thermophysical data. The inclusion of a variable volume shift factor resulted in highly accurate predictions of CO_2 gas density over a wide range of pressure and temperature conditions.

The EOS and the thermophysical correlations used to develop the new TOUGH2 module can handle CO_2-CH_4-H_2S-N_2 gas mixtures. Hence, owing to its compatibility with TOUGHREACT, the new module can be used to develop a new TOUGHREACT module to predict the impact of microbial activity on the fate and trapping of CO_2 in geological CO_2 storage sites under biotic conditions where microbial activity can be reflected by the formation of CO_2, CH_4, H_2S, and N_2 biogases.

3.6. Acknowledgement

This is Oklahoma State University Boone Pickens School of Geology contribution number 2017-74

3.7. References

Akinfiev, N. N., and Diamond, L. W., 2003, Thermodynamic description of aqueous nonelectrolytes at infinite dilution over a wide range of state parameters: Geochimica et Cosmochimica Acta, v. 67, no. 4, p. 613-629.

Al-Khoury, R., and Bundschuh, J., 2014, Computational Models for CO2 Geo-sequestration & Compressed Air Energy Storage, CRC Press.

Altunin, V., 1975, Thermophysical properties of carbon dioxide, Publishing House of Standards Moscow.

Andersen, G., Probst, A., Murray, L., and Butler, S., An Accurate PVT Model for Geothermal Fluids as Represented by H2O-NaCl-CO2, in Proceedings Mixtures, Proceedings 17th Workshop on Geothermal Reservoir Engineering1992, Citeseer.

Basso, O., Lascourreges, J.-F., Le Borgne, F., Le Goff, C., and Magot, M., 2009, Characterization by culture and molecular analysis of the microbial diversity of a deep subsurface gas storage aquifer: Research in microbiology, v. 160, no. 2, p. 107-116.

Battistelli, A., and Marcolini, M., 2009, TMGAS: a new TOUGH2 EOS module for the numerical simulation of gas mixtures injection in geological structures: International Journal of Greenhouse Gas Control, v. 3, no. 4, p. 481-493.

Cai, M., Jiménez, N., Krüger, M., Guo, H., Jun, Y., Straaten, N., and Richnow, H. H., 2015a, Potential for aerobic and methanogenic oil biodegradation in a water flooded oil field (Dagang oil field): Fuel, v. 141, p. 143-153.

Cai, M., Yu, C., Wang, R., Si, Y., Masakorala, K., Yuan, H., Yao, J., and Zhang, J., 2015b, Effects of oxygen injection on oil biodegradation and biodiversity of reservoir microorganisms in Dagang oil field, China: International Biodeterioration & Biodegradation, v. 98, p. 59-65.

Committee, I. F., 1967, A formulation of the thermodynamic properties of ordinary water substance: Memoirs of the Faculty of Engineering, Kyoto University, v. IFC Secretariat, Düsseldorf, Germany.

Dolfing, J., Larter, S. R., and Head, I. M., 2008, Thermodynamic constraints on methanogenic crude oil biodegradation: The ISME journal, v. 2, no. 4, p. 442-452.

Fujiwara, K., Mukaidani, T., Kano, S., Hattori, Y., Maeda, H., Miyagawa, Y., Tkakabayashi, K., and Okatsu, K., Research study for microbial restoration of methane deposit with subsurface CO2 sequestration into depleted gas/oil fields, in Proceedings SPE Asia Pacific Oil & Gas Conference and Exhibition2006, Society of Petroleum Engineers.

Garcia, J. E., 2001, Density of aqueous solutions of CO2: Lawrence Berkeley National Laboratory.

Guide, S. U. s., 2015, Advanced process and thermal reservoir simulator: by Computer Modelling Group Ltd., Alberta Canadá.

Haas Jr, J. L., 1976, Thermodynamics properties of the coexisting phases and thermochemical properties of the NaCl component in boiling NaCl solutions: US, Geol. Surv., Bull.;(United States), v. 1421.

Hitchon, B., 1996, Aquifer disposal of carbon dioxide: hydrodynamic and mineral trapping-proof of concept.

Itavaara, M., Nyyssonen, M., Kapanen, A., Nousiainen, A., Ahonen, L., and Kukkonen, I., 2011, Characterization of bacterial diversity to a depth of 1500 m in the Outokumpu deep borehole, Fennoscandian Shield: FEMS Microbiol Ecol, v. 77, no. 2, p. 295-309.

Jones, D., Head, I., Gray, N., Adams, J., Rowan, A., Aitken, C., Bennett, B., Huang, H., Brown, A., and Bowler, B., 2008, Crude-oil biodegradation via methanogenesis in subsurface petroleum reservoirs: Nature, v. 451, no. 7175, p. 176-180.

Kotelnikova, S., 2002, Microbial production and oxidation of methane in deep subsurface: Earth-Science Reviews, v. 58, no. 3, p. 367-395.

Larter, S., and di Primio, R., 2005, Effects of biodegradation on oil and gas field PVT properties and the origin of oil rimmed gas accumulations: Organic Geochemistry, v. 36, no. 2, p. 299-310.

Lee, B. I., and Kesler, M. G., 1975, A generalized thermodynamic correlation based on three-parameter corresponding states: AIChE Journal, v. 21, no. 3, p. 510-527.

Lei, H., Li, J., Li, X., and Jiang, Z., 2016, EOS7Cm: An improved TOUGH2 module for simulating non-isothermal multiphase and multicomponent flow in CO 2–H 2 S–CH 4–brine systems with high pressure, temperature and salinity: Computers & Geosciences, v. 94, p. 150-161.

Liu, J.-F., Sun, X.-B., Yang, G.-C., Mbadinga, S. M., Gu, J.-D., and Mu, B.-Z., 2015a, Analysis of microbial communities in the oil reservoir subjected to CO2-flooding by using functional genes as molecular biomarkers for microbial CO2 sequestration: Frontiers in microbiology, v. 6.

Liu, J.-F., Sun, X.-B., Yang, G.-C., Mbadinga, S. M., Gu, J.-D., and Mu, B., 2015b, Analysis of Microbial Communities in the Oil Reservoir Subjected to CO2-Flooding by Using Functional Genes as Molecular Biomarkers for Microbial CO2 Sequestration: Frontiers in Microbiology, v. 6.

Lorenz, S., Maric, D., and Rirschl, C., 2000, Eine analytische Funktion zur Bestimmung der Enthalpie wässriger NaCl Lösungen, draft report: Institut für Sicherheitstechnologie, Köln, Germany.

Morozova, D., Wandrey, M., Alawi, M., Zimmer, M., Vieth, A., Zettlitzer, M., Würdemann, H., and Group, C. S., 2010, Monitoring of the microbial community composition in saline aquifers during CO 2 storage by fluorescence in situ hybridisation: International Journal of Greenhouse Gas Control, v. 4, no. 6, p. 981-989.

Mu, A., Boreham, C., Leong, H. X., Haese, R., and Moreau, J. W., 2014, Changes in the deep subsurface microbial biosphere resulting from a field-scale CO2 geosequestration experiment: Frontiers in Microbiology, v. 5.

NIST, 2017, Thermophysical Properties of Fluid Systems, http://webbook.nist.gov/chemistry/fluid/.

Oldenburg, C. M., Moridis, G. J., Spycher, N., and Pruess, K., 2004, EOS7C version 1.0: TOUGH2 module for carbon dioxide or nitrogen in natural gas (methane) reservoirs: Lawrence Berkeley National Laboratory.

Peet, K. C., Freedman, A. J., Hernandez, H. H., Britto, V., Boreham, C., Ajo-Franklin, J. B., and Thompson, J. R., 2015, Microbial growth under supercritical CO2: Applied and environmental microbiology, v. 81, no. 8, p. 2881-2892.

Peng, D.-Y., and Robinson, D. B., 1976, A new two-constant equation of state: Industrial & Engineering Chemistry Fundamentals, v. 15, no. 1, p. 59-64.

Phillips, S., 1981, A technical databook for geothermal energy utilization: Lawrence Berkeley National Laboratory.

Pitzer, K. S., 1973, Thermodynamics of electrolytes. I. Theoretical basis and general equations: The Journal of Physical Chemistry, v. 77, no. 2, p. 268-277.

Poling, B. E., Prausnitz, J. M., and O'connell, J. P., 2001, The properties of gases and liquids, Mcgraw-hill New York.

Pruess, K., 1991, TOUGH2: A general-purpose numerical simulator for multiphase fluid and heat flow, Lawrence Berkeley Lab. Berekeley, California.

Pruess, K., 2005, TOUGH2-ECO2N Users Guide.

Pruess, K., and Spycher, N., 2007, ECO2N – A fluid property module for the TOUGH2 code for studies of CO2 storage in saline aquifers: Energy Conversion and Management, v. 48, no. 6, p. 1761-1767.

Quiñones-Cisneros, S. E., Zéberg-Mikkelsen, C. K., and Stenby, E. H., 2000, The friction theory (f-theory) for viscosity modeling: Fluid Phase Equilibria, v. 169, no. 2, p. 249-276.

-, 2001a, The friction theory for viscosity modeling: extension to crude oil systems: Chemical engineering science, v. 56, no. 24, p. 7007-7015.

-, 2001b, One parameter friction theory models for viscosity: Fluid Phase Equilibria, v. 178, no. 1, p. 1-16.

Rathnaweera, T. D., Ranjith, P. G., Perera, M. S. A., and Haque, A., 2016, Influence of CO2–Brine Co-injection on CO2 Storage Capacity Enhancement in Deep Saline Aquifers: An Experimental Study on Hawkesbury Sandstone Formation: Energy & Fuels, v. 30, no. 5, p. 4229-4243.

Schmidt, K. A., Quinones-Cisneros, S. E., Carroll, J. J., and Kvamme, B., 2008, Hydrogen sulfide viscosity modeling: Energy & Fuels, v. 22, no. 5, p. 3424-3434.

Scott, A. R., Kaiser, W., and Ayers Jr, W. B., 1994, Thermogenic and secondary biogenic gases, San Juan basin, Colorado and New Mexico--implications for coalbed gas producibility: AAPG bulletin, v. 78, no. 8, p. 1186-1209.

Shabani, B., and Vilcáez, J., 2017, Prediction of CO2-CH4-H2S-N 2 gas mixtures solubility in brine using a non-iterative fugacity-activity model relevant to CO2-MEOR: Journal of Petroleum Science and Engineering, v. 150, p. 162-179.

Spycher, N., and Pruess, K., 2005, CO2–H2O mixtures in the geological sequestration of CO2. II. Partitioning in chlorine brine at 12-100 C and up tp 600 bar: Geochim. Cosmochim. Acta, v. 69, no. 13, p. 3309-3320.

Spycher, N., Pruess, K., and Ennis-King, J., 2003, CO 2-H 2 O mixtures in the geological sequestration of CO 2. I. Assessment and calculation of mutual solubilities from 12 to 100 C and up to 600 bar: Geochimica et cosmochimica acta, v. 67, no. 16, p. 3015-3031.

Sugai, Y., Purwasena, I. A., Sasaki, K., Fujiwara, K., Hattori, Y., and Okatsu, K., 2012, Experimental studies on indigenous hydrocarbon-degrading and hydrogen-producing bacteria in an oilfield for microbial restoration of natural gas deposits with CO 2 sequestration: Journal of Natural Gas Science and Engineering, v. 5, p. 31-41.

Vilcáez, J., 2015a, Numerical modeling and simulation of microbial methanogenesis in geological CO 2 storage sites: Journal of Petroleum Science and Engineering, v. 135, p. 583-595.

-, 2015b, Stimulating effect of protein-rich matter on the biogenic conversion of CO2 to CH4: Journal of CO2 Utilization, v. 10, no. 0, p. 60-66.

Vilcáez, J., Li, L., Wu, D., and Hubbard, S. S., 2013, Reactive Transport Modeling of Induced Selective Plugging by Leuconostoc Mesenteroides in Carbonate Formations: Geomicrobiology Journal, v. 30, no. 9, p. 813-828.

Vilcáez, J., Morad, S., and Shikazono, N., 2017, Pore-scale simulation of transport properties of carbonate rocks using FIB-SEM 3D microstructure: Implications for field scale solute transport simulations: Journal of Natural Gas Science and Engineering, v. 42, p. 13-22.

Vilcáez, J., Suto, K., and Inoue, C., 2008, Modeling the auto-thermal performance of a thermophilic bioleaching heap employing mesophilic and thermophilic microbes: Hydrometallurgy, v. 94, no. 1–4, p. 82-92.

Xu, T., Sonnenthal, E., Spycher, N., and Pruess, K., 2006, TOUGHREACT—a simulation program for non-isothermal multiphase reactive geochemical transport in variably saturated geologic media: applications to geothermal injectivity and CO 2 geological sequestration: Computers & Geosciences, v. 32, no. 2, p. 145-165.

Xu, T., Sonnenthal, E., Spycher, N., and Zheng, L., 2014, TOUGHREACT V3. 0-OMP Reference Manual: A Parallel Simulation Program for Non-Isothermal Multiphase Geochemical Reactive Transport. LBNL-DRAFT: University of California, Berkeley, CA, v. 94720.

Zhang, D., and Song, J., 2014, Mechanisms for geological carbon sequestration: Procedia IUTAm, v. 10, p. 319-327.

Ziabakhsh-Ganji, Z., and Kooi, H., 2012, An equation of state for thermodynamic equilibrium of gas mixtures and brines to allow simulation of the effects of impurities in subsurface CO 2 storage: International Journal of Greenhouse Gas Control, v. 11, p. S21-S34.

CHAPTER IV

TOUGHREACT-CO2Bio – a new module to simulate geological carbon storage under biotic conditions (Part 1): the multiphase flow of CO_2-CH_4-H_2-H_2S gas mixtures

Babak Shabani, Javier Vilcáez*

Boone Pickens School of Geology, Oklahoma State University, Stillwater, OK 74078, USA

4.1. Abstract

A new TOUGHREACT module named CO2Bio is introduced to simulate geological carbon storage (GCS) under biotic conditions. CO2Bio is developed by incorporating into TOUGHREACT an expanded thermodynamic model capable of predicting the mutual solubility of CO_2-CH_4-H_2S-H_2 gas mixtures and brine. Simple but robust thermophysical correlations are adopted in CO2Bio to calculate density, viscosity and enthalpy of CO_2-CH_4-H_2S-H_2 gas mixtures. CO2Bio can predict the kinetic microbial production and/or consumption of CO_2, CH_4, H_2S, and H_2 gases, and the multiphase flow of CO_2-CH_4-H_2S-H_2 gas mixtures and brine at deep geological formation conditions. The multiphase flow capabilities of CO2Bio are verified by comparing its simulation results with other reliable multiphase simulation programs including the ECO2N module of TOUGHREACT, the EOS7C module of TOUGH2, and CMG-GEM©. Simulated scenarios include injection of CO_2 into a radial infinite acting saline aquifer, extraction of dissolved CH_4 from CH_4-saturated water by CO_2 injection, and injection of CO_2 mixed with H_2S as an impurity into a saline

aquifer. To verify the field-scale applicability of TOUGHREACT-CO2Bio, we conducted simulations for alternate injection of CO_2 and brine into the Cushing-Drumright oil reservoir of Oklahoma where the supply of nutrients such as protein-rich matter was assumed to result in the stimulation of microbial production of H_2 and CH_4 from the degradation of n-alkanes. Our simulation results confirm that TOUGHREACT-CO2Bio is capable of predicting the multiphase flow of CO_2-CH_4-H_2S-H_2 gas mixtures and brine.

Keywords: Geological carbon storage, Methanogenesis, CO_2-CH_4-H_2S-H_2 gas mixture, Thermophysical properties, TOUGHREACT-CO2Bio

*Corresponding author: vilcaez@okstate.edu (J. Vilcáez)

4.2. Introduction

Methanogenic biodegradation of crude oil (mostly n-alkanes) is a well-known process that occurs in oil reservoirs (Dolfing et al., 2008; Jones et al., 2008a; Larter and di Primio, 2005; Scott et al., 1994), and its stimulation has been seen as a pathway for a new enhanced oil recovery method (Cai et al., 2015a; Cai et al., 2015b; Jones et al., 2008b; Vilcáez, 2015b). Biodegradation of crude oil under anaerobic conditions generates acetate and H_2 as metabolic products (Eq. (1)). While the generated acetate is converted into CH_4 and CO_2 by acetoclastic methanogens via fermentation (Eq. (2)), the generated CO_2 is converted into CH_4 by hydrogenotrophic microbes via the reduction pathway with H_2 (Eq. (3)):

$$4C_{16}H_{34} + 64H_2O \rightarrow 32CH_3COO^- + 32H^+ + 68H_2 \quad (1)$$

$$32CH_3COO^- + 32H^+ \rightarrow 32CH_4 + 32CO_2 \quad (2)$$

$$196H_2 + 64CO_2 \rightarrow 49CH_4 + 15CO_2 + 98H_2O \quad (3)$$

H_2 is a key component for CH_4 production from CO_2 by hydrogenotrophic methanogens in oil reservoirs. The injection of CO_2 into depleted oil reservoirs increases its availability for CH_4 production

and decreases the pH of the formation water to acidic pH (4-6) levels where the activity of H_2-forming fermentative microbes is highest. For this, the combined injection of CO_2 and petroleum produced water supplied with nutrients such as protein-rich matter has been proposed to stimulate the microbial conversion of residual crude oil and CO_2 (substrates) to CH_4 in depleted oil reservoirs (Vilcáez, 2015a; Vilcáez, 2015b). The produced CH_4 in depleted oil reservoirs can be recovered more easily than residual crude oil. This highlights the promising potential of a shift towards a CH_4-based energy economy where microbially produced CH_4 in depleted oil reservoirs is commercialized as an energy source.

The stimulating effect of the combined injection of CO_2 and petroleum produced water supplied with nutrients such as protein-rich matter on the microbial conversion of crude oil (mostly n-alkanes) and CO_2 to CH_4 has been proven using formation water and crude oil collected from depleted oil reservoirs in Oklahoma (Vilcáez et al., 2018). The reported stimulating effect of CO_2 is in agreement with previous studies showing that CO_2 can be converted to CH_4 by indigenous anaerobic microbial communities in oil reservoirs (Jones et al., 2008a; Mayumi et al., 2011), and that CO_2 promotes the growth of H_2-forming microbes in depleted oil reservoirs (Liu et al., 2015; Sugai et al., 2012). The results of these studies highlight the need for simulation tools to not only predict the physical and chemical fate, but also the microbiological fate of CO_2 injected into depleted oil reservoirs. This can be considered for either geological storage of CO_2 or for enhanced oil recovery through the stimulation of microbial conversion of n-alkanes and CO_2 to CH_4.

Owing to its multiphase and geochemical capabilities, the latest version of TOUGHREACT (Xu et al., 2014), which includes microbial capabilities could be used to predict the physical, chemical, and microbiological fate of CO_2 injected into deep saline aquifers or depleted oil reservoirs (if crude oil is assumed to remain immobile). However, the ECO2N module of TOUGHREACT that is currently widely used to predict the physical and chemical fate of CO_2 in deep saline aquifers can only handle pure CO_2 (Pruess and Spycher, 2007). This limits its applicability to predict the microbiological effect of CO_2 in deep saline aquifers and depleted oil reservoirs. The microbial conversion of crude oil and

CO_2 to CH_4, for instance, involves the continuous production and/or consumption of CO_2, H_2, and acetate. This can affect the extent of the dissolution and mineral trapping of CO_2 as well as the kinetics of CH_4 production. Therefore, in this work we developed a new TOUGHREACT module, named CO2Bio, to predict the long-term trapping and fate of CO_2 in deep saline aquifers and depleted oil reservoirs under biotic conditions. This module accounts for the kinetics of the microbial production and/or consumption of CO_2, CH_4, H_2, and H_2S gases, as well as the multiphase flow of CO_2-CH_4-H_2-H_2S gas mixtures and brine. In this article, we introduce the multiphase flow capabilities of CO2Bio. The microbial capabilities of CO2Bio will be introduced in a subsequent article.

An important interaction that affects the multiphase flow of gas mixtures and brine is their mutual solubility. Therefore, thermodynamic models have been developed to predict the mutual solubility of CO_2-SO_2-H_2S-CH_4-N_2 gas mixtures and brine (Ziabakhsh-Ganji and Kooi, 2012), CO_2-H_2S-CH_4-N_2 gas mixtures and brine (Shabani and Vilcáez, 2017), and CO_2-CH_4-H_2S gas mixtures and brine (Li et al., 2014). Unfortunately, available thermodynamic models that have been developed to predict the mutual solubility of gas mixtures and brine do not account for the presence of H_2. Accounting for the presence of H_2 is important because H_2 constitutes a bottleneck for the microbial conversion of CO_2 to CH_4 (Eq. (3)). In this work, to be able to develop a new TOUGHREACT module (CO2Bio), which is capable of simulating the fate of CO_2 in deep geological formations under biotic conditions, we expanded the capabilities of the thermodynamic model of Ziabakhsh-Ganji and Kooi (2012) to predict the mutual solubility of CO_2-CH_4-H_2-H_2S gas mixtures and brine. The original thermodynamic model of Ziabakhsh-Ganji and Kooi can predict the mutual solubility of CO_2-SO_2-H_2S-CH_4-N_2 gas mixtures and brine within a wide range of pressure, temperature, and salinity conditions. Here, we did not include SO_2 and N_2 in CO2Bio, because these two components have no role in the microbial conversion of CO_2 and/or crude oil to CH_4 in deep saline aquifers or depleted oil reservoirs. We included H_2S in CO2Bio, because sulfate reducing bacteria (SRB) under the availability of high concentrations of sulfate ions can outcompete methanogenic microbes for H_2 and acetate. Therefore,

including the possibility of H_2S formation by SRB is crucial to assess the feasibility of CH_4 production in depleted oil reservoirs and deep saline aquifers.

The expansion of the capabilities of Ziabakhsh-Ganji and Kooi's thermodynamic model to predict the mutual solubility of CO_2-CH_4-H_2-H_2S gas mixtures and brine involves the estimation of thermodynamic parameters to calculate the fugacity and activity coefficients of CO_2, CH_4, H_2, and H_2S in the gas and liquid phases in equilibrium. Ideally, this should be done by correlating results from the thermodynamic model with experimental data of mutual solubility of CO_2-CH_4-H_2-H_2S gas mixtures and brine. However, experimental data of CO_2-CH_4-H_2-H_2S gas mixtures and brine mutual solubility at high pressures (> 100 bar) and temperatures (> 50 °C) are not readily available in literature. Hence, in this work we estimated the required parameters to predict the mutual solubility of H_2 and brine by correlating results of the thermodynamic model with simulation results obtained using a thermodynamic model developed to predict the solubility of pure H_2 in brine.

Many correlations can be found in literature, which can be used to predict thermophysical properties (density, viscosity and enthalpy) of gas mixtures. For example, Shabani and Vilcáez (2018) used a simple approach to calculate the thermophysical properties of CO_2-H_2S-CH_4-N_2 gas mixtures to develop a fast TOUGH2 module to simulate the multiphase flow of CO_2-H_2S-CH_4-N_2 gas mixtures and brine. We used this approach in CO2Bio to calculate the thermophysical properties of CO_2-CH_4-H_2-H_2S gas mixtures.

The flow capabilities of TOUGHREACT-CO2Bio are introduced in three sections. Section 2, which describes the general computational features of TOUGHREACT, differences between ECO2N and CO2Bio, multiphase capabilities of CO2Bio, and main equations used in CO2Bio to calculate the mutual solubility of CO_2-H_2S-CH_4-H_2 gas mixtures and brine, and the thermophysical properties of CO_2-H_2S-CH_4-H_2 gas mixtures; section 3, which compares simulation results obtained with TOUGHREACT-CO2Bio against the simulation results obtained with TOUGHREACT-ECO2N,

TOUGH2-EOS7C, and CMG-GEM© for various lab- and field-scale scenarios; and section 4, which summarizes the main findings of our study.

4.3. Methodology

TOUGHREACT uses a sequential iteration approach to solve the combined system of flow and solute transport equations. The governing equations for multiphase fluid and heat flow, and solute transport have the same structures, which are derived from the law of conservation of mass (or energy). TOUGHREACT uses the integral finite difference method (IFDM) to solve the fluid (and heat) flow equation. After solving the flow equation, the updated fluid velocities and phase saturations are used to calculate the solutes transport. The solute transport equation applied to the gas and liquid phases in equilibrium is solved on a component-by-component basis. The resulting concentrations obtained from solving the solute transport equation are used to calculate the conversion of solutes due to chemical reactions (precipitation/dissolution, oxidation/reduction, sorption/desorption, ion exchange, and organic matter microbial degradation). The system of combined equilibrium and kinetic chemical reaction equations are solved using Newton-Raphson's method (Xu et al., 2006) on the cell-by-cell basis. TOUGHREACT modules such as ECO2N have been used for a wide variety of geochemical, mineralogical and hydrological problems, such as the impact of mineral trapping of CO_2 (Darby et al., 2009; Xu et al., 2003; Xu et al., 2004), and biogeochemical nitrogen cycling and reactive transport in the vadose zone system (Gu et al., 2009; Maggi et al., 2008).

CO2Bio is developed using ECO2N as a framework. The main difference is that while ECO2N calculates the fugacity coefficient of CO_2 as a function of pressure, temperature, and composition using Spycher and Pruess' thermodynamic model (Spycher and Pruess, 2005), CO2Bio calculates the fugacity coefficients of CO_2, CH_4, H_2S, H_2, and H_2O in the gas phase as a function of pressure, temperature and composition, using an expanded version of the thermodynamic model of Ziabakhsh-Ganji and Kooi (2012). Also, while ECO2N provides a tabulated database for the estimation of CO_2 thermophysical properties of the gas phase, CO2Bio uses simple correlations to estimate

thermophysical properties of the gas phase. In CO2Bio, the oil phase in depleted oil reservoirs injected with CO_2 is assumed to remain immobile. The presence of an oil phase is taken into account by treating the oil phase as an immobile mineral phase. In CO2Bio, the immobile oil phase serves as a source of biodegradable crude oil (e.g., n-alkanes) in the aqueous phase.

4.3.1. TOUGHREACT-CO2Bio

The components that are taken into account in CO2Bio are CO_2, CH_4, H_2S, H_2, H_2O and NaCl. All components except NaCl can be present in both liquid and gas phases. NaCl is considered completely soluble in the aqueous phase, but if it reaches the saturation point, it starts to precipitate and is present in both the liquid and solid phases. The effect of precipitation and dissolution of NaCl on porosity and permeability is taken into account following the approach of ECO2N.

The total mole fractions of CO_2, CH_4, H_2S, H_2, and H_2O components in the system (Z_i) and the mass fraction (X_{NaCl}) or solid saturation (S_s) of NaCl, along with temperature (T) and pressure (P) constitute the primary variables of the system. All possible combinations of the liquid, gas and solid phase compositions can be handled by CO2Bio, except when H_2O is not a constituent of the liquid phase. When NaCl precipitates, the mass fraction of NaCl in the aqueous phase will correspond to the saturation concentration of NaCl in the aqueous phase at the given temperature. S_s is used as the primary variable in the case where NaCl precipitates, otherwise, in the absence of NaCl in the solid phase, X_{NaCl} is used as a primary variable. Table 4.1 summarizes the primary variables in CO2Bio.

Table 4.1. Primary variables in CO2Bio.

	1	2	3	4	5	6	7 (NK+1)
Single and two phase	P	X_{NaCl} or S_s	Z_{CO2}	Z_{H2S}	Z_{H2}	Z_{CH4}	T

4.3.2. Mutual solubility of CO_2-CH_4-H_2S-H_2 gas mixtures and brine

The thermodynamic model of Ziabakhsh-Ganji and Kooi (2012) is expanded in this work to predict the mutual solubility of CO_2-CH_4-H_2S-H_2 gas mixtures and brine. This model was developed by equating the chemical potential of each component in the aqueous and gas phases in equilibrium:

$$h_i \gamma_i x_i = P \emptyset_i y_i \tag{4}$$

where ϕ_i is fugacity coefficient of component i, P is pressure, x_i and y_i are the molar fraction of component i in the aqueous and gas phases in equilibrium, h_i is Henry's constant of component i, and γ_i is the activity coefficient of component i. Peng and Robinson (1976) EOS is used to calculate ϕ_i, and Henry's constant (h_i) is calculated using the following equation:

$$lnh_i = (1-\eta) lnf^0_{H2O} + \eta ln\left(\frac{RT}{MW_{H2O}} \rho^0_{H2O}\right) + 2\rho^0_{H2O} \Delta B \tag{5}$$

$$\Delta B = \tau + \beta \left(\frac{10^3}{T}\right)^{0.5} \tag{6}$$

where T is temperature in kelvin, MW_{H2O} is the molecular mass of water (18.015 g/mol), f_{H2O}^0 is the fugacity and ρ_{H2O}^0 is the density of pure water in g/cm^3, R is universal gas constant, η is a constant for each gas dissolved in water, ΔB represents the difference in interaction between dissimilar molecules and that between identical solvent molecules, and τ (cm^3/g) and β (cm^{3}K$^{0.5}$/g) are adjustable parameters. Activity coefficient of component i is calculated from:

$$\ln \gamma_i = \sum_c 2 m_c \lambda_{i-c} + \sum_c \sum_a m_a m_c \zeta_{i-a-c} \tag{7}$$

where m_a and m_c are anions and cations molalities, respectively, $\lambda_{i\text{-}c}$ and $\zeta_{i\text{-}a\text{-}c}$ are second and third order interaction parameters. The dependency of the interaction parameters on pressure and temperature were modeled using:

$$Par(T,P) = c_1 + c_2 T + \frac{c_3}{T} + c_4 P + \frac{c_5}{P} + c_6 \frac{P}{T} + c_7 \frac{T}{P^2} + \frac{c_8 P}{630-T} + c_9 T ln(P) + c_{10} \frac{P}{T^2} \tag{8}$$

where Par(T, P) is either $\lambda_{i\text{-}c}$ or $\xi_{i\text{-}a\text{-}c}$, T is temperature in kelvin, P is pressure in bar, and c_i (i=1 to 10) are parameters estimated using a fitting procedure.

Knowing the total mole fraction of each component in the system (Z_i), the mole fraction of each component in the gas and liquid phase (y_i and x_i) for a given pressure, temperature and salinity is calculated by vapor-liquid flash calculation using Rachford-Rice equation:

$$\sum_{i=1}^{nk} \frac{Z_i(K_i-1)}{1+n^v(K_i-1)} = 0,\ x_i = \frac{Z_i}{1+n^v(K_i-1)},\ y_i = \frac{K_i Z_i}{1+n^v(K_i-1)} \quad (9)$$

where nk is the number of components in the system, K_i is the equilibrium constant ($K_i = y_i/x_i$) (Eq. 4), and n^v is mole fraction of the gas phase in the system.

Experimental data of H_2 solubility in brine at high pressures (> 100 bar) and temperatures (> 50 °C) are not readily available in literature. Here we used the Li et al. (2018) thermodynamic model's predictions of H_2 solubility in brine to obtain values of η, β, τ, and c_i (i=1 to 10). These parameters are needed to expand the thermodynamic model of Ziabakhsh-Ganji and Kooi (2012) to account for H_2. The thermodynamic model of Li et al. (2018) can accurately predict the mutual solubility of H_2 and brine within the range of 273-373 K, 1-50 MPa, and 0-5 mol-NaCl/kg. The accuracy of this model has been tested for binary mixtures of H_2-CH_4 and H_2-N_2 (Li et al., 2018). We used a linear regression method in two steps to obtain the values of these parameters. First, we obtained the values of η, β and τ in Eq. (5) from the mutual solubility data of H_2 and pure water. Then, we obtained the value of c_i in Eq. (8) using H_2 solubility data in brine. Table 4.2 and 4.3 summarizes the values of η, β, τ, and c_i (i=1 to 10) parameters for H_2. The values of these parameters for CO_2, CH_4, and H_2S can be found in Ziabakhsh-Ganji and Kooi (2012).

Table 4.2. Parameters for calculation of Henry's constant.

Gas	η	τ	β
H_2	0.294994	-4.23407	5.41551

Table 4.3. Second and third order interaction parameters for H_2.

Constant	$\lambda_{H2\text{-}Na}$	$\xi_{H2\text{-}Na\text{-}Cl}$
c_1	-2.1432831	-0.0040631
c_2	0.0031411257	0.0
c_3	392.20546	0.0
c_4	-0.0000286012	-0.000003665
c_5	0.0	0.17004
c_6	0.002352716	-0.000418
c_7	0.0	0.000588
c_8	-0.0024422	-0.000391
c_9	0.0000029806	0.0
c_{10}	-0.389	0.19913

4.3.3. Thermophysical properties of the gas phase

Accurate estimations of thermophysical properties (density, viscosity, and enthalpy) of each fluid phase are important to simulate the multiphase flow of fluids in porous media. The approach of Shabani and Vilcáez (2018) is used in CO2Bio to calculate the thermophysical properties of the gas phase.

4.3.3.1. Density

The density of the gas phase in CO2Bio is calculated using Peng-Robinson EOS:

$$v_g = \frac{Z_g RT}{P} \tag{10}$$

$$\rho = \frac{MW_g}{v_g + c} \tag{11}$$

where Z_g is the gas compressibility factor, T is temperature in kelvin, P is pressure bar, v_g is the molar volume, R is the universal gas constant in $cm^3 \cdot bar/K \cdot mol$, ρ is the gas density in g/cm^3, MW_g is the molecular weight of the gas phase in g/mol, and c is the volume shift factor (Shabani and Vilcáez, 2017; Shabani and Vilcáez, 2018). We calibrated the values of c for each gas component using National Institute of Standards and Technology (NIST) density data. Table 4.4 lists the calibrated c values for

each gas component. Note that c value of CO_2 is a function of the reduced temperature ($T_r = T/T_c$) and reduced pressure ($P_r = P/P_c$), where Tc and Pc are the critical temperature and pressure of the component. Using CO2Bio, this approach allowed us to reproduce densities for pure CO_2, H_2S, CH_4, and H_2 gases and mixture gases from the original NIST with less than 1% error (Fig. 1).

Table 4.4. Volume shift factors of gas components.

Gas	Volume shift factor (c)
CO_2*	$T_r^{6.27844} * (-8.18682 * P_r^{-0.94163} + 0.94612) + 2.49642$
CH_4	-0.1557
H_2S	-0.1195
H_2	-2.959

* From Shabani and Vilcáez (2018)

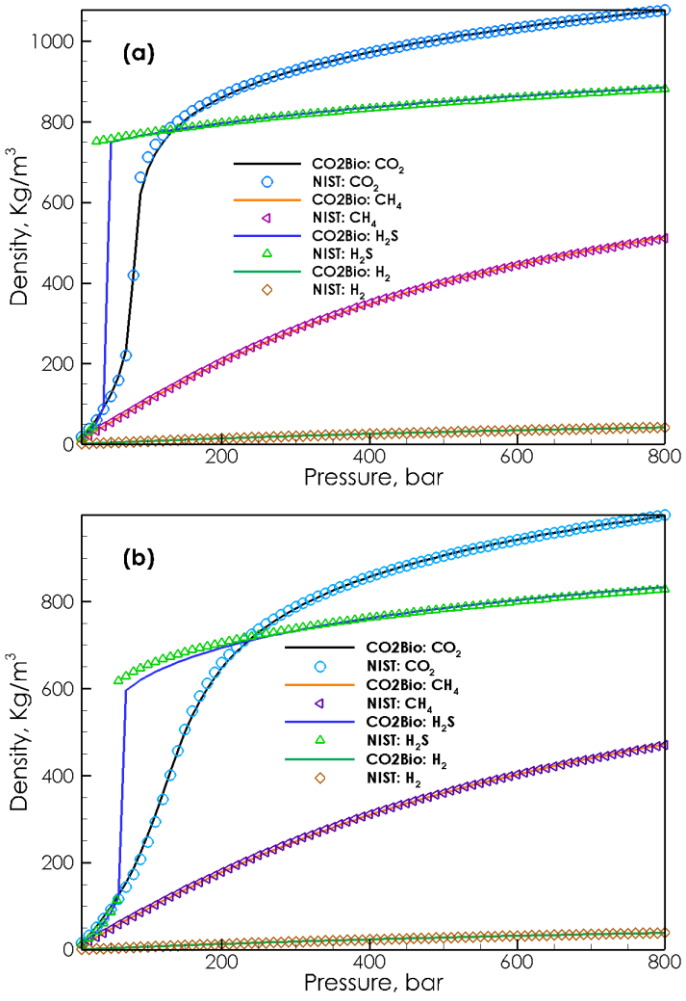

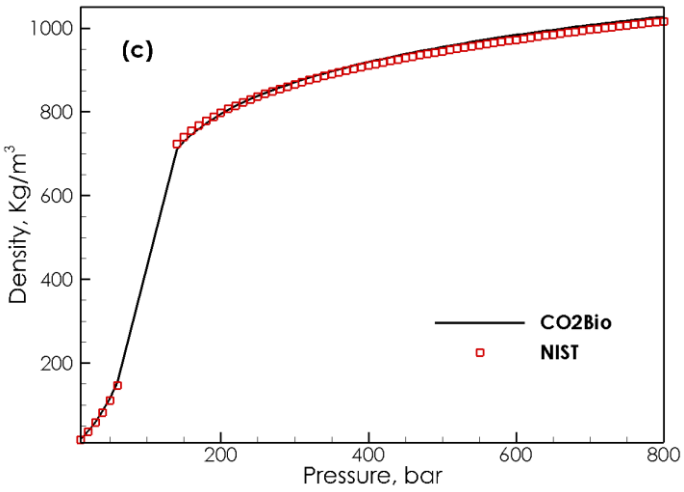

Fig. 4.1. Comparison between densities of pure CO_2, H_2S, CH_4, and H_2 gas obtained from the NIST database and CO2Bio using Peng-Robinson EOS at (a) 35 °C, (b) 70 °C, and for (c) a ternary mixture of CO_2 (90%), CH_4 (5%), and H_2S (5%) at 35 °C.

4.3.3.2. Viscosity

The viscosity of the gas phase in CO2Bio is calculated using the one parameter friction theory (Quiñones-Cisneros et al., 2000; Quiñones-Cisneros et al., 2001) in conjunction with Peng-Robinson EOS. According to the one-parameter friction theory, the viscosity (μ) of the gas phase can be calculated as the sum of the friction viscosity (μ_f) and the diluted viscosity (μ_o).

$$\mu = \mu_o + \mu_f \tag{12}$$

where

$$\mu_f = k_r p_r + k_a p_a, \mu_o = 40.785 \frac{\sqrt{MW_i \times T}}{v_{c_i}^{2/3} \Omega_i^*} F_{c_i} \tag{13}$$

here, k_r and k_a are repulsive and attractive viscous friction coefficients, p_r and p_a are repulsive and attractive pressures in bar calculated from Peng-Robinson EOS, MW_i is the molecular weight of component i in g/mol, T is temperature in kelvin, v_{ci} is the critical volume of component i in cm^3/mol,

F_{ci} is an empirical factor for component i which is a function of acentric factor and dipole moment, and Ω^*_i is the reduced collision integral for component i, which is a function of reduced temperature.

The viscosities of a ternary mixture of CO_2 (90%), H_2S (5%), and CH_4 (5%) at 35 ˚C obtained using CO2Bio and the NIST database are compared in Fig. 2. The estimated error of viscosity calculations for pure CO_2, CH_4, H_2S, and H_2 gases at pressures ranging between 1 and 800 bar and temperatures ranging between 5 to 95 °C is about 5%.

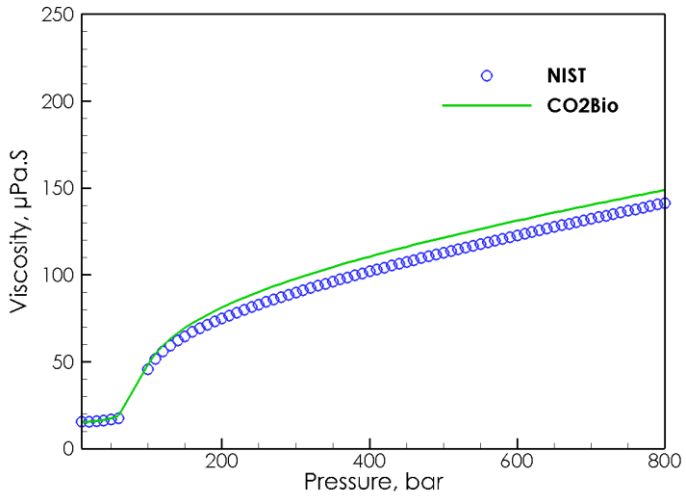

Fig. 4.2. Comparison between the viscosity of a ternary mixture of CO_2 (90%), CH_4 (5%), and H_2S (5%) calculated using CO2Bio and obtained from the NIST database at 35 °C.

4.3.3.3. Enthalpy

The gas phase enthalpy in CO2Bio is calculated as the sum of the ideal gas mixture enthalpy and the departure enthalpy with either Peng-Robinson EOS or Lee-Kesler EOS:

$$H_g = \sum_{i=1}^{n_c} y_i . H_{g_i}^{ideal} + H_g^{departure} \quad (14)$$

where

$$H_{g_i}^{ideal} = H_{g_i}^{reference} + \int_{T_1}^{T_2} C_{pg} dT \quad (15)$$

Here, $H_{g_i}^{ideal}$ is the ideal gas enthalpy in kJ/kg, $H_{g_i}^{reference}$ is the reference enthalpy of each component at 273.16 K (temperature of the triple point of water) in kJ/kg, and C_{pg} is the specific heat capacity that is calculated as a function of temperature using a fourth order polynomial equation in kJ/kg·K, and $H_g^{departure}$ is the departure enthalpy in kJ/kg, which is the difference between the enthalpy of an ideal gas and a real gas at the same pressure and temperature.

A comparison of the enthalpy of a ternary mixture of CO_2 (90%), H_2S (5%), and CH_4 (5%) at 35 ˚C obtained from the NIST database and calculated using CO2Bio is shown in Fig. 3. We found the estimated error of enthalpy calculation for pure CO_2, CH_4, H_2S, and H_2 gases to be less than 2%.

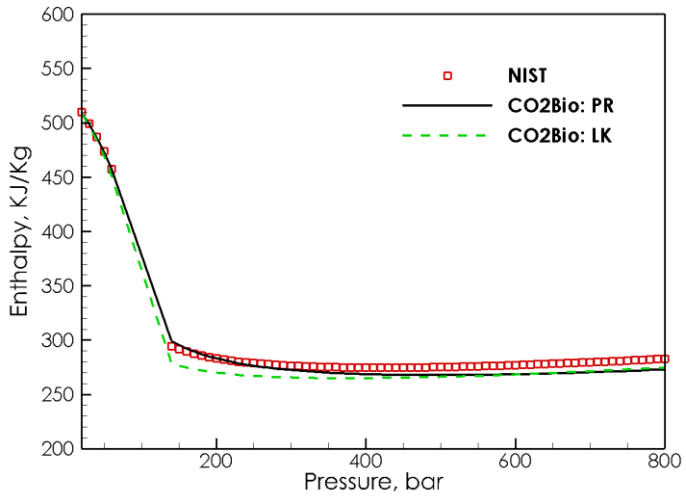

Fig. 4.3. Comparison between enthalpy of a ternary mixture of CO_2, CH_4, and H_2S calculated using CO2Bio and obtained from the NIST database at 35 ℃.

4.3.4. Thermophysical properties of the liquid phase

The approach of ECO2N is used in CO2Bio to estimate the thermophysical properties of the liquid phase. Since the liquid phase mainly consists of brine, the thermophysical properties of brine are first calculated and then corrections are made to take into account the dissolution of CO_2 in the liquid phase. We did not consider the effect of dissolution of CH_4, H_2S, and H_2 in brine on thermophysical properties (density, viscosity, and enthalpy) of the liquid phase in CO2Bio. The amounts of CH_4, H_2S, and H_2 in deep saline aquifers used for GCS will be considerably smaller than the amounts of CO_2

injected. This is due to the low availability of organic matter in deep saline aquifers. Whereas, in depleted oil reservoirs where the availability of organic matter (e.g., n-alkanes) will be higher, the current version of CO2Bio can only handle scenarios where the dissolution of H_2S, CH_4 and H_2 has a negligible effect on the thermophysical properties of the liquid phase.

4.4. Verification and application

The verification of simulation programs is essential to gain confidence in the results obtained from their application to the real world. This can be done through comparisons with simulation results obtained from widely employed simulation programs of similar capabilities, analytical solutions of the governing equations, and/or reliable experimental results. Experimental data on the multiphase flow of CO_2-CH_4-H_2S-H_2 gas mixtures in porous media is not readily available. In addition, obtaining an analytical solution of the governing equations of multiphase flow of CO_2-CH_4-H_2S-H_2 gas mixtures in porous media is practically impossible. Hence, we verified the accuracy of the multiphase flow capabilities of TOUGHREACT-CO2Bio through comparisons against simulation results obtained using TOUGHREACT-ECO2N, TOUGH2-EOS7C and GEM-CMG©. Moreover, our goal is to demonstrate the capability of TOUGHREACT-CO2Bio to simulate the multiphase flow of CO_2-CH_4-H_2S-H_2 gas mixtures at field-scale. Therefore, we simulated the alternate injection of CO_2 and brine into the Cushing-Drumright oil reservoir of Oklahoma assuming constant rates of H_2 and CH_4 production attributed to the possible biodegradation of crude oil (n-alkanes).

4.4.1. Non-isothermal radial flow of CO_2 in a saline aquifer

A non-isothermal radial flow of CO_2 in a homogeneous infinite acting saline aquifer (Pruess, 2005) was simulated using TOUGHREACT-CO2Bio and TOUGHREACT-ECO2N. The initial temperature and pressure of the aquifer are 45 °C and 120 bar, respectively. NaCl mass fraction of the formation water is 1%. The aquifer thickness is 100 m, and CO_2 is injected into the aquifer at a constant rate of 100 kg/s. Simulation results obtained with TOUGHREACT-CO2Bio and TOUGHREACT-

ECO2N after five years of CO_2 injection are compared in Fig. 4. TOUGHREACT-CO2Bio yields essentially the same results obtained with TOUGHREACT-ECO2N (less than 1% relative error), confirming the capability of TOUGHREACT- CO2Bio to simulate the flow of pure CO_2 in saline aquifers.

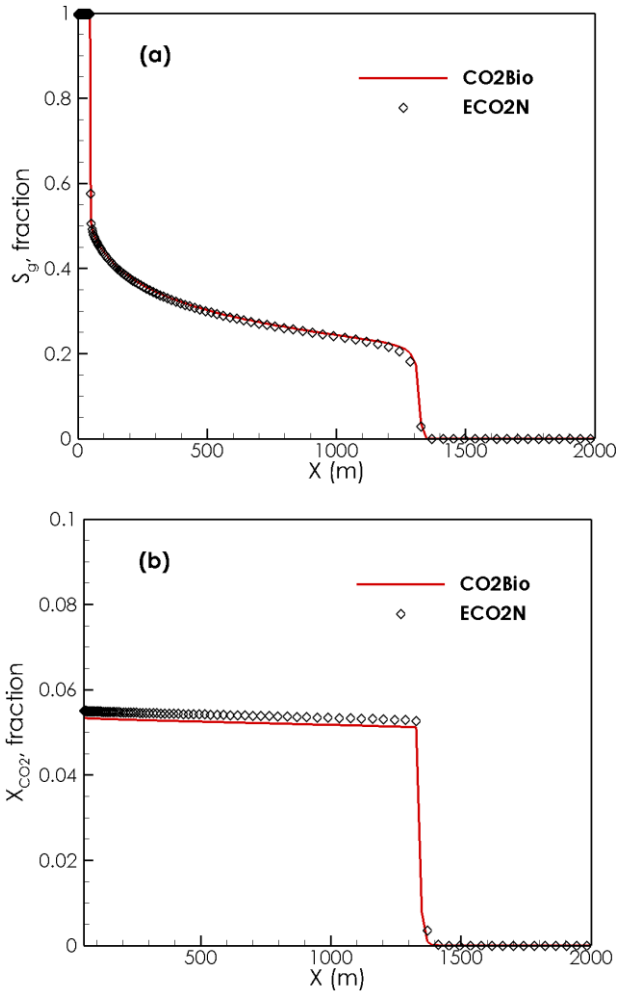

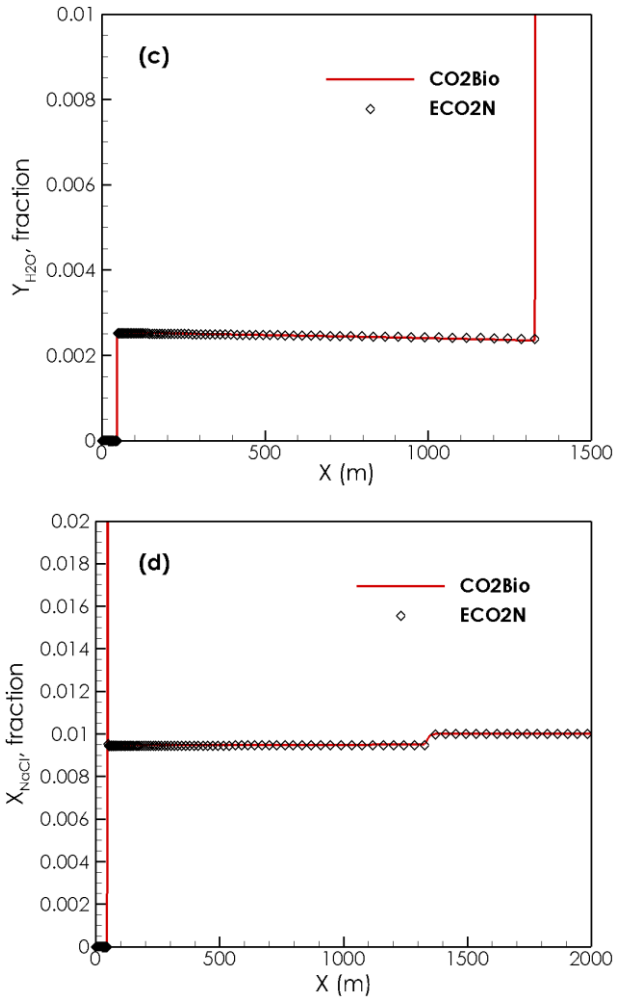

Fig. 4.4. Comparison of simulation results of non-isothermal radial flow of CO_2 in a homogeneous infinite acting saline aquifer obtained with TOUGHREACT-CO2Bio and TOUGHREACT-ECO2N: (a) gas saturation (S_g), (b) CO_2 mass fraction in the aqueous phase (XCO_2), (c) H_2O mass fraction in the gas phase (YH_2O), and (d) NaCl mass fraction (X_{NaCl}) in the aqueous phase, after five years of CO_2 injection at 100 kg/s.

4.4.2. Extraction of dissolved CH_4 in water by CO_2 injection

To verify the accuracy of the multiphase and multicomponent flow predictions of TOUGHREACT-CO2Bio, CO_2 injection at 9.4×10^{-4} kg/s into a 61 m long one-dimensional horizontal column containing CH_4-saturated water (Taggart, 2010) was simulated using TOUGHREACT-CO2Bio and the results compared against the simulation results obtained using TOUGH2-EOS7C (Oldenburg

et al., 2013) (Fig. 5). The initial pressure and temperature of the column are 204 bar and 91.8 °C, respectively. The results obtained with TOUGHREACT-CO2Bio are in close agreement with the results obtained with TOUGH2-EOS7C (3% relative error), demonstrating the multicomponent capabilities of TOUGHREACT-CO2Bio.

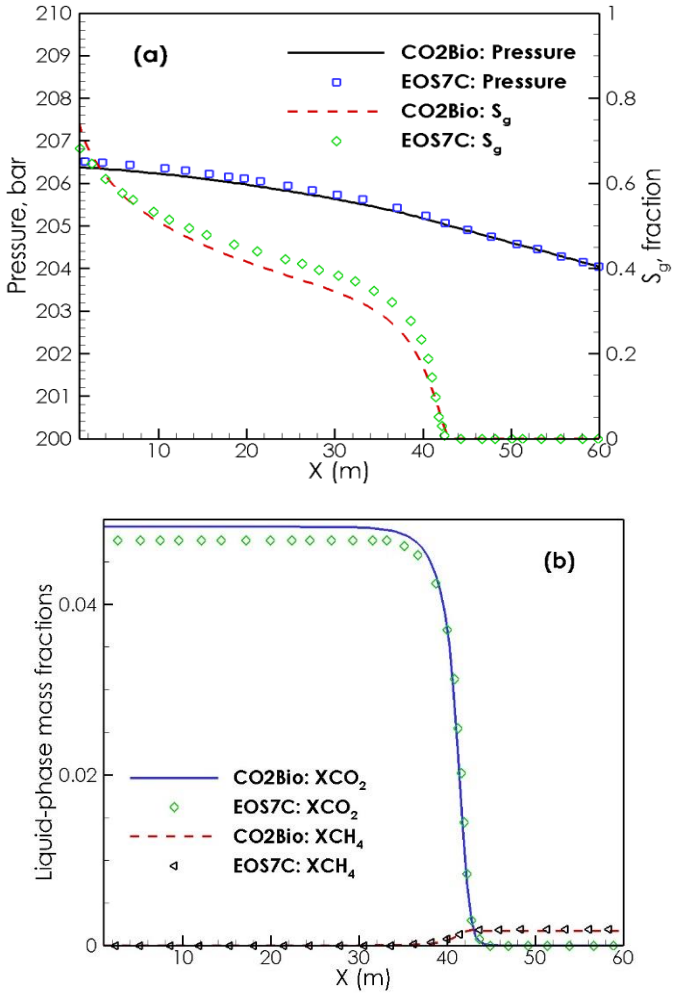

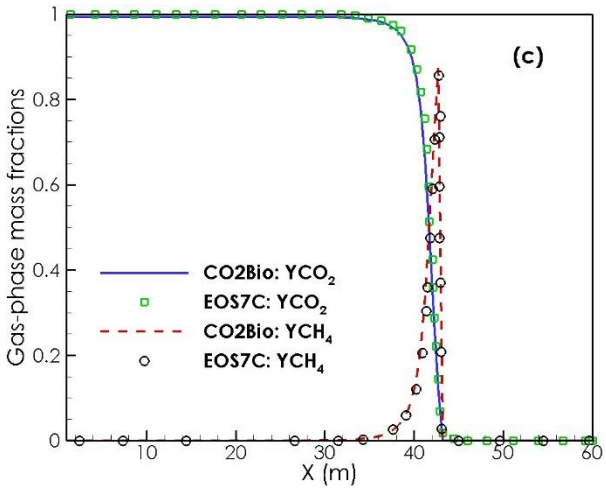

Fig. 4.5. Comparison of simulation results of CO_2 injection at a rate of 9.4×10^{-4} kg/s into a 61 m long one-dimensional horizontal column containing CH_4-saturated water obtained with TOUGHREACT-CO2Bio and TOUGH2-EOS7C after 3 days of CO_2 injection: (a) Reservoir pressure and gas saturation (S_g), (b) CO_2 and CH_4 mass fraction in the aqueous phase (XCO_2, XCH_4), and (c) CO_2 and CH_4 mass fraction in the gas phase (YCO_2, YCH_4).

4.4.3. Co-injection of CO_2 with H_2S as an impurity into a deep saline aquifer

To further verify the accuracy of the multiphase and multicomponent flow predictions of TOUGHREACT-CO2Bio, a simulation of CO_2 (98%) and H_2S (2%) co-injection into a 24.38 m long one-dimensional sand-packed coil filled with saline water was conducted using TOUGHREACT-CO2Bio to replicate simulation results of gas saturation obtained using CMG-GEM© (data from Bachu and Bennion (2009)) at different times. The initial pressure and temperature are 135 bar and 61 °C, respectively. NaCl mass fraction of the aquifer is 11%. The injection rate of CO_2 and H_2S are 1.017×10^{-6} and 2.075×10^{-8} kg/s, respectively. Simulation results obtained with TOUGHREACT-CO2Bio are in good agreement with the simulations results obtained with CMG-GEM© software, confirming the multicomponent capabilities of TOUGHREACT-CO2Bio. We consider the minor difference between the two simulation results to be due to numerical dispersion and differences in the thermodynamic models used in TOUGHREACT-CO2Bio and CMG-GEM© to calculate the mutual solubility of gas mixtures and brine.

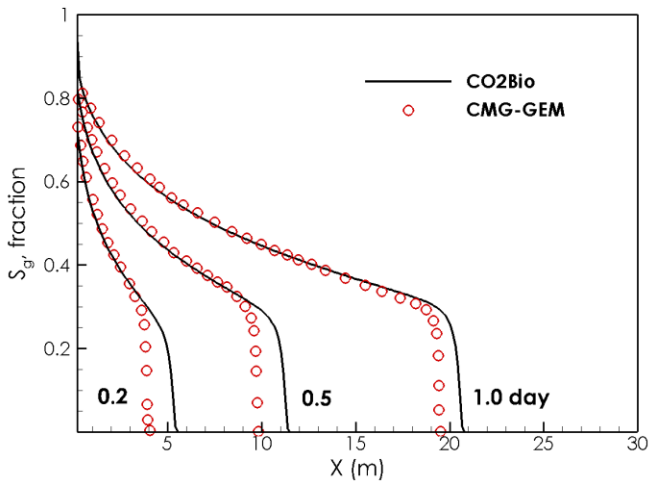

Fig. 4.6. Comparison of simulation results CO_2 (98%) and H_2S (2%) co-injection into a 24.38 m long one-dimensional sand-packed coil filled with saline water obtained with TOUGHREACT-CO2Bio and CMG-GEM© at different times.

4.4.4. Alternate injection of CO_2 and formation water into a depleted oil reservoir

To demonstrate the capability of TOUGHREACT-CO2Bio to simulate the multiphase flow of CO_2-CH_4-H_2S-H_2 gas mixtures at the field-scale under biotic conditions, the 3D alternate injection of CO_2 and formation water (brine) into the Cushing oil field of Oklahoma was simulated assuming constant rates of H_2 and CH_4 production attributed to the biodegradation of n-alkanes. TOUGHREACT-CO2Bio aims to capture the transport rates of CO_2, CH_4, H_2S, and H_2 gases in the aqueous and gas phases in equilibrium as they are produced and/or consumed in the aqueous phase due to microbial activity. Therefore, to assess the capability of TOUGHREACT-CO2Bio to capture the transport of H_2, which constitutes the bottleneck for the microbial conversion of CO_2 to CH_4, H_2 consumption by methanogens is not included in the simulation. The geological model of the Cushing-Drumright oil reservoir used for the simulations is shown in Fig. 7. Porosity is 11.9-20%, and permeability is 6-53 mD. The thickness of the Cushing-Drumright oil reservoir is 331 m. The initial pressure and temperature of the oil reservoir increase with depth at gradients of 0.0875 bar/m and 0.025 °C/m, respectively. This make the pressure and temperature reaching 92.2 bar and 46.35 °C, respectively at

the bottom layer of the reservoir. The NaCl mass fraction in the reservoir is 0.01. Crude oil in the reservoir, which constitutes the source of n-alkanes in the aqueous phase, is assumed to remain immobile.

The simulation was carried out for the alternate injection of CO_2 and formation water. One injection well and one production well are placed in the model. A constant bottomhole pressure of 80 bar is assigned to the production well. The injection rates of CO_2 and formation water, as well as the production rates of H_2 and CH_4 used for the simulation in each alternate injection cycle are summarized in Table 4.5, where Total (theoretical) is the total mass of each gas (CO_2, CH_4 and H_2) in the system calculated manually using the total masses of injected and/or produced gases, and Total (CO2Bio) is the total mass of each gas in the system reported by CO2Bio at the end of simulation. The injection of formation water supplied with nutrients such as protein-rich matter is assumed to result in the stimulation of the microbial production of H_2 and CH_4 from the biodegradation of n-alkanes after a complete cycle of CO_2 and water injection. Therefore, during the first cycle of CO_2 and formation water alternate injection (1: CO_2 and 1: Brine), H_2 and CH_4 productions are zero in the simulation. The production of H_2 and CH_4 is included in the second cycle of CO_2 and formation water injection (2: CO_2 and 2: Brine). In this simulation setup, the production of H_2 and CH_4 is assumed to take place around the injection well within an area covering 690 m × 740 m at the bottom of the reservoir in two layers with average thickness of 15 m (240 cells). This corresponds to the area flooded with the formation water during the first cycle of the alternate injection. It is noteworthy that the injected (CO_2) and produced (CH_4 and H_2) gases do not reach the production well after the two simulated cycles (720 days).Worldwide, the rates of CH_4 production from crude oil biodegradation in different oil reservoirs have been reported to range from 0.001 to 6.4 μg/L·h (Nazima et al., 2017). Based on this information, CH_4 and H_2 production rates of 5.0×10^{-5} kg/s were used for simulations.

Table 4.5. Scheme of alternate injection of CO_2 and produced water used for field-scale simulations.

Cycles	Duration	CO_2 injection	Brine injection	CH_4 production	H_2 production

	(days)	(kg/s)	(kg/s)	(kg/s)	(kg/s)
1: CO_2	180	2	0	0	0
1: Brine	180	0	2	0	0
2: CO_2	180	2	0	1.2×10^{-2} *	1.2×10^{-2} *
2: Brine	180	0	2	1.2×10^{-2} *	1.2×10^{-2} *
Total (theoretical)	720	62208000	-	373248	373248
Total (CO2Bio)	720	62201754	-	373248	373248

*Total production rate of CH_4 and H_2 within 240 cells (5.11×10^5 m^2) around the injection well

Figs. 8 and 9 show the simulated mass fractions of CO_2, CH_4 and H_2 in the aqueous phase around the injection well after the first and second cycles of alternate injection of CO_2 and formation water (Table 4.5). As expected, during the first cycle of CO_2 injection, CO_2 migrated upward due to buoyancy forces and then expanded laterally due to advection. The injection of formation water following the injection of CO_2 resulted in the horizontal displacement of CO_2 away from the injection well. During the second cycle, similar upward and lateral movement of CO_2 followed by the displacement of CO_2 due to the injection of formation water occurred (Figs. 8a-b). During the second cycle of alternate injection, the produced CH_4 and H_2 exhibited migration behavior similar to CO_2. This is due to fact that all three gases have lower density than formation water (Fig. 9a-b). Mass balances of CO_2, CH_4, and H_2 input into the oil reservoir reported by TOUGHREACT-CO2Bio is in excellent agreement with manually calculated mass balances. The relative error of in-place mass balance for each component is less than 0.01 %.

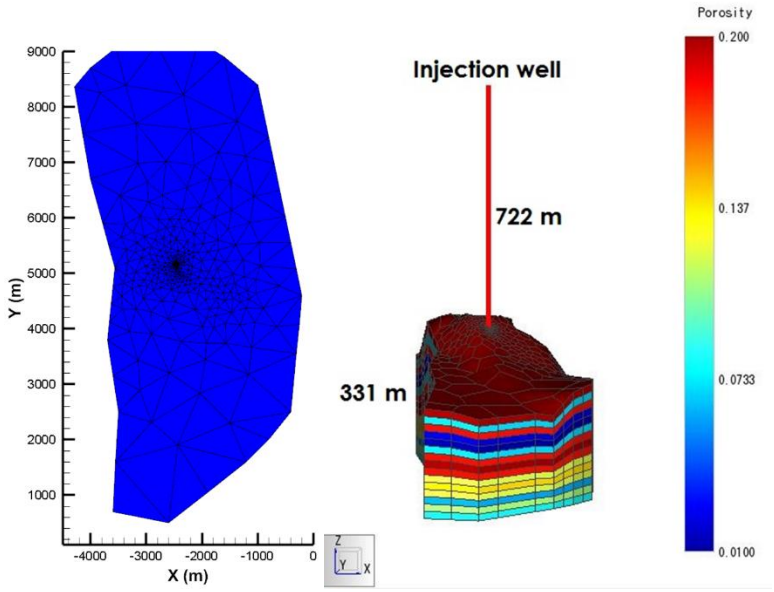

Fig. 4.7. Tope (left) and lateral (right) views of the geological model of the Cushing-Drumright oil reservoir (Shabani and Vilcáez, 2018)

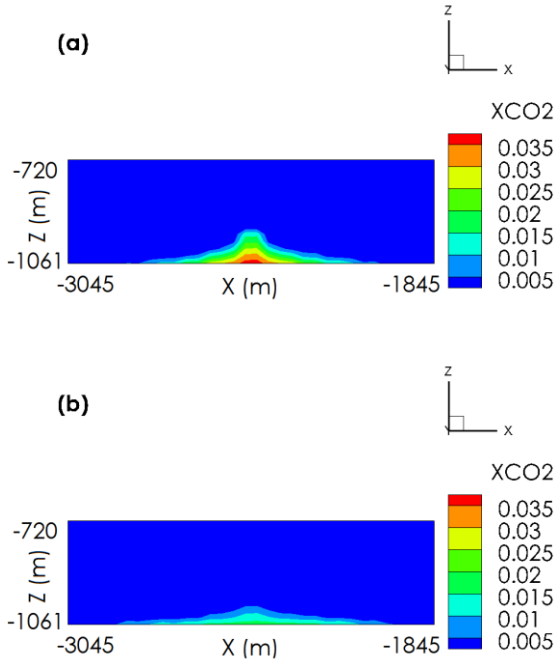

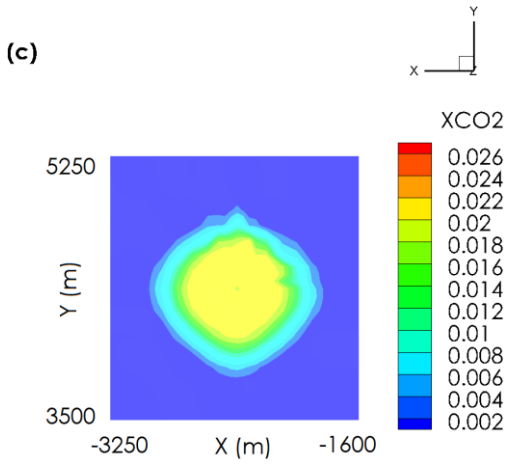

Fig. 4.8. Alternate injection of CO_2 and formation water (Table 4.5): (a) and (b) Cross-sectional views of the simulated distribution of CO_2 mass fraction in the aqueous phase after 540 days and 720 days, respectively, (c) Top view of CO_2 mass fraction in the aqueous phase after 720 days.

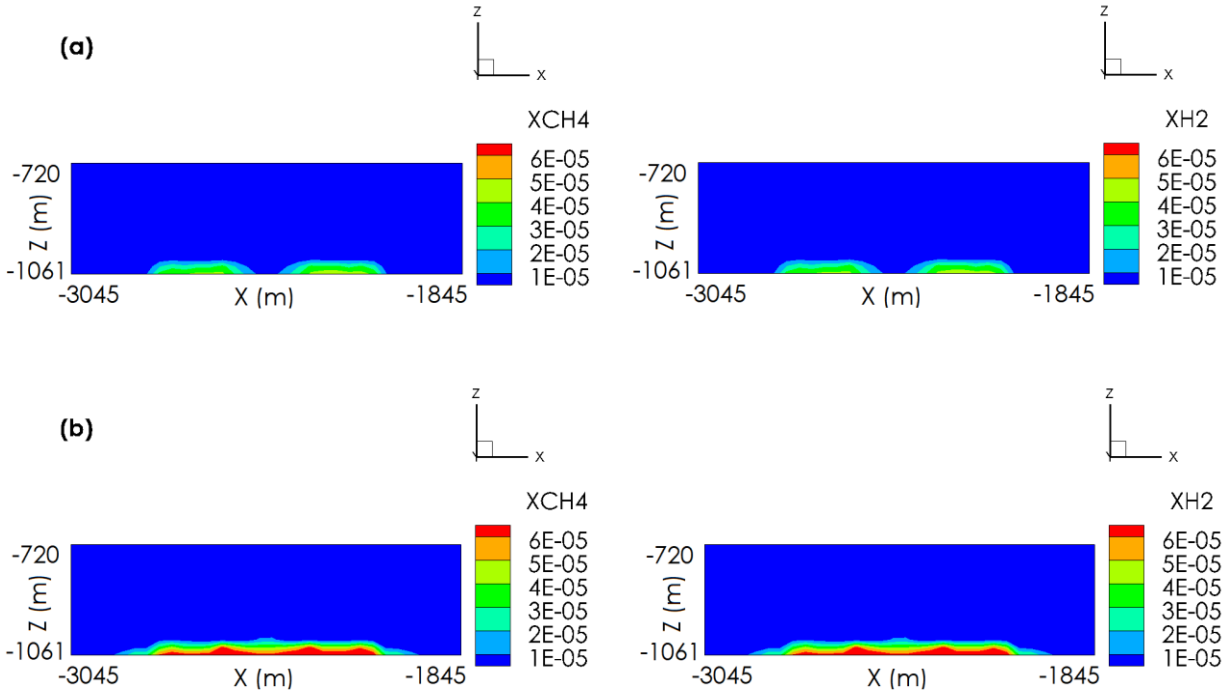

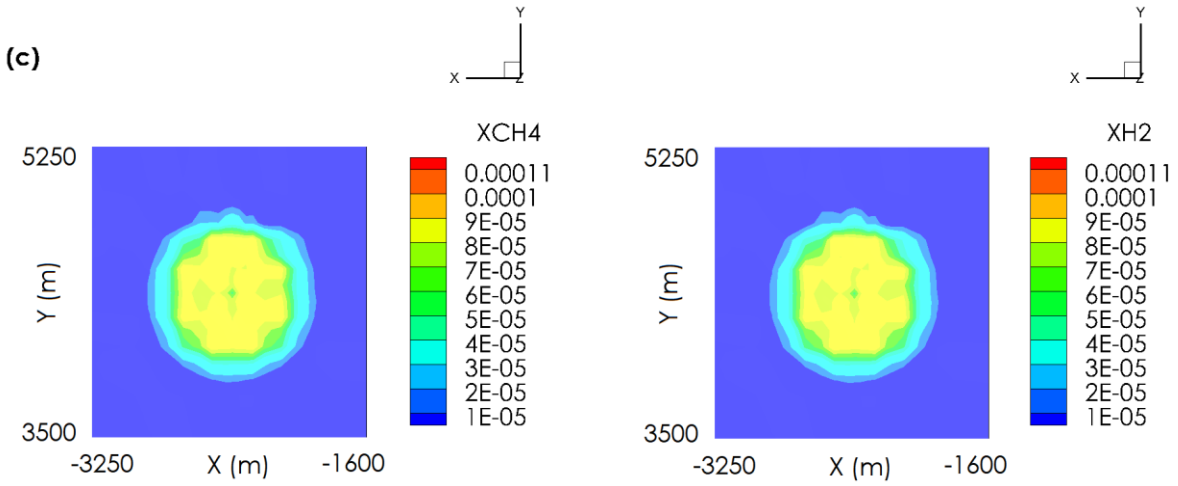

Fig. 4.9. Alternate injection of CO2 and formation water (Table 4.5): (a) and (b) Cross-sectional view of the simulated distribution of CH4 (left) and H2 (right) mass fraction in the aqueous phase after 540 days and 720 days, respectively, (c) Top view of CH4 (left) and H2 (right) mass fraction in the aqueous phase after 720 days.

Fig. 10 shows the gas and aqueous mass fractions of CH_4 and H_2 in the radial direction after the two cycles of CO_2 and formation water injection (Table 4.5). As expected, the gas and aqueous mass fractions of CH_4 and H_2 in the gas phase increase with increasing distance from the injection well. This is due to the advective transport of CH_4 and H_2. However, the gas mass fraction of H_2 reaches higher levels than the mass fractions of CH_4 in the gas phase. This is due to the higher solubility of CH_4 than H_2 in the formation water (Kaye and Lady, 1986). We attribute the more subtle difference between the mass fractions of CH_4 and H_2 in the liquid phase to the low production rates of CH_4 and H_2. Fig. 11 shows the aqueous mass fraction of CO_2 in the radial direction after each injection period of the two simulated cycles (Table 4.5). As expected, low mass fractions of CO_2 near the wellbore are concomitant with the brine injection periods, and high mass fractions of CO_2 near the wellbore are concomitant with the CO_2 injection periods. The results confirm that TOUGHREACT-CO2Bio is capable of capturing the different transport rates of CO_2, CH_4, and H_2 in the gas and aqueous phases.

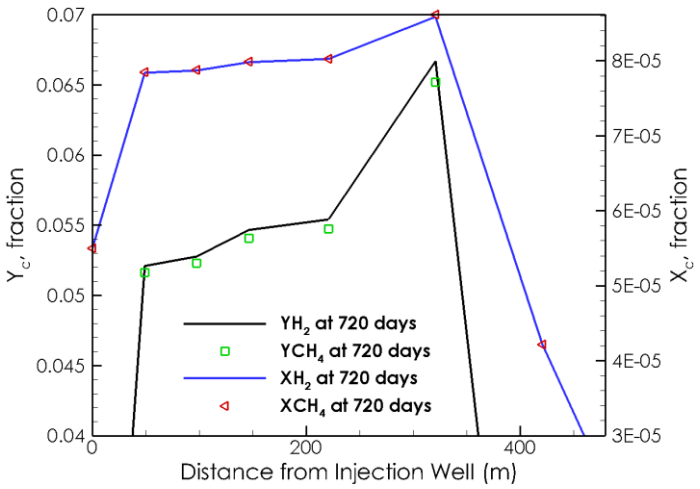

Fig. 4.10. Radial mass fractions distribution of CH_4 and H_2 in the aqueous (X_c) and gas (Y_c) phases around the injection well after 720 days of CO_2 and formation water injection (Table 4.5).

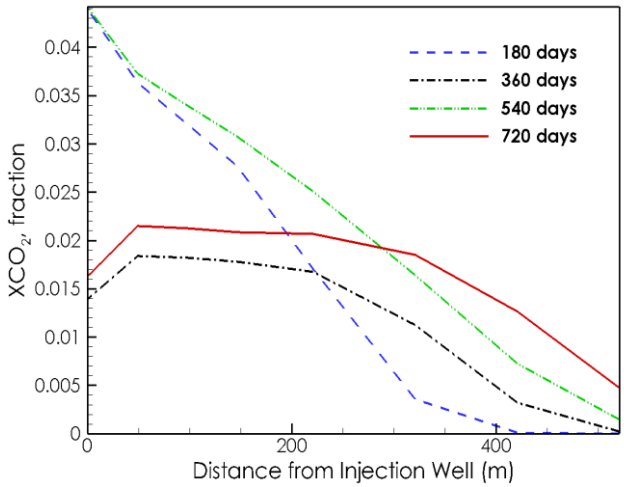

Fig. 4.11. Radial mass fraction distribution of CO_2 in the aqueous phase around the injection well after each injection period (Table 4.5).

4.5. Conclusion

The newly developed module of TOUGHREACT named CO2Bio is suitable for the simulation of multiphase flow of CO_2-CH_4-H_2-H_2S gas mixtures at deep geological formations under biotic conditions when CO_2, CH_4, H_2, and H_2S gases are produced and/or consumed by indigenous microbial communities. The predictions of CO2Bio are in good agreement with predictions of other widely employed and reliable software. Minor differences between the simulated results obtained with CO2Bio

and other software is attributed to the intrinsic differences between the approaches used to calculate the thermophysical properties, the mutual solubility of CO_2-CH_4-H_2-H_2S gas mixtures and brine, and numerical dispersion. In general, the estimated thermophysical properties of the gas phase using the selected thermophysical correlations used in CO2Bio are in excellent agreement with NIST thermophysical data. The applicability of TOUGHREACT-CO2Bio to predict the kinetics of CO_2 and/or crude oil microbial conversion to CH_4 in deep saline aquifers or depleted oil reservoirs under flow conditions will be presented in a subsequent article.

4.6. Acknowledgement

We thank to the Geological Society of America (GSA) for partial financial support of the Ph.D. research of the first author. This is Oklahoma State University Boone Pickens School of Geology contribution number 2018-94.

4.7. References

Bachu, S., Bennion, D. B., 2009. Chromatographic partitioning of impurities contained in a CO2 stream injected into a deep saline aquifer: Part 1. Effects of gas composition and in situ conditions. International Journal of Greenhouse Gas Control. 3, 458-467.

Cai, M., et al., 2015a. Potential for aerobic and methanogenic oil biodegradation in a water flooded oil field (Dagang oil field). Fuel. 141, 143-153.

Cai, M., et al., 2015b. Effects of oxygen injection on oil biodegradation and biodiversity of reservoir microorganisms in Dagang oil field, China. International Biodeterioration & Biodegradation. 98, 59-65.

Darby, E. B., et al., 2009. Geochemical modeling of near-surface CO2 interactions: The critical element in cost-effective long-term monitoring. Energy Procedia. 1, 2389-2395.

Dolfing, J., et al., 2008. Thermodynamic constraints on methanogenic crude oil biodegradation. The ISME journal. 2, 442.

Gu, C., et al., 2009. Aqueous and gaseous nitrogen losses induced by fertilizer application. Journal of Geophysical Research: Biogeosciences. 114.

Jones, D., et al., 2008a. Crude-oil biodegradation via methanogenesis in subsurface petroleum reservoirs. Nature. 451, 176-180.

Jones, D., et al., 2008b. Crude-oil biodegradation via methanogenesis in subsurface petroleum reservoirs. Nature. 451, 176.

Kaye, G. W. C., Lady, T. H., 1986. Tables of Physical and Chemical Constants. Longman.

Larter, S., di Primio, R., 2005. Effects of biodegradation on oil and gas field PVT properties and the origin of oil rimmed gas accumulations. Organic Geochemistry. 36, 299-310.

Li, D., et al., 2018. A unified phase equilibrium model for hydrogen solubility and solution density. International Journal of Hydrogen Energy. 43, 512-529.

Li, J., et al., 2014. Modeling of CO2-CH4-H2S-brine based on cubic EOS and fugacity-activity approach and their comparisons. Energy Procedia. 63, 3598-3607.

Liu, J.-F., et al., 2015. Analysis of microbial communities in the oil reservoir subjected to CO2-flooding by using functional genes as molecular biomarkers for microbial CO2 sequestration. Frontiers in microbiology. 6, 236.

Maggi, F., et al., 2008. A mechanistic treatment of the dominant soil nitrogen cycling processes: Model development, testing, and application. Journal of Geophysical Research: Biogeosciences. 113.

Mayumi, D., et al., 2011. Evidence for syntrophic acetate oxidation coupled to hydrogenotrophic methanogenesis in the high-temperature petroleum reservoir of Yabase oil field (Japan). Environmental microbiology. 13, 1995-2006.

Nazima, T. N., et al., 2017. Radiotracer assay of microbial processes in petroleum reservoirs. Advances in Biotechnology & Microbiology. 2, 10.19080/AIBM.2017.02.555591.

Oldenburg, C. M., et al., 2013. The role of CO2 in CH4 exsolution from deep brine: Implications for geologic carbon sequestration. Greenhouse Gases: Science and Technology. 3, 359-377.

Peng, D.-Y., Robinson, D. B., 1976. A new two-constant equation of state. Ind. Eng. Chem. Fundam. 15, 59-64.

Pruess, K., ECO2N: A TOUGH2 fluid property module for mixtures of water, NaCl, and CO2. Lawrence Berkeley Laboratory, California, 2005, pp. 66.

Pruess, K., Spycher, N., 2007. ECO2N – A fluid property module for the TOUGH2 code for studies of CO2 storage in saline aquifers. Energy Conversion and Management. 48, 1761-1767.

Quiñones-Cisneros, S. E., et al., 2000. The friction theory (f-theory) for viscosity modeling. Fluid Phase Equilibria. 169, 249-276.

Quiñones-Cisneros, S. E., et al., 2001. One parameter friction theory models for viscosity. Fluid Phase Equilibria. 178, 1-16.

Scott, A. R., et al., 1994. Thermogenic and secondary biogenic gases, San Juan basin, Colorado and New Mexico--implications for coalbed gas producibility. AAPG bulletin. 78, 1186-1209.

Shabani, B., Vilcáez, J., 2017. Prediction of CO2-CH4-H2S-N2 gas mixtures solubility in brine using a non-iterative fugacity-activity model relevant to CO2-MEOR. Journal of Petroleum Science and Engineering. 150, 162-179.

Shabani, B., Vilcáez, J., 2018. A fast and robust TOUGH2 module to simulate geological CO2 storage in saline aquifers. Computers & Geosciences. 111, 58-66.

Spycher, N., Pruess, K., 2005. CO2-H2O Mixtures in the Geological Sequestration of CO2. II. Partitioning in Chloride Brines at 12–100 C and up to 600 bar. Geochimica et Cosmochimica Acta. 69, 3309-3320.

Sugai, Y., et al., 2012. Experimental studies on indigenous hydrocarbon-degrading and hydrogen-producing bacteria in an oilfield for microbial restoration of natural gas deposits with CO 2 sequestration. Journal of Natural Gas Science and Engineering. 5, 31-41.

Taggart, I. J., 2010. Extraction of dissolved methane in brines by CO2 injection: Implication for CO2 sequestration. SPE Reservoir Evaluation & Engineering. 13, 791-804.

Vilcáez, J., 2015a. Numerical modeling and simulation of microbial methanogenesis in geological CO2 storage sites. Journal of Petroleum Science and Engineering. 135, 583-595.

Vilcáez, J., 2015b. Stimulating effect of protein-rich matter on the biogenic conversion of CO2 to CH4. Journal of CO2 Utilization. 10, 60-66.

Vilcáez, J., et al., 2018. Stimulation of methanogenic crude oil biodegradation in depleted oil reservoirs. Fuel. 232, 581-590.

Xu, T., et al., 2003. Reactive geochemical transport simulation to study mineral trapping for CO2 disposal in deep arenaceous formations. Journal of Geophysical Research: Solid Earth. 108.

Xu, T., et al., 2004. Numerical simulation of CO2 disposal by mineral trapping in deep aquifers. Applied geochemistry. 19, 917-936.

Xu, T., et al., 2006. TOUGHREACT—a simulation program for non-isothermal multiphase reactive geochemical transport in variably saturated geologic media: applications to geothermal injectivity and CO 2 geological sequestration. Computers & Geosciences. 32, 145-165.

Xu, T., et al., 2014. TOUGHREACT V3. 0-OMP Reference Manual: A Parallel Simulation Program for Non-Isothermal Multiphase Geochemical Reactive Transport. LBNL-DRAFT. University of California, Berkeley, CA. 94720.

Ziabakhsh-Ganji, Z., Kooi, H., 2012. An equation of state for thermodynamic equilibrium of gas mixtures and brines to allow simulation of the effects of impurities in subsurface CO2 storage. International Journal of Greenhouse Gas Control. 11, S21-S34.

CHAPTER V

TOUGHREACT-CO2BIO – A NEW MODULE TO SIMULATE GEOLOGICAL CARBON STORAGE UNDER BIOTIC CONDITIONS (PART 2): THE BIO-GEOCHEMICAL REACTIVE TRANSPORT OF CO_2-CH_4-H_2-H_2S GAS MIXTURES

Babak Shabani, Javier Vilcáez*, Jack Pashin

Boone Pickens School of Geology, Oklahoma State University, Stillwater, OK 74078, USA

5.1. Abstract

The capabilities of TOUGHREACT-CO2Bio to simulate the multiphase flow of CO_2-CH_4-H_2-H_2S gas mixtures and brine in deep geological formations were presented in Shabani and Vilcáez (2019). The CO2Bio capabilities are extended to predict the kinetics of CO_2 and/or crude oil biodegradation to CH_4. The microbial gas generation is then coupled with multiphase flow using a sequential iteration method. To verify the ability of CO2Bio to predict bio-geochemical generation of CH_4 and H_2, the results of an experimental data of methanogenic crude oil biodegradation though the combined supply of CO_2 and protein-rich matter in anaerobic microcosms were simulated. To confirm the capability of CO2Bio to simulate the bio-geochemical reactive transport of CO_2-CH_4-H_2-H_2S gas mixtures and brine in deep geological formations under biotic condition, the 3D alternate injection of CO_2 and produced water in a section of Cushing oilfield is simulated. The simulation results show that CO2Bio is capable of modeling the complex multiphase-multicomponent reactive transport of CO_2-CH_4-H_2S-H_2 gas mixtures and brine under biotic conditions.

Key words: Geological carbon storage; CO_2-CH_4-H_2-H_2S gas mixture; TOUGHREACT-CO2Bio; Microbial gas generation.

*Corresponding author: vilcaez@okstate.edu (J. Vilcáez)

5.2. Introduction

In part 1 of this study (Shabani and Vilcáez, 2019) the capabilities of TOUGHREACT-CO2Bio to simulate the multiphase-multicomponent flow of CO_2-CH_4-H_2S-H_2 and brine in deep geological formations and depleted oil reservoirs were presented. CO2Bio is developed based on the ECO2N module of TOUGHREACT. CO2Bio uses an expanded thermodynamic model and robust thermophysical correlations to handle the multiphase-multicomponent flow of CO_2-CH_4-H_2S-H_2 gas mixtures and brine in deep geological formations. In part 2 of this study, the capabilities of CO2Bio is extended to couple the reactive solute transport with the flow. Similar to part 1, the focus of this study is to simulate the biodegradation of crude oil in depleted oil reservoirs by alternate injection of CO_2 and produced water supplied with a nutrient solution. The idea is that the injection of CO_2 into depleted oil reservoirs decreases the pH of the formation water to acidity levels ($4 < pH < 6$). The injected CO_2 can also serve as a source of carbon to produce methane (Vilcáez et al., 2018). The nutrient solution, which mainly consists of carbohydrates and proteins, accelerates the activity of targeted microbial communities (e.g. methanogens) and helps them grow over other inhabitant microbial communities in depleted oil reservoirs. This leads to the higher microbial production of CH_4 from biodegradation of the remaining crude oil in the reservoir.

In the following sections, first, the formulation of biodegradation kinetics used in TOUGHREACT-CO2Bio is presented. Then, the approach to incorporate the generated gases from microbial reactions to the flow is explained. Afterward, the experimental data of methanogenic crude oil biodegradation is simulated. Finally, the 3D alternate injection of CO_2 and produced water into a

section of Cushing oilfield is simulated to verify the capability of TOUGHREACT-CO2Bio to model the complex bio-geochemical reactive transport in deep geological formations.

5.3. Microbial capabilities of TOUGHREACT

TOUGHREACT applies a sequential iteration method to solve the combined system of flow and solute transport equations. The governing equations for multiphase fluid (and heat) flow, and solute transport have the same structure, which is derived from the conservation of mass (or energy) law.

The geochemical system in TOUGHREACT is defined by N_c aqueous primary (basis) species and secondary species. The secondary species include aqueous complexes, gaseous and precipitated (mineral) species. The number of secondary species must be equal to the number of reactions, and they can be represented as a linear combination of the set of primary species:

$$S_i = \sum_{j=1}^{N_c} v_{ij} S_j \qquad i = 1, \dots, N_R \tag{1}$$

Where S denotes chemical species, N_R is the number of secondary species, j is the basis species index, i is the secondary species index, and v_{ij} is the stoichiometric coefficient of j-th primary species in the i-th reaction (Xu et al., 2014). A general-rate law is used in TOUGHREACT to define aqueous and sorption kinetics and biodegradation as follows:

$$r_i = \sum_{s=1}^{M} \begin{Bmatrix} k_{i,s} & rate\ constant \\ \times \prod_{j=1}^{N_l} \left(\gamma_j^{v_{i,j}} C_j^{v_{i,j}} \right) & product\ terms \\ \times \prod_{k=1}^{N_m} \left(\frac{C_{i,k}}{K_{Mi,k} + C_{i,k}} \right) & Monod\ terms \\ \times \prod_{p=1}^{N_p} \left(\frac{I_{i,p}}{I_{i,p} + C_{i,p}} \right) & inhibition\ terms \end{Bmatrix} \tag{2}$$

Where r_i is the reaction rate of the i-th reaction, M is the number of mechanisms or pathways, s is the mechanism counter, k is the rate constant (maximum specific growth constant for biodegradation), N_l is the number of reacting species in the product term, γ_j is the activity coefficient of species j, C_j is the concentration of species j, $v_{i,j}$ is the stoichiometry coefficient, N_m is the number of Monod factors, $C_{i,k}$

is the concentration of k-th Monod species, $K_{Mi,k}$ is the k-th Monod half-saturation constant of the i-th species, N_p is the number of inhibition factors, $C_{i,p}$ is the concentration of the p-th inhibition species, and $I_{i,p}$ is the p-th inhibition constant.

5.4. Microbial capabilities of TOUGHREACT-CO2Bio

Following the approach of Vilcáez (2015), the microbial communities that are involved in the simulation study contain the methanogens, sulfate reducing bacteria, and H_2-forming fermentative bacteria (X_1, X_2… X_5). These microbes have been known to coexist in oil reservoirs (Lin et al., 2014, Xiao et al., 2013, Youssef et al., 2009, Liu et al., 2015).

X_1: H_2-forming fermentative bacteria

X_2: Acetotrophic methanogens

X_3: Acetotrophic sulfate reducing bacteria

X_4: Hydrogenotrophic methanogens

X_5: Hydrogenotrophic sulfate reducing bacteria

Table 5.1 summarizes the metabolism reactions of each microbe. All types of microbes in the microbial community are symbolized by the same molecular formula $C_5H_7O_2N$ (Rittmann and McCarty, 2012). The carbohydrate and protein that are contained in the nutrient solution are represented by the molecular formula of sucrose ($C_{12}H_{22}O_{11}$) and serine ($C_3H_7O_3N$). The remaining crude oil in the depleted oil reservoirs is considered to be immobile. In this study, Hexadecane ($C_{16}H_{34}$) is considered as the source of biodegradable hydrocarbon in depleted oil reservoirs.

Table 5.1. Microbial metabolism reactions (modified from Vilcáez (2015))

Microbe	Stoichiometric reaction
X_1	$2.777C_{12}H_{22}O_{11} + NH_4^+ + 45.333H_2O \rightarrow$ $2.777CH_3COO^- + 22.777HCO_3^- + 45.555H_2 + 26.555H^+ + C_5H_7O_2N$

	$125C_3H_7O_3N + 237H_2O \rightarrow$
	$124NH_4^+ + 125CH_3COO^- + 120HCO_3^- + 115H_2 + 121H^+ + C_5H_7O_2N$
	$5.952C_{16}H_{34} + NH_4^+ + 106.048H_2O \rightarrow$
	$41.667CH_3COO^- + 6.905HCO_3^- + 115H_2 + 49.571H^+ + C_5H_7O_2N$
X_2	$44.444CH_3COO^- + NH_4^+ + 22.278H_2O + 51.5H^+ \rightarrow$
	$36.389HCO_3^- + 47.5CH_4 + C_5H_7O_2N$
X_3	$27.778CH_3COO^- + NH_4^+ + 28.75SO_4^{2-} + 61.5H^+ \rightarrow$
	$50.556HCO_3^- + 28.75H_2S + 16.889H_2O + C_5H_7O_2N$
X_4	$125H_2 + NH_4^+ + 33.75HCO_3^- + 32.75H^+ \rightarrow$
	$99.25H_2O + 28.75CH_4 + C_5H_7O_2N$
X_5	$200H_2 + NH_4^+ + 47.5SO_4^{2-} + 99H^+ \rightarrow$
	$5HCO_3^- + 47.5H_2S + 203H_2O + C_5H_7O_2N$

In TOUGHREACT-CO2Bio, a pH inhibition term (I_{pH}) is included in the kinetic reaction mathematical formulation to account for the upper (pH_{UL}) and lower (pH_{LL}) limits at which microbial species are completely inhibited. Thus the reaction rate of the X-th microbe can be written as:

$$r_{x_i} = r_i \times I_{pH_i} \tag{3}$$

$$I_{pH_i} = Exp\left[-3\left(\frac{pH - pH_{UL_i}}{pH_{UL_i} - pH_{LL_i}}\right)^2\right] \tag{4}$$

The upper and lower pH limits for microbes are listed in Table 5.2. All kinetic parameters relevant to methanogenic and sulfate reduction reactions were reported in Vilcáez (2015).

Table 5.2. pH inhibition coefficients (as recommended in the ADM1 (Batstone et al., 2002)).

	X_1	X_2	X_3	X_4	X_5
$pH_{UL,i}$	5.5	7.0	5.5	6.0	6.5*
$pH_{LL,i}$	4.0	6.0	4.5	5.0	5.0*

* (Vilcáez, 2015)

5.5. Incorporation of microbial gas generation into the flow equations

In TOUGHREACT, the discretization of the flow equations results in a set of nonlinear algebraic equations, where the time-dependent primary thermodynamic variables of all grid are unknowns. These equations are casted in residual form and solved for the thermodynamic variables using Newton-Raphson method. For each grid block, there are NEQ equations (usually NEQ = NK + 1, NK is number of primary variables), so that for a flow system with NEL grid blocks represents a total of NEL x NEQ coupled non-linear equations (Pruess et al., 1999). Hence, the residual matrix contains NEL x NEQ variables. By solving the system of equations at each time step, the velocity and thermophysical properties of fluids are calculated. The calculated values then are used to solve the transport equations. The transport equations are solved on a component by component basis through all grid blocks of the system and the calculated concentrations are stored in a total concentration matrix (Bharali et al.), whereas the chemical reaction equations are solved in a grid by grid basis through all compounds in each grid block. The algorithm to couple transport and chemical equations basically consists of alternating the calculation of transport and chemical reaction equations.

In TOUGHREACT-CO2Bio, CO_2(aq), CH_4(aq), H_2(aq) and H_2S(aq) are included in the chemical input file as primary variables. CH_4(aq), H_2(aq) and H_2S(aq) can be generated through microbial activity in the aqueous phase (Table 1). In each time step, the generated amounts of CH_4(aq), H_2(aq) and H_2S(aq) are fed back to the flow equation. To do so, the residual form of the discretized flow equation is modified for each primary variable by including the calculated chemical primary variables from the chemical part. Then, the equilibrium between the aqueous and gas phases for each component is calculated using the thermodynamic model.

On the other hand, when the concentration of CO_2(aq), CH_4(aq), H_2(aq) and H_2S(aq) from the flow equation is higher than their equivalent concentration from the reactive part, the difference is calculated and added to the total concentration matrix for the corresponding component.

5.6. Verification of the model

5.6.1. Batch microbial conversion of crude oil to methane

To verify the ability of CO2Bio to predict bio-geochemical generation of CH_4 and H_2, the results of an experimental data (Vilcáez et al., 2018) of methanogenic crude oil biodegradation though the combined supply of CO_2 and protein-rich matter in anaerobic microcosms at ambient pressure and 50℃ were simulated. In the experiment, collected formation water and oil samples of Stillwater oilfield in Oklahoma were transferred to anaerobic media serum vials that were supplemented with a nutrient solution (e.g. protein rich matter) and $NaHCO_3$ as a source of CO_2. N_2 was used to bubble out the remaining oxygen in the headspace of the microcosms at the beginning of the experimentation. Fig. 5.1 shows the experimental results of methanogenic crude oil biodegradation.

Each vial has 250 cc volume, and 120 cc of them were filled with the formation water, oil, and nutrient solution. The experimental system was simulated using a cube of the same size. The chemical composition of the Stillwater formation water was used in the model (Table 5.4). Hexadecane ($C_{16}H_{34}$) was considered as the source of the hydrocarbon in the reservoir. The nutrient solution was assumed to be consisted of 30% sucrose (as carbohydrate source) and 70% serine (protein source). To model the gas-filled part of the vials, which was initially filled with N_2, CO_2 gas were included in the model. The reason for this assumption is that CO2Bio does not account for N_2 in its thermodynamic model. The maximum specific growth constant and Monod half-saturation constant of the species are reported in Table 5.3.

Figs. 5.2-5.4 shows the predicted results using CO2Bio. As it is seen, the trend of H_2 and CH_4 generation and/or consumption were correctly projected. As it is expected, the higher rate of H_2 and CH_4 generation at the beginning of the experiment is a result of the nutrient source consumption (Fig. 5.3), and it is followed by the lower rate of CH_4 generation, which is mainly resulted by degradation of crude oil. Fig. 5.4 shows the growth of microbial communities in the system. As it is seen, the

availability of nutrients was resulted in the stimulation of methanogenic and H_2-forming fermentative microbes, which indeed triggered the generation of CH_4.

Table 5.3. The maximum specific growth constant and Monod half-saturation constant of the species (modified from Vilcáez (2015))

Microorganism and limiting nutrient	Maximum specific growth rate (1/s)	Half-saturation constant (mol/l)
X_1-$C_{16}H_{34}$	1.900×10^{-8}	2.0×10^{-5}
X_1-$C_3H_7O_3N$	4.777×10^{-7}	2.0×10^{-4}
X_1- $C_{12}H_{22}O_{11}$	4.777×10^{-6}	2.0×10^{-4}
X_2-CH_3COO^-	1.777×10^{-5}	3.0×10^{-3}
X_3-CH_3COO^-	8.333×10^{-8}	2.0×10^{-4}
X_4-H_2	3.888×10^{-6}	6.6×10^{-6}
X_5-H_2	4.444×10^{-7}	1.3×10^{-6}

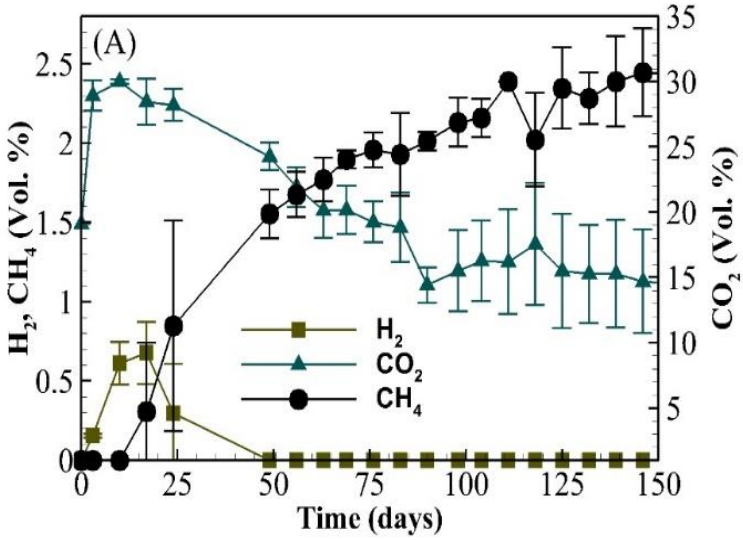

Fig. 5.1. Experimental data of generation/consumption of CH_4 and H_2 vs. time (Vilcáez et al., 2018)

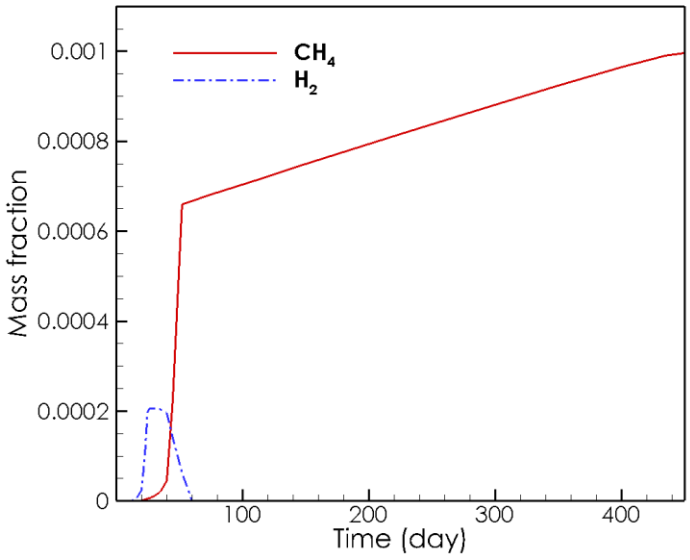

Fig. 5.2. Simulated data of generation/consumption of CH_4 and H_2 vs. time

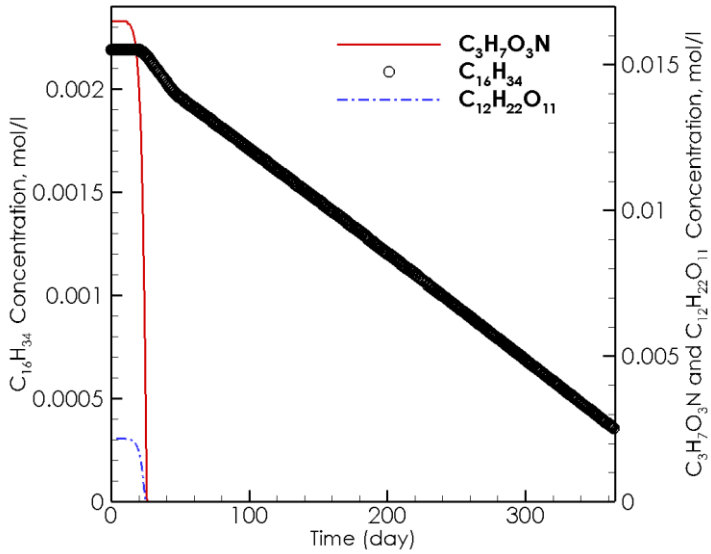

Fig. 5.3. Simulated concentration of $C_{16}H_{34}$, $C_3H_7O_3N$ and $C_{12}H_{22}O_{11}$ vs. time

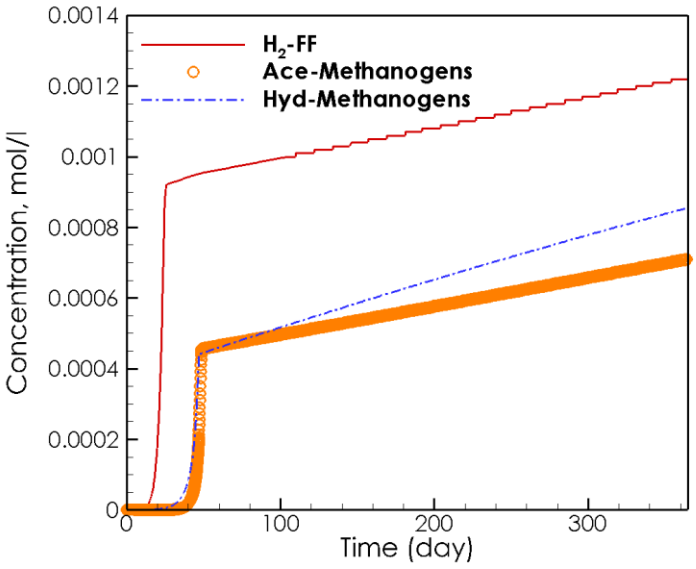

Fig. 5.4. Simulated concentration of microbes vs. time

The capability of TOUGHREACT-CO2Bio to simulate the multiphase flow of CO_2-CH_4-H_2S-H_2 gas mixture and brine in deep geological formations has been presented in part 1 of this study (Shabani and Vilcáez, 2019). Here, we simulated a batch experiment of microbial biodegradation of crude oil to methane, and compared the simulated results with experimental data. In another case, a section of Cushing oil field was modeled to simulate the alternate injection of CO_2 and produced water supplied with nutrients to biodegrade the remaining crude oil to methane.

5.6.2. Alternate injection of CO_2 and produced water

To show the capability of TOUGHREACT-CO2Bio to simulate the coupled multiphase flow and reactive solute transport of CO_2-CH_4-H_2S-H_2 gas mixture and brine in porous media, a 3D alternate injection of CO_2 and produced water in a section of Cushing-Drumright oil reservoir was simulated.

Fig. 5.5 shows the simulated reservoir model. The model dimension is 289.65×341.725×307.723 m^3. The reservoir is discretized into 3375 cells (15×15×15). The model has 15 different layers, with the porosity ranges from 11.9 to 20 %, and permeability of 6-53 mD. The initial pressure and temperature at the bottom layer of the reservoir are 92.2 bar and 46.35℃.

The Cushing oil reservoir is majorly consisted of sandstone. Hence, the reservoir model is considered to be consisted of quartz and calcite minerals. Similar to the batch simulation, Hexadecane is considered as the source of hydrocarbon in the reservoir. The hydrocarbon phase (e.g. hexadecane) is assumed to be immobile in the reservoir, however, it contributes to the flow by the aqueous kinetic reaction reported in Table 5.1. The initial water composition of the reservoir is equivalent to the concentration of formation water of Stillwater oil field of Oklahoma (Table 5.4).

Table 5.4. The chemical composition of the formation water

Component	**Concentration (mol/l)**
H^+	1.995×10^{-6}
Ca^{+2}	1.725×10^{-1}
Mg^{+2}	4.443×10^{-2}
Na^+	1.537
K^+	1.000×10^{-12}
$SiO_2(aq)$	7.262×10^{-4}
$CO_2(aq)$	1.000×10^{-12}
HCO_3^-	1.639×10^{-3}
SO_4^{-2}	4.154×10^{-4}
Cl^-	2.061
$CH_4(aq)$	1.000×10^{-12}
$H_2(aq)$	1.000×10^{-12}
$H_2S(aq)$	1.000×10^{-12}
NH^{4+}	4.838×10^{-3}
CH_3COO^-	1.000×10^{-12}
$C_{16}H_{34}$	2.208×10^{-4}
$C_3H_7O_3N$	1.000×10^{-12}
$C_{12}H_{22}O_{11}$	1.000×10^{-12}
X_1	5.440×10^{-8}
X_2	5.440×10^{-8}
X_3	5.440×10^{-8}
X_4	5.440×10^{-8}
X_5	5.440×10^{-8}
$O_2(aq)$	1.000×10^{-12}

One injection point and one production point are placed in the model. The reservoir simulation includes 6 months of stabilization phase, 6 months of CO_2 injection and 6 months of produced water injection. In the stabilization phase, the program run for 6 months to reach the steady state condition. In this period, the biodegradation of Hexadecane occurs under natural microbial mechanisms in the reservoir. The program then restarted from the stabilization period for CO_2 injection period. CO_2 was

injected at the constant rate of 0.2 kg/s at the bottom two layers of the reservoir for 6 months. As mentioned in the introduction section, the injected CO_2 decreases the pH level of the reservoir, and it also serves as a source of carbon to produce methane. The CO_2 injection period was then followed by produced water injection. The produced water (formation water) is supplied with a nutrient solution and recycled to the reservoir. The nutrient solution consists of 30% sucrose and 70% serine. The total concentration of the nutrient solution in the injected water is 2.5 g/l. The nutrient solution is assumed to be completely soluble in the injection water.

Fig. 5.6 demonstrates the 3D gas distribution in the reservoir at the end of the simulation. As it is seen, the generated biogenic CH_4 swept up in a bank of CH_4 saturated phase and moved ahead of gas moving front. This is mainly because of the sweeping effect of the injected CO_2 and the lower viscosity of the generated gases. Injected CO_2 also extracts the dissolved CH_4 in the aqueous phase.

Because some key kinetic parameters for microbial degradation of hydrocarbons at reservoir pressure and temperature are not known yet (such as rate constants), this work did not aim to conduct an economic analysis of biogenic production of CH_4 through the alternate injection of CO_2 and produced water into depleted oil reservoirs.

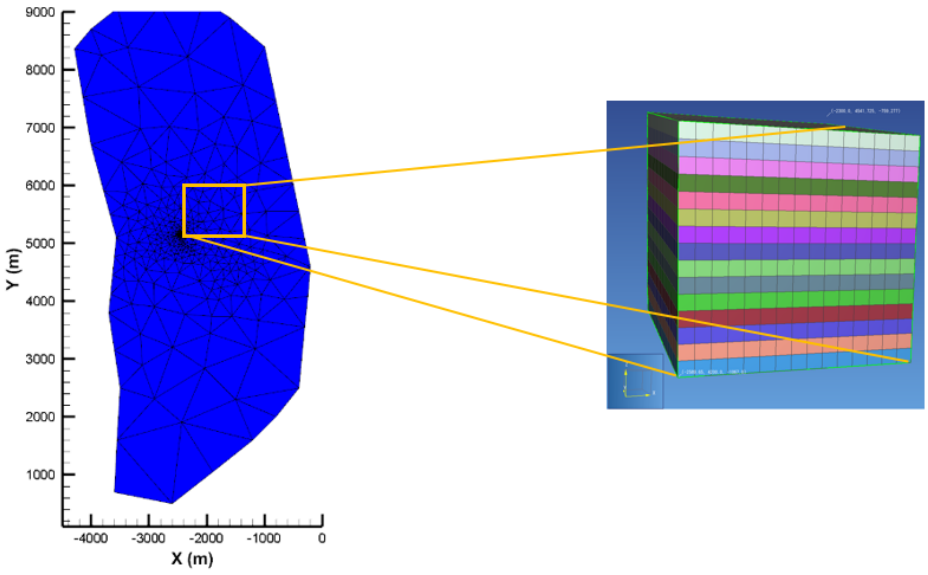

Fig. 5.5. The simulated reservoir model

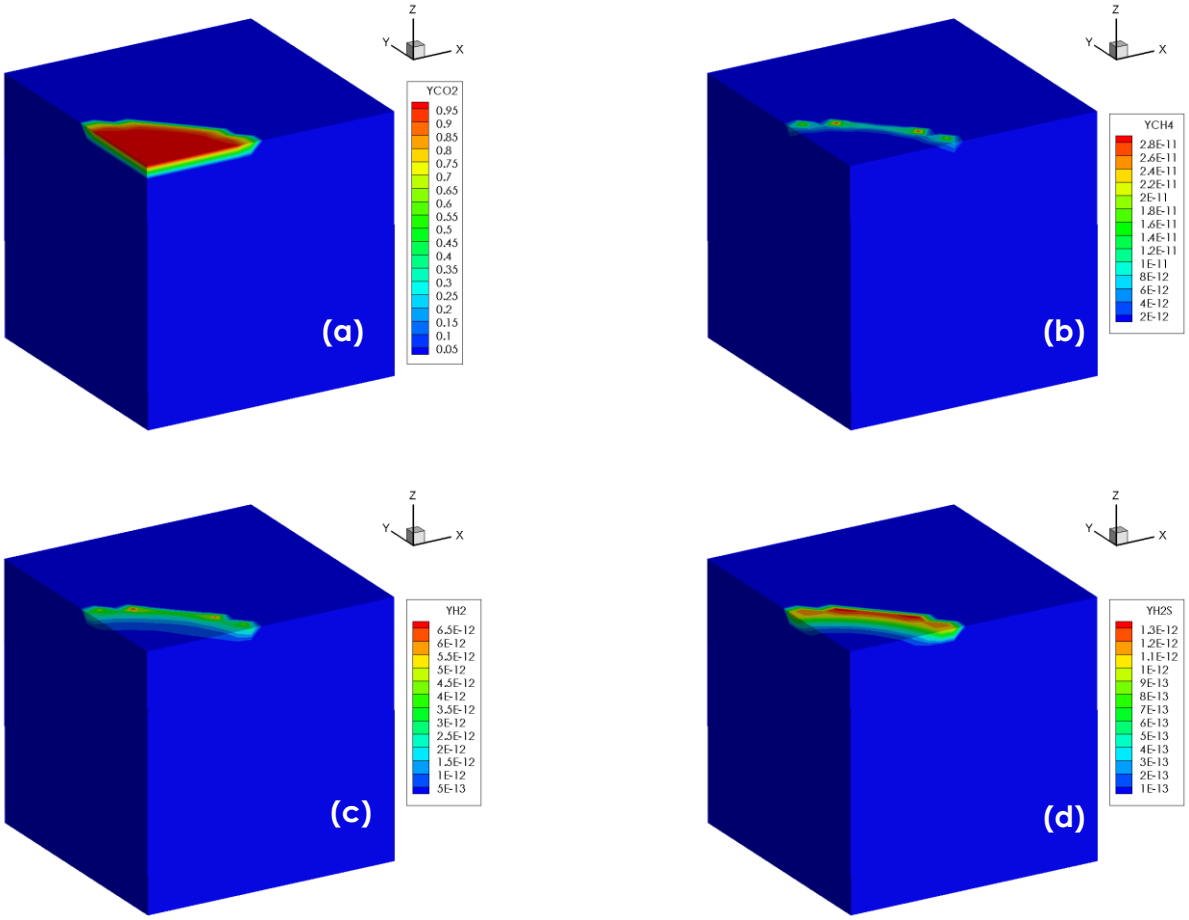

Fig. 5.6. Gas distribution in the reservoir at the end of the simulation; a) CO_2, b) CH_4, c) H_2 and d) H_2S

5.7. Conclusion

CO2Bio is a new module of TOUGHREACT, which is mainly developed to simulate the reactive flow of CO_2-CH_4-H_2-H_2S gas mixtures and brine in deep geological formations under biotic conditions. In CO2Bio, the microbial generation of CH_4, H_2 and H_2S is coupled with the multiphase-multicomponent fluid flow. CO2Bio is capable of predicting the kinetics of CO_2 and/or crude oil microbial conversion to CH_4 in deep saline aquifers or depleted oil reservoirs. The idea of alternate injection of CO_2 and produced water into depleted oil reservoirs to convert the remaining crude oil to methane convey the impression of a promising method not only to mitigate the CO_2 emission to the atmosphere, but also to produce natural gas, which is the cleanest fossil fuel energy source. However, more experimental data is needed to study the economic feasibility of the microbial conversion of crude oil to methane in field scale.

5.8. References

BATSTONE, D. J., KELLER, J., ANGELIDAKI, I., KALYUZHNYI, S., PAVLOSTATHIS, S., ROZZI, A., SANDERS, W., SIEGRIST, H. & VAVILIN, V. 2002. The IWA anaerobic digestion model no 1 (ADM1). Water Science and Technology, 45**,** 65-73.

LIN, J., HAO, B., CAO, G., WANG, J., FENG, Y., TAN, X. & WANG, W. 2014. A study on the microbial community structure in oil reservoirs developed by water flooding. Journal of Petroleum Science and Engineering, 122**,** 354-359.

LIU, J.-F., SUN, X.-B., YANG, G.-C., MBADINGA, S. M., GU, J.-D. & MU, B.-Z. 2015. Analysis of microbial communities in the oil reservoir subjected to CO2-flooding by using functional genes as molecular biomarkers for microbial CO2 sequestration. Frontiers in microbiology, 6**,** 236.

RITTMANN, B. E. & MCCARTY, P. L. 2012. Environmental biotechnology: principles and applications, Tata McGraw-Hill Education.

SHABANI, B. & VILCÁEZ, J. 2019. TOUGHREACT-CO2Bio–a new module to simulate geological carbon storage under biotic conditions (Part 1): the multiphase flow of CO2-CH4-H2-H2S gas mixtures. Journal of Natural Gas Science and Engineering.

VILCÁEZ, J. 2015. Numerical modeling and simulation of microbial methanogenesis in geological CO2 storage sites. Journal of Petroleum Science and Engineering, 135**,** 583-595.

VILCÁEZ, J., YORK, J., YOUSSEF, N. & ELSHAHED, M. 2018. Stimulation of methanogenic crude oil biodegradation in depleted oil reservoirs. Fuel, 232**,** 581-590.

XIAO, M., ZHANG, Z.-Z., WANG, J.-X., ZHANG, G.-Q., LUO, Y.-J., SONG, Z.-Z. & ZHANG, J.-Y. 2013. Bacterial community diversity in a low-permeability oil reservoir and its potential for enhancing oil recovery. Bioresource technology, 147**,** 110-116.

XU, T., SONNENTHAL, E., SPYCHER, N. & ZHENG, L. 2014. TOUGHREACT V3. 0-OMP reference manual: a parallel simulation program for non-isothermal multiphase geochemical reactive transport. University of California, Berkeley.

YOUSSEF, N., ELSHAHED, M. S. & MCINERNEY, M. J. 2009. Microbial processes in oil fields: culprits, problems, and opportunities. Advances in applied microbiology, 66**,** 141-251.

CHAPTER VI

CONCLUSIONS

In this dissertation I investigated the feasibility of field scale stimulation of microbial conversion of CO_2 and crude oil to CH_4 in depleted oil reservoirs. To achieve this goal, I have developed a new module for the well-known reactive transport simulator TOUGHREACT, named CO2Bio, to simulate the multiphase-multicomponent reactive transport of CO_2-CH_4-H_2S-H_2 gas mixtures and brine under biotic conditions. CO2Bio is developed by incorporating into TOUGHREACT an expanded thermodynamic model capable of predicting the mutual solubility of CO_2-CH_4-H_2S-H_2 gas mixtures and brine. Simple but robust thermophysical correlations are adopted in CO2Bio to calculate density, viscosity and enthalpy of CO_2-CH_4-H_2S-H_2 gas mixtures. In CO2Bio, the microbial gas generation is coupled with multiphase flow using a sequential iteration method. Thus, CO2Bio can predict the kinetic microbial production and/or consumption of CO_2, CH_4, H_2S, and H_2 gases, and the multiphase flow of CO_2-CH_4-H_2S-H_2 gas mixtures and brine at deep geological formation conditions. The multiphase flow capabilities of CO2Bio are verified by comparing its simulation results with other reliable multiphase simulation programs including the ECO2N module of TOUGHREACT, the EOS7C module of TOUGH2, and CMG-GEM©. To verify the capability of CO2Bio to simulate the bio-geochemical reactive transport of CO_2-CH_4-H_2-H_2S gas mixtures and brine in deep geological formations under biotic condition, the 3D alternate injection of CO_2 and produced water in a section of Cushing oil field in Oklahoma is simulated. The idea of alternate injection of CO_2 and produced water into depleted oil reservoirs to convert the remaining crude oil to methane convey the impression of a promising method not only to mitigate the CO_2

emission to the atmosphere, but also to produce natural gas, which is the cleanest fossil fuel energy source. The simulation results showed that CO2Bio is capable of modeling the complex multiphase-multicomponent reactive transport of CO_2-CH_4-H_2S-H_2 gas mixtures and brine under biotic conditions. However, more experimental data is needed to study the economic feasibility of the microbial conversion of crude oil to methane in field scale.

VITA

Babak Shabani

Candidate for the Degree of

Doctor of Philosophy

Thesis: BENEFICIAL USE OF PRODUCED WATER AND CARBON DIOXIDE IN DEPLETED OIL RESERVOIRS: IN-SITU MICROBIAL CONVERSION OF CRUDE OIL TO METHANE

Major Field: Geology

Biographical:

Education:

Completed the requirements for the Doctor of Philosophy in Geology at Oklahoma State University, Stillwater, Oklahoma in May, 2019.

Completed the requirements for the Master of Science in Petroleum Engineering-Drilling and Production at Amirkabir University of Technology (Polytechnic), Tehran, Iran in 2011.

Completed the requirements for the Bachelor of Science in Petroleum Engineering-Drilling at Petroleum University of Technology, Ahwaz, Iran in 2008.

Experience: Graduate Research and Teaching Associate at Oklahoma State University.

Professional Memberships: Society of Petroleum Engineers, Geological Society of America, American Association of Petroleum Geologists.